Scientific Inquiry and Review (SIR)
Volume 7 Issue2, 2023
ISSN (P): 2521-2427, ISSN (E): 2521-2435
Homepage: https://journals.umt.edu.pk/index.php/SIR

Article QR

Title: **Shape-Preserving Curve and Surface Data Embedding Algorithm**

Author (s): Farheen Ibraheem[1], Shamaila Samreen[2], Muhammad Bilal Riaz[3], Tayba Arooj[4]

Affiliation (s):
[1]Forman Christian College, A Chartered University-FCCU, Lahore-Pakistan
[2]University of Engineering and Technology- Lahore-Pakistan
[3]Gdansk University of Technology – Poland
[4]Lahore College for Women University, Lahore, Pakistan

DOI: https://doi.org/10.32350/sir.72.01

History: Received: December 08, 2022, Revised: March 20, 2023, Accepted: March 21, 2023, Published: June 15, 2023

Citation: Ibraheem F, Samreen S, Riaz MB, Arooj T. Shape-Preserving curve and surface data embedding algorithm Pakistan. *Sci Inq Rev.* 2023;7(2):1–37. https://doi.org/10.32350/sir.72.01

Copyright: © The Authors

Licensing: This article is open access and is distributed under the terms of Creative Commons Attribution 4.0 International License

Conflict of Interest: Author(s) declared no conflict of interest

A publication of
The School of Science
University of Management and Technology, Lahore, Pakistan

Shape-Preserving Curve and Surface Data Embedding Algorithm

Farheen Ibraheem[1*], Shamaila Samreen[2], Muhammad Bilal Riaz[3], and Tayba Arooj[4]

[1]Forman Christian College, A Chartered University-FCCU, Lahore, Pakistan
[2]University of Engineering and Technology, Lahore, Pakistan
[3]Faculty of Applied Physics and Mathematics, Gdansk University of Technology, Poland
[4]Lahore College for Women University, Lahore, Pakistan

ABSTRACT

In this study, shape preserving data driven rational cubic schemes are developed. A rational cubic piecewise function (quadratic denominator and cubic numerator) with two parameters was transformed to C^1 rational cubic piecewise function. Constraints were derived on free parameters by means of some mathematical derivations to train and demonstrate convex curve. The scheme, then, was advanced to partially blended rational bi-cubic function with eight free parameters which were controlled to ascertain convex surface. A numerical comparison with certain existing schemes manifested that the proposed method was economical. The proposed scheme was put into visualization of convex 2D and 3D data using MATLAB software packet. Additionally, the suggested approach produced a more visually appealing interpolating curve for scientific visualization for specific data sets.

Keywords: convex data, convex surface, rational functions, shape preservation

1. INTRODUCTION

A considerable amount of raw data that represents the experiment's outcomes is typically obtained by the scientists when the experiments are carried out in the lab. For instance, the data in a chemical experiment might be the distillation curve, whereas in a biology experiment, it could be the movement of the relevant cell within the system. Additionally, any experiment may have error or noise in the data collecting procedures. The type of error could be systematic, biased, or random. Other methods of data processing, such as data fitting and data smoothing or filtering were applied to these types of data. Interpolation is a preferable alternative for the data if

* Corresponding Author: farheenibraheem@fccollege.edu.pk

the data is clean, which means there are probably no errors. However, if the data contains noise, approximation, smoothing, or de-noising may be advantageous to gain fruitful results. There are several popular techniques for processing the data including linear regression, polynomial regression (or fitting), any non-polynomial fitting, cubic splines, and smoothing splines. Interpolation, on the other hand, addresses the problem of creating curve or surface that must also maintain the data's geometric shape when it is approximated which is subject of the current research.

Science and engineering, both rely on these continuous visual representations of discrete scientific data in particular which are coherent with intrinsic properties of the data. Computational methods used in these realms are terms as shape preserving algorithms. The design of shape preserving data embedded curves and surfaces lies at the heart of several scientific disciplines in the digital age including computer-aided geometric design (CAGD), computer graphics, and computer-aided design (CAD). These applied areas combine via computational software packets, ideas from numerical techniques, visualization, differential geometry, and linear algebra. Surface and curve drawing schemes offered architects a competitive edge over traditional drafting tool and optimized the likelihood of realizing their ideas by exhibiting their thoughts on computer displays in remarkable short amount of time.

Moreover, the design of machine software, robotics, and chemical processes are among the many fields in which shape-preserving approaches are widely used. For designing ceramics, cutting wood for wooden furniture and creating ornaments, a lathe is utilized. The design of the lathe path is made by using shape-preserving software. Shape-preserving interpolation techniques are employed in both, chemistry and robotics, to plan the path of the robots. In chemistry, they are used for PARFAC modelling of the fluorescence data. There are more applications in the areas of signal processing and photogrammetric data manipulation. Convexity, monotonicity, and positivity are the most dominant data types. All of these applications have to be retained in the process of visualization.

The usual data interpolation algorithms present the data smoothly, however, fail to intact its shapes. The existing shape-preserving algorithms restrain the derivatives at the knots to envisage convex, monotone, and positive data as convex, monotone, and positive surfaces and curves and operate effectively with specific conditions, for instance, the solution of

ordinary and partial differential equations cannot be interpolated by these shape-preserving methods. Another strategy is to add additional knots between the existing data points. Even though these techniques maintain the forms of the data, the amount of computing work has grown larger.

The motivation behind the current research was to devise an efficient and economic algorithm that not only delivers smooth visualizations but confirms convexity in the visual attribute. This research addressed the convex surface and curve interpolation which has become a fundamental element of numerous applications in several areas, such as airplane and automotive industries, architecture, mechanical engineering, and computer graphics. Likewise, convexity in yield curve measures the extent at which price of a bond changes with the rate of interest prevalent in market. It benefits the stakeholders to anticipate price of a bond if market interest rate changes. Furthermore, indifference curve in economics which ranks a consumer's preference for a combination of goods represents convex structure.

Shape conserving convex interpolation was well explored in past few decades and some eminent contributions are [1–26]. The control points of the boundary of 2D shape are optimized using B'ezier curve in [1] and [2]. BFGS diagonal approximation method was employed in [3] to solve B spline curve fitting problem. Surface reconstruction, using B spline and BFGS diagonal approximation, was discussed in [4]. Kvasov [6] presented two algorithms to preserve the monotonicity and convexity of the discrete data by using weighted C^1 quadratic splines. Verlan [7] proposed an algorithm of C^2 interpolation utilizing splines of arbitrary degree for discrete data to achieve the convexity conservation of data. Moreover, in [8–10] convexity preserving techniques were global.

Brodlie and Butt [11] presented a piecewise cubic C^1 interpolant to preserve the convexity of the data. Hussain et al. [12] suggested a local shape preserving interpolation scheme through GC^1 bi-quadratic trigonometric spline. The scheme comprised of four free parameters in each rectangular domain. These free parameters were controlled so that no possible fluctuations could be seen. This scheme maintained the smoothness of positive and monotone 3D data. Sarfraz et al. [14] constructed a rational cubic function with two parameters in the vision of captivating positive data. Simple constraints were manipulated on two parameters in the illustration of rational cubic function and extended rational bi-cubic

partially blended function. The scheme was local with an approximation order of $O(h_i^3)$. Sarfraz et al. [15] developed the smooth shape preserving methods deploying piecewise rational cubic and the rational bi-cubic function to conserve the convexity for 2D and 3D data. The data dependent constraints on free parameters were evaluated to achieve the shape of convex data. The convexity conserving schemes yielded adequate degrees of freedom to facilitate the researcher and user. The convex shape of the data was not preserved by the techniques in [17] when the data was presented with derivatives.

To retain the shape of convex data, Costantini and Fontanella [22] created a semi-global approach. However, this scheme was not economical as degree of interpolant in some rectangular patches became excessively high and the polynomial patches tended to be linear in x and/or y. The resulting surfaces, also, failed to attain a visually pleasant look. In order to create convex surfaces, Asaturyan [23] each rectangular grid was divided into nine smaller rectangles. This scheme was not local which means that by altering the data for one sub rectangle's edge in the x direction, a modification was made to the grid for all of the sub rectangle's edges that were originally situated in the x direction. The convex data visualization techniques created in [24] were global.

In [25], the proposed approach kept the convexity of the surface along the grid lines, but failed to preserve the convexity inside the grids, leading to unfavorable flat areas because second order mixed partial derivatives vanished. A univariate C^2 cubic spline was utilized to preserve convexity. A C^2 quartic \ quadratic interpolant was used by authors in [26] to visualize monotone, convex, and positive data set.

The convex shape of the data was not preserved by the techniques in [17, 25] when the data was presented with derivatives.

The main focus of the current paper was to derive data dependent constraints on parameters in the description of piece wise rational cubic and bi-cubic functions in [14] to hold convexity. The research conducted for this purpose was discussed in several sections. Section 2 and Section 3 presents a review of piece wise rational cubic and rational bi-cubic function [14] to be employed. Convexity preserving constraints for curve and surface data were developed in Section 4. Section 5 provides implementation of rational scheme developed on 2D and 3D data sets and corresponding numerical

results were demonstrated in Section 6. Proposed research algorithm was concluded in Section 7**.**

2. RATIONAL CUBIC FUNCTION

The rational cubic function introduced by Sarfraz et al. [14] is explained in this section.

Suppose that (u_j, v_j), where $j = 0,1,2,\dots,n$ are the set of given data points defined over the interval $[a, b]$ such that $a = u_0 < u_1 < u_2 < \cdots < u_n = b$. The piecewise rational cubic function with two parameters ϱ_j and σ_j defined over the each subinterval $I_j = [u_{j+1}, u_j]$ where $j = 0,1,2,3,\dots,n-1$ is given by:

$$T_j(u) = \frac{P_j(\xi)}{Q_j(\xi)}, \tag{2.1}$$

where

$$P_j(\xi) = \varrho_j v_j(1-\xi)^3 + \{\varrho_j v_j + h_j \varrho_j d_j + 2v_j\}(1-\xi)^2\xi + \{\sigma_j v_{j+1} - h_j\sigma_j d_{j+1} + 2v_{j+1}\}(1-\xi)\,\xi^2 + \sigma_j v_{j+1}\xi^3,$$

$$Q_j(\xi) = \varrho_j(1-\xi)^2 + 2(1-\xi)\xi + \sigma_j\xi^2,$$

$$\xi = \frac{(u-u_j)}{h_j},\ h_j = u_{j+1} - u_j.$$

The rational cubic function defined in **Eq**. (**2**. **1**) is C^1 if the following characteristics hold,

$$T_j(u_j) = v_j, T_j(u_{j+1}) = v_{j+1}, T_j^{(1)}(u_j) = d_j, T_j^{(1)}(u_{j+1}) = d_{j+1} \tag{2.2}$$

where $T^{(1)}$ signifies derivative with respect to 'u' and d_j symbolizes the derivative values at the knots u_j. Interestingly, taking $\varrho_j = \sigma_j = 1$, rational cubic spline takes the form of standard cubic Hermite spline in each interval $I_j = [u_j, u_{j+1}]$.

3. RATIONAL BI-CUBIC FUNCTION

In this section, the rational cubic function in **Eq**. (**2**. **1**) is expanded to a rational bi-cubic function specified over three-dimensional set of data points $\{(u_j, v_j, \tilde{G}_{j,l}): j = 0,1,2,\dots,n;\ l = 0,1,2,\dots,m\}$with the rectangular

grid M $= [u_0, u_n] \times [v_0, v_m]$. Let $\tilde{\mu}: a = u_0 < u_1 < u_2 < \cdots < u_n = b$ be the partition of $[a, b]$ and $\tilde{\pi}: c = v_0 < v_1 < v_2 < \cdots < v_n = d$ be the partition of $[c, d]$. The rational bi-cubic partially blended function can be defined over each rectangular patch $I_j = [u_j, u_{j+1}] \times [v_l, v_{l+1}]$ as:

$$T(u, v) = -EGN^T, \tag{3.1}$$

where

$$G = \begin{pmatrix} 0 & T(u, v_l) & T(u, v_{l+1}) \\ T(u_j, v) & T(u_j, v_l) & T(v_j, v_{l+1}) \\ T(u_{j+1}, v) & T(u_{j+1}, v_l) & T(u_{j+1}, v_{l+1}) \end{pmatrix}, \tag{3.2}$$

$$E = [-1 \quad \tau_0(\xi) \quad \tau_1(\xi)],$$

$$N = [-1 \quad \lambda_0(\eta) \quad \lambda_1(\eta)],$$

where

$\tau_0 = (1-\xi)^2(1+2\xi),\ \tau_1 = \xi^2(3-2\xi),\ \lambda_0 = (1-\eta)^2(1+2\eta),\ \lambda_1 = \eta^2(3-2\eta).$

Furthermore, $\xi = \frac{(u-u_j)}{h_j} \qquad 0 \le \xi \le 1\,, \qquad \eta = \frac{(v-v_l)}{\bar{h}_l} \qquad 0 \le \eta \le 1,$

$h_j = u_{j+1} - u_j,\ \bar{h}_l = v_{l+1} - v_l.$

The rational cubic function $T(u, v_l), T(u, v_{l+1}), T(u_j, v), T(u_{j+1}, v)$ similar to **Eq.** $(\mathbf{2.1})$ are attained and specified over the boundary of rectangular portion as:

$$T(u, v_l) = \frac{\sum_{l=0}^{3}(1-\xi)^{3-l}\xi^l M_l}{Q_1(\xi)}, \tag{3.3}$$

where

$M_0 = \varrho_{j,l}\tilde{G}_{j,l},$

$M_1 = \varrho_{j,l}\tilde{G}_{j,l} + h_j\varrho_{j,l}\tilde{G}^u_{j,l} + 2\tilde{G}_{j,l},$

$M_2 = \sigma_{j,l}\tilde{G}_{j+1,l} - h_j\sigma_{j,l}\tilde{G}^u_{j+1,l} + 2\tilde{G}_{j+1,l}, M_3 = \sigma_{j,l}\tilde{G}_{j+1,l}$

$Q_1(\xi) = \varrho_{j,l}(1-\xi)^2 + (1-\xi)\xi + \sigma_{j,l}\xi^2$

with $\varrho_{j,l}$ and $\sigma_{j,l}$ shape parameters.

Likewise,

$$T(u, v_{l+1}) = \frac{\sum_{l=0}^{3}(1-\xi)^{3-l}\xi^{l}N_l}{Q_2(\xi)}, \tag{3.4}$$

where

$N_0 = \varrho_{j,l+1}\tilde{G}_{j,l+1}$, $N_1 = \varrho_{j,l+1}\tilde{G}_{j,l+1} + h_j\varrho_{j,l+1}\tilde{G}^{u}_{j,l+1} + 2\tilde{G}_{j,l+1}$,

$N_2 = \sigma_{j,l+1}\tilde{G}_{j+1,l+1} - h_j\sigma_{j,l+1}\tilde{G}^{u}_{j+1,l+1} + 2\tilde{G}_{j+1,l+1}$, $N_3 = \sigma_{j,l+1}\tilde{G}_{j+1,l+1}$,

$Q_2(\xi) = \varrho_{j,l+1}(1-\xi)^2 + (1-\xi)\xi + \sigma_{j,l+1}\xi^2$

with shape parameter $\varrho_{j,l+1}$ and $\sigma_{j,l+1}$.

Further, we have,

$$T(u_j, v) = \frac{\sum_{j=0}^{3}(1-\eta)^{3-j}\eta^{j}J_j}{Q_3(\eta)}, \tag{3.5}$$

where

$J_0 = \bar{\varrho}_{j,l}\tilde{G}_{j,l}$, $J_1 = \bar{\varrho}_{j,l}\tilde{G}_{j,l} + \bar{h}_j\bar{\varrho}_{j,l}\tilde{G}^{u}_{j,l} + 2\tilde{G}_{j,l}$,

$J_2 = \bar{\sigma}_{j,l}\tilde{G}_{j,l+1} - \bar{h}_j\bar{\sigma}_{j,l}\tilde{G}^{u}_{j,l+1} + 2\tilde{G}_{j,l+1}$, $J_3 = \bar{\sigma}_{j,l}\tilde{G}_{j,l+1}$,

$Q_3(\eta) = \bar{\varrho}_{j,l}(1-\eta)^2 + (1-\eta)\eta + \bar{\sigma}_{j,l}\eta^2$

with shape parameter $\bar{\varrho}_{j,l}$ and $\bar{\sigma}_{j,l}$.

Lastly,

$$T(u_{j+1}, v) = \frac{\sum_{j=0}^{3}(1-\eta)^{3-j}\eta^{j}K_j}{Q_4(\eta)}, \tag{3.6}$$

where

$K_0 = \bar{\varrho}_{j+1,l}\tilde{G}_{j+1,l}$, $K_1 = \bar{\varrho}_{j+1,l}\tilde{G}_{j+1,l} + \bar{h}_j\bar{\varrho}_{j+1,l}\tilde{G}^{u}_{j+1,l} + 2\tilde{G}_{j+1,l}$,

$K_2 = \bar{\sigma}_{j+1,l}\tilde{G}_{j+1,l+1} - \bar{h}_j\bar{\sigma}_{j+1,l}\tilde{G}^{u}_{j+1,l+1} + 2\tilde{G}_{j+1,l+1}$, $K_3 = \bar{\sigma}_{j+1,l}\tilde{G}_{j+1,l+1}$,

$Q_4(\eta) = \bar{\varrho}_{j+1,l}(1-\eta)^2 + (1-\eta)\eta + \bar{\sigma}_{j+1,l}\eta^2$

With shape parameters $\bar{\varrho}_{j+1,l}$ and $\bar{\sigma}_{j+1,l}$.

4. THE PROPOSED ALGORITHM

This section uses the rational cubic function and rational bi-cubic function to build convexity-preserving for regular surface data (2).

4.1. Convex Curve Model

Assume that $\{(u_j, v_j); j = 0,1,2, \dots, n\}$ represents the given convex data set defined over the interval $[a, b]$ where $a = u_0 < u_1 < u_2 < \cdots < u_n = b$ and $d_j; j = 0,1,2, \dots, n$ designates the derivative values at the point $u_j; j = 0,1,2, \dots, n$.

Also, let

$\check{\Delta}_j = \frac{v_{j+1} - v_j}{h_j}$.

Additionally, the following condition is fulfilled by the derivative values:

$\check{\Delta}_j \leq \check{\Delta}_{j+1}$

$d_j \leq d_{j+1}, d_j \leq \check{\Delta}_j \leq d_{j+1},$

$\varrho_j \; and \; \sigma_j$ are the parameters in the interval $[u_j, u_{j+1}]$.

The piecewise rational cubic function $T_j(u)$ defined in **Eq.** $(\mathbf{2.1})$ is convex, if

$T_j^{(2)}(u) \geq 0, u_0 \leq u \leq u_n$

The value of $T_j^{(2)}(u)$ is computed as follows:

$$T_j^{(2)}(u) = \frac{\sum_{j=0}^{5} (1-\xi)^{5-j} \xi^j \hat{a}_j}{h_j \left(Q_j(\xi)\right)^3}, \tag{4.1}$$

where

$\hat{a}_0 = 2\varrho_j^2 \sigma_j \check{\Delta}_j + 4\varrho_j^2 \check{\Delta}_j - 2\varrho_j^2 \sigma_j d_{j+1} - 4\varrho_j^2 d_j,$

$\hat{a}_1 = -2\varrho_j \sigma_j d_{j+1} - 4\varrho_j d_j - 3\varrho_j \sigma_j d_j + 5\varrho_j \sigma_j \check{\Delta}_j + 4\varrho_j \check{\Delta}_j,$

$\hat{a}_2 = 3\sigma_j^2 d_{j+1} - \varrho_j \sigma_j d_{j+1} - 2\varrho_j d_j - 6\varrho_j \sigma_j d_j + 7\varrho_j \sigma_j \check{\Delta}_j + 2\varrho_j \check{\Delta}_j - 3\sigma_j^2 \check{\Delta}_j,$

$\hat{a}_3 = 6\varrho_j\sigma_j d_{j+1} + 2\sigma_j d_{j+1} - 3\varrho_j^2 d_j + \varrho_j\sigma_j d_j + 3\varrho_j^2\check{\Delta}_j - 7\varrho_j\sigma_j\check{\Delta}_j - 2\sigma_j\check{\Delta}_j,$

$\hat{a}_4 = 3\varrho_j\sigma_j d_{j+1} + 4\sigma_j d_{j+1} + 2\varrho_j\sigma_j d_j - 5\varrho_j\sigma_j\check{\Delta}_j - 4\sigma_j\check{\Delta}_j,$

$\hat{a}_5 = -2\varrho_j\sigma_j^2\check{\Delta}_j + 4\sigma_j^2\check{\Delta}_j + 2\varrho_j\sigma_j^2 d_j + 4\sigma_j^2 d_{j+1}.$

The denominator quantity $Q_j(\xi)$ in (9) is a cube quantity and is positive if

$\varrho_j \geq 0, \qquad \sigma_j \geq 0.$

In addition to this, the requisite condition for convexity in each subinterval is given as:

$\hat{a}_j \geq 0; \qquad j = 0,1,2,3,5.$

After numerous manipulations, we successfully procure the constraints on σ_j and ϱ_j given by

$$\sigma_j > \max\left\{0, \frac{2(d_j - \check{\Delta}_j)}{(-d_{j+1} - 6d_j + 7\check{\Delta}_j)}\right\} \tag{4.2}$$

$$\varrho_j > \max\left\{0, \frac{2(\check{\Delta}_j - d_{j+1})}{(d_j + 6d_{j+1} - 7\check{\Delta}_j)}\right\} \tag{4.3}$$

which can be rearranged as

$$\sigma_j = \kappa_j + \max\left\{0, \frac{2(d_j - \check{\Delta}_j)}{(-d_{j+1} - 6d_j + 7\check{\Delta}_j)}\right\}, \qquad \kappa_j > 0$$

$$\varrho_j = \varepsilon_j + \max\left\{0, \frac{2(\check{\Delta}_j - d_{j+1})}{(d_j + 6d_{j+1} - 7\check{\Delta}_j)}\right\}, \qquad \varepsilon_j > 0$$

The above discussion is summarized as:

Theorem 1: Assume that $\{(u_j, v_j); j = 0,1,2,\dots,n\}$ be a convex data set. Then, the convexity is sustained by the piecewise rational cubic function defined in (1), if in each subinterval $[u_j, u_{j+1}]$, $j = 0,1,2,\dots,n$ the parameters σ_j, ϱ_j satisfy the conditions :

$$\sigma_j = \kappa_j + \max\left\{0, \frac{2(d_j - \check{\Delta}_j)}{(-d_{j+1} - 6d_j + 7\check{\Delta}_j)}\right\}, \qquad \kappa_j > 0$$

$$\varrho_j = \varepsilon_j + \max\left\{0, \frac{2(\check{\Delta}_j - d_{j+1})}{(d_j + 6d_{j+1} - 7\check{\Delta}_j)}\right\}. \qquad \varepsilon_j > 0$$

5. CONVEX SURFACE MODEL

Consider a convex data set $\{(u_j, v_l, \tilde{G}_{j,l}); j = 0,1,2,\dots,n, l = 0,1,2,\dots,m\}$ demarcated over the rectangular mesh $[u_j, u_{j+1}] \times [v_j, v_{j+1}]$ for $j = 0,1,2,\dots,n-1, l = 0,1,2,\dots,m-1$ such that the following necessary conditions for convexity are settled:

$\check{\Delta}_{j,l} \leq \check{\Delta}_{j+1,l}$, $\tilde{G}^u_{j,l} \leq \tilde{G}^u_{j+1,l}$, $\tilde{\Delta}_{j,l} \leq \tilde{\Delta}_{j,l+1}$, $\tilde{G}^v_{j,l} \leq \tilde{G}^v_{j,l+1}$

$\check{\Delta}_{j,l} = \frac{\tilde{G}_{j+1,l} - \tilde{G}_{j,l}}{h_j}$, $\tilde{\Delta}_{j,l} = \frac{\tilde{G}_{j,l+1} - \tilde{G}_{j,l}}{\bar{h}_l}$

$\tilde{G}^u_{j,l} \leq \check{\Delta}_{j,l} \leq \tilde{G}^u_{j+1,l}$, $\tilde{G}^v_{j,l} \leq \tilde{\Delta}_{j,l} \leq \tilde{G}^v_{j,l+1}$

Now, convexity for the surface patch defined in $(\mathbf{3.1})$ holds if all the boundary curves $(\mathbf{3.3}), (\mathbf{3.4}), (\mathbf{3.5})$ *and* $(\mathbf{3.6})$ are convex.

Consequently, the boundary curve $\mathrm{T}(u, v_l)$ is convex if $T_j^{(2)}(u, v_l) \geq 0$ i.e.,

$$T_j^{(2)}(u, v_l) = \frac{\sum_{l=0}^{5}(1-\xi)^{5-l}\xi^l \hat{b}_l}{h_j(Q_1(\xi))^3}\,, \tag{5.1}$$

where

$$\hat{b}_0 = 2\varrho^2_{j,l}\sigma_{j,l}\tilde{\Delta}_{j,l} + 4\varrho^2_{j,l}\tilde{\Delta}_{j,l} - 2\varrho^2_{j,l}\sigma_{j,l}\tilde{G}^u_{j+1,l} - 4\varrho^2_{j,l}\tilde{G}^u_{j,l},$$

$$\hat{b}_1 = -2\varrho_{j,l}\sigma_{j,l}\tilde{G}^u_{j+1,l} - 4\varrho_{j,l}\tilde{G}^u_{j,l} - 3\varrho_{j,l}\sigma_{j,l}\tilde{G}^u_{j,l} + 5\varrho_{j,l}\sigma_{j,l}\tilde{\Delta}_{j,l} + 4\varrho_{j,l}\tilde{\Delta}_{j,l},$$

$$\hat{b}_2 = 3\sigma^2_{j,l}\tilde{G}^u_{j+1,l} - \varrho_{j,l}\sigma_{j,l}\tilde{G}^u_{j+1,l} - 2\varrho_{j,l}\tilde{G}^u_{j,l} - 6\varrho_{j,l}\sigma_{j,l}\tilde{G}^u_{j,l} + 7\varrho_{j,l}\sigma_{j,l}\tilde{\Delta}_{j,l} + 2\varrho_{j,l}\tilde{\Delta}_{j,l} - 3\sigma^2_{j,l}\tilde{\Delta}_{j,l},$$

$$\hat{b}_3 = 6\varrho_{j,l}\sigma_{j,l}\tilde{G}^u_{j+1,l} + 2\sigma_{j,l}\tilde{G}^u_{j+1,l} - 3\varrho^2_{j,l}\tilde{G}^u_{j,l} + \varrho_{j,l}\sigma_{j,l}\tilde{G}^u_{j,l} + 3\varrho^2_{j,l}\tilde{\Delta}_{j,l} - 7\varrho_{j,l}\sigma_{j,l}\tilde{\Delta}_{j,l} - 2\sigma_{j,l}\tilde{\Delta}_{j,l},$$

$$\hat{b}_4 = 3\varrho_{j,l}\sigma_{j,l}\tilde{G}^u_{j+1,l} + 4\sigma_{j,l}\tilde{G}^u_{j+1,l} + 2\varrho_{j,l}\sigma_{j,l}\tilde{G}^u_{j,l} - 5\varrho_{j,l}\sigma_{j,l}\tilde{\Delta}_{j,l} - 4\sigma_{j,l}\tilde{\Delta}_{j,l},$$

$$\hat{b}_5 = -2\varrho_{j,l}\sigma^2_{j,l}\tilde{\Delta}_{j,l} + 4\sigma^2_{j,l}\tilde{\Delta}_{j,l} + 2\varrho_{j,l}\sigma^2_{j,l}\tilde{G}^u_{j,l} + 4\sigma^2_{j,l}\tilde{G}^u_{j+1,l}.$$

Now, for positive $T_j^{(2)}(u, v_l)$, the numerator $\sum_{l=0}^{5}(1-\xi)^{5-l}\xi^l \hat{b}_l \geq 0$,

If

$\hat{b}_l \geq 0, l = 0,1,2,3,4,5$

After frequent calculations, following constraints were inferred,

$$\sigma_{j,l} > \max\left\{0, \frac{2\left(\tilde{G}^u_{j,l} - \tilde{\Delta}_{j,l}\right)}{\left(-\tilde{G}^u_{j+1,l} - 6\tilde{G}^u_{j,l} + 7\tilde{\Delta}_{j,l}\right)}\right\},$$

$$\varrho_{j,l} > \max\left\{0, \frac{2\left(\tilde{\Delta}_{j,l} - \tilde{G}^u_{j+1,l}\right)}{\left(\tilde{G}^u_{j,l} + 6\tilde{G}^u_{j+1,l} - 7\tilde{\Delta}_{j,l}\right)}\right\},$$

Correspondingly, $\mathrm{T}(u, v_{l+1})$ is convex if $T_j^{(2)}(u, v_{l+1}) \geq 0$ i.e.,

$$T_j^{(2)}(u, v_{l+1}) = \frac{\sum_{l=0}^{5}(1-\xi)^{5-l}\xi^l \hat{c}_l}{h_j (Q_2(\xi))^3}, \tag{5.2}$$

where

$\hat{c}_0 = 2\varrho^2_{j,l+1}\sigma_{j,l+1}\tilde{\Delta}_{j,l+1} + 4\varrho^2_{j,l+1}\tilde{\Delta}_{j,l+1} - 2\varrho^2_{j,l+1}\sigma_{j,l+1}\tilde{G}^u_{j+1,l+1} - 4\varrho^2_{j,l+1}\tilde{G}^u_{j,l+1}$,

$\hat{c}_1 = -2\varrho_{j,l+1}\sigma_{j,l+1}\tilde{G}^u_{j+1,l+1} - 4\varrho_{j,l+1}\tilde{G}^u_{j,l+1} - 3\varrho_{j,l+1}\sigma_{j,l+1}\tilde{G}^u_{j,l+1} + 5\varrho_{j,l+1}\sigma_{j,l+1}\tilde{\Delta}_{j,l+1} + 4\varrho_{j,l+1}\tilde{\Delta}_{j,l+1}$,

$\hat{c}_2 = 3\sigma^2_{j,l+1}\tilde{G}^u_{j+1,l+1} - \varrho_{j,l+1}\sigma_{j,l+1}\tilde{G}^u_{j+1,l+1} - 2\varrho_{j,l+1}\tilde{G}^u_{j,l+1} - 6\varrho_{j,l+1}\sigma_{j,l+1}\tilde{G}^u_{j,l+1} + 7\varrho_{j,l+1}\sigma_{j,l+1}\tilde{\Delta}_{j,l+1} + 2\varrho_{j,l+1}\tilde{\Delta}_{j,l+1} - 3\sigma^2_{j,l+1}\tilde{\Delta}_{j,l+1}$,

$\hat{c}_3 = 6\varrho_{j,l+1}\sigma_{j,l+1}\tilde{G}^u_{j+1,l+1} + 2\sigma_{j,l+1}\tilde{G}^u_{j+1,l+1} - 3\varrho^2_{j,l+1}\tilde{G}^u_{j,l+1} + \varrho_{j,l+1}\sigma_{j,l+1}\tilde{G}^u_{j,l+1} + 3\varrho^2_{j,l+1}\tilde{\Delta}_{j,l+1} - 7\varrho_{j,l+1}\sigma_{j,l+1}\tilde{\Delta}_{j,l+1} - 2\sigma_{j,l+1}\tilde{\Delta}_{j,l+1}$,

$\hat{c}_4 = 3\varrho_{j,l+1}\sigma_{j,l+1}\tilde{G}^u_{j+1,l+1} + 4\sigma_{j,l+1}\tilde{G}^u_{j+1,l+1} + 2\varrho_{j,l+1}\sigma_{j,l+1}\tilde{G}^u_{j,l+1} - 5\varrho_{j,l+1}\sigma_{j,l+1}\tilde{\Delta}_{j,l+1} - 4\sigma_{j,l+1}\tilde{\Delta}_{j,l+1}$,

$\hat{c}_5 = -2\varrho_{j,l+1}\sigma^2_{j,l+1}\tilde{\Delta}_{j,l+1} + 4\sigma^2_{j,l+1}\tilde{\Delta}_{j,l+1} + 2\varrho_{j,l+1}\sigma^2_{j,l+1}\tilde{G}^u_{j,l+1} + 4\sigma^2_{j,l+1}\tilde{G}^u_{j+1,l+1}$.

For the numerator $\sum_{l=0}^{5}(1-\xi)^{5-l}\xi^l \hat{c}_l \geq 0$,

We must have

$\hat{c}_l \geq 0, l = 0,1,2,3,4,5.$

which yields,

$$\sigma_{j,l+1} > \max\left\{0, \frac{2\left(\tilde{G}^u_{j,l+1} - \tilde{\Delta}_{j,l+1}\right)}{\left(-\tilde{G}^u_{j+1,l+1} - 6\tilde{G}^u_{j,l+1} + 7\tilde{\Delta}_{j,l+1}\right)}\right\},$$

$$\varrho_{j,l+1} > \max\left\{0, \frac{2\left(\tilde{\Delta}_{j,l+1} - \tilde{G}^u_{j+1,l+1}\right)}{\left(\tilde{G}^u_{j,l+1} + 6\tilde{G}^u_{j+1,l+1} - 7\tilde{\Delta}_{j,l+1}\right)}\right\}.$$

Identically, $\mathrm{T}(u_j, v)$ is convex if $T_j^{(2)}(u_j, v) \geq 0$ i.e.,

$$T_j^{(2)}(u_j, v) = \frac{\sum_{j=0}^{5}(1-\xi)^{5-j}\xi^j \hat{r}_j}{\bar{h}_l(Q_3(\xi))^3}, \tag{5.3}$$

where

$$\hat{r}_0 = 2\bar{\varrho}^2_{j,l}\bar{\sigma}_{j,l}\check{\Delta}_{j,l} + 4\bar{\varrho}^2_{j,l}\check{\Delta}_{j,l} - 2\bar{\varrho}^2_{j,l}\bar{\sigma}_{j,l}\tilde{G}^v_{j,l+1} - 4\bar{\varrho}^2_{j,l}\tilde{G}^v_{j,l},$$

$$\hat{r}_1 = -2\bar{\varrho}_{j,l}\bar{\sigma}_{j,l}\tilde{G}^v_{j,l+1} - 4\bar{\varrho}_{j,l}\tilde{G}^v_{j,l} - 3\bar{\varrho}_{j,l}\bar{\sigma}_{j,l}\tilde{G}^v_{j,l} + 5\bar{\varrho}_{j,l}\bar{\sigma}_{j,l}\check{\Delta}_{j,l} + 4\bar{\varrho}_{j,l}\check{\Delta}_{j,l},$$

$$\hat{r}_2 = 3\bar{\varrho}^2_{j,l}\tilde{G}^v_{j,l+1} - \bar{\varrho}_{j,l}\bar{\sigma}_{j,l}\tilde{G}^v_{j,l+1} - 2\bar{\varrho}_{j,l}\tilde{G}^v_{j,l} - 6\bar{\varrho}_{j,l}\bar{\sigma}_{j,l}\tilde{G}^v_{j,l} + 7\bar{\varrho}_{j,l}\bar{\sigma}_{j,l}\check{\Delta}_{j,l} + 2\bar{\varrho}_{j,l}\check{\Delta}_{j,l} - 3\bar{\varrho}^2_{j,l}\check{\Delta}_{j,l},$$

$$\hat{r}_3 = 6\bar{\varrho}_{j,l}\bar{\sigma}_{j,l}\tilde{G}^v_{j,l+1} + 2\bar{\sigma}_{j,l}\tilde{G}^v_{j,l+1} - 3\bar{\varrho}^2_{j,l}\tilde{G}^v_{j,l} + \bar{\varrho}_{j,l}\bar{\sigma}_{j,l}\tilde{G}^v_{j,l} + 3\bar{\varrho}^2_{j,l}\check{\Delta}_{j,l} - 7\bar{\varrho}_{j,l}\bar{\sigma}_{j,l}\check{\Delta}_{j,l} - 2\bar{\sigma}_{j,l}\check{\Delta}_{j,l},$$

$$\hat{r}_4 = 3\bar{\varrho}_{j,l}\bar{\sigma}_{j,l}\tilde{G}^v_{j,l+1} + 4\bar{\sigma}_{j,l}\tilde{G}^v_{j,l+1} + 2\bar{\varrho}_{j,l}\bar{\sigma}_{j,l}\tilde{G}^v_{j,l} - 5\bar{\varrho}_{j,l}\bar{\sigma}_{j,l}\check{\Delta}_{j,l} - 4\bar{\sigma}_{j,l}\check{\Delta}_{j,l},$$

$$\hat{r}_5 = -2\bar{\varrho}_{j,l}\bar{\sigma}^2_{j,l}\check{\Delta}_{j,l} + 4\bar{\sigma}^2_{j,l}\check{\Delta}_{j,l} + 2\bar{\varrho}_{j,l}\bar{\sigma}^2_{j,l}\tilde{G}^v_{j,l} + 4\bar{\sigma}^2_{j,l}\tilde{G}^v_{j,l+1}.$$

Likewise, $\sum_{j=0}^{5}(1-\xi)^{5-j}\xi^j\hat{r}_j \geq 0,$

if

$\hat{r}_j \geq 0; j = 0,1,2,3,4,5.$

This provides the following constraints,

$$\bar{\sigma}_{j,l} > \max\left\{0, \frac{2\left(\tilde{G}^v_{j,l} - \check{\Delta}_{j,l}\right)}{\left(-\tilde{G}^v_{j,l+1} - 6\tilde{G}^v_{j,l} + 7\check{\Delta}_{j,l}\right)}\right\},$$

$$\bar{\varrho}_{j,l} > \max\left\{0, \frac{2\left(\check{\Delta}_{j,l} - \tilde{G}^v_{j,l+1}\right)}{\left(\tilde{G}^v_{j,l} + 6\tilde{G}^v_{j,l+1} - 7\check{\Delta}_{j,l}\right)}\right\}.$$

Eventually, T$\left(u_{j+1}, v\right)$ is convex if $T_j^{(2)}(u_{j+1}, v) \geq 0$ i.e.,

$$T_j^{(2)}(u_{j+1}, v) = \frac{\sum_{j=0}^{5}(1-\xi)^{5-j}\xi^j \hat{s}_j}{\bar{h}_l(Q_4(\xi))^3}, \tag{5.4}$$

where

$\hat{s}_0 = 2\bar{\varrho}_{j+1,l}^2\bar{\sigma}_{j+1,l}\check{\Delta}_{j+1,l} + 4\bar{\varrho}_{j+1,l}^2\check{\Delta}_{j+1,l} - 2\bar{\varrho}_{j+1,l}^2\bar{\sigma}_{j+1,l}\tilde{G}_{j+1,l+1}^v - 4\bar{\varrho}_{j+1,l}^2\tilde{G}_{j+1,l}^v,$

$\hat{s}_1 = -2\bar{\varrho}_{j+1,l}\bar{\sigma}_{j+1,l}\tilde{G}_{j+1,l+1}^v - 4\bar{\varrho}_{j+1,l}\tilde{G}_{j+1,l}^v - 3\bar{\varrho}_{j+1,l}\bar{\sigma}_{j+1,l}\tilde{G}_{j+1,l}^v + 5\bar{\varrho}_{j+1,l}\bar{\sigma}_{j+1,l}\check{\Delta}_{j+1,l} + 4\bar{\varrho}_{j+1,l}\check{\Delta}_{j+1,l},$

$\hat{s}_2 = 3\bar{\varrho}_{j+1,l}^2\tilde{G}_{j+1,l+1}^v - \bar{\varrho}_{j+1,l}\bar{\sigma}_{j+1,l}\tilde{G}_{j+1,l+1}^v - 2\bar{\varrho}_{j+1,l}\tilde{G}_{j+1,l}^v - 6\bar{\varrho}_{j+1,l}\bar{\sigma}_{j+1,l}\tilde{G}_{j+1,l}^v + 7\bar{\varrho}_{j+1,l}\bar{\sigma}_{j+1,l}\check{\Delta}_{j+1,l} + 2\bar{\varrho}_{j+1,l}\check{\Delta}_{j+1,l} - 3\bar{\varrho}_{j+1,l}^2\check{\Delta}_{j+1,l},$

$\hat{s}_3 = 6\bar{\varrho}_{j+1,l}\bar{\sigma}_{j+1,l}\tilde{G}_{j+1,l+1}^v + 2\bar{\sigma}_{j+1,l}\tilde{G}_{j+1,l+1}^v - 3\bar{\varrho}_{j+1,l}^2\tilde{G}_{j+1,l}^v + \bar{\varrho}_{j+1,l}\bar{\sigma}_{j+1,l}\tilde{G}_{j+1,l}^v + 3\bar{\varrho}_{j+1,l}^2\check{\Delta}_{j+1,l} - 7\bar{\varrho}_{j+1,l}\bar{\sigma}_{j+1,l}\check{\Delta}_{j+1,l} - 2\bar{\sigma}_{j+1,l}\check{\Delta}_{j+1,l},$

$\hat{s}_4 = 3\bar{\varrho}_{j+1,l}\bar{\sigma}_{j+1,l}\tilde{G}_{j+1,l+1}^v + 4\bar{\sigma}_{j+1,l}\tilde{G}_{j+1,l+1}^v + 2\bar{\varrho}_{j+1,l}\bar{\sigma}_{j+1,l}\tilde{G}_{j+1,l}^v - 5\bar{\varrho}_{j+1,l}\bar{\sigma}_{j+1,l}\check{\Delta}_{j+1,l} - 4\bar{\sigma}_{j+1,l}\check{\Delta}_{j+1,l},$

$\hat{s}_5 = -2\bar{\varrho}_{j+1,l}\bar{\sigma}_{j+1,l}^2\check{\Delta}_{j+1,l} + 4\bar{\sigma}_{j+1,l}^2\check{\Delta}_{j+1,l} + 2\bar{\varrho}_{j+1,l}\bar{\sigma}_{j+1,l}^2\tilde{G}_{j+1,l}^v + 4\bar{\sigma}_{j+1,l}^2\tilde{G}_{j+1,l+1}^v.$

Likewise, $\sum_{j=0}^{5}(1-\xi)^{5-j}\xi^j\hat{s}_j \geq 0$, if

$\hat{s}_j \geq 0; j = 0,1,2,3,4,5$

This provides the following constraints,

$$\bar{\sigma}_{j+1,l} > \max\left\{0, \frac{2\left(\tilde{G}_{j+1,l}^v - \check{\Delta}_{j+1,l}\right)}{\left(-\tilde{G}_{j+1,l+1}^v - 6\tilde{G}_{j+1,l}^v + 7\check{\Delta}_{j+1,l}\right)}\right\},$$

$$\bar{\varrho}_{j+1,l} > \max\left\{0, \frac{2\left(\check{\Delta}_{j+1,l} - \tilde{G}_{j+1,l+1}^v\right)}{\left(\tilde{G}_{j+1,l}^v + 6\tilde{G}_{j+1,l+1}^v - 7\check{\Delta}_{j+1,l}\right)}\right\}.$$

This discussion is briefed as:

Theorem 2: The visualization of 3D convex data as convex surface for Bi-cubic partially blended rational function in (3) can be rendered if in each rectangular mesh $I = \left[u_j, u_{j+1}\right] \times [v_l, v_{l+1}]$, the parameters

$\varrho_{j,l}$, $\sigma_{j,l}$, $\varrho_{j,l+1}$, $\sigma_{j,l+1}$, $\bar{\varrho}_{j,l}$, $\bar{\sigma}_{j,l}$, $\bar{\varrho}_{j+1,l}$, $\bar{\sigma}_{j+1,l}$, assure the following constraints:

$$\sigma_{j,l} > \max\left\{0, \frac{2\left(\tilde{G}^{u}_{j,l} - \tilde{\Delta}_{j,l}\right)}{\left(-\tilde{G}^{u}_{j+1,l} - 6\tilde{G}^{u}_{j,l} + 7\tilde{\Delta}_{j,l}\right)}\right\}, \varrho_{j,l} > \max\left\{0, \frac{2\left(\tilde{\Delta}_{j,l} - \tilde{G}^{u}_{j+1,l}\right)}{\left(\tilde{G}^{u}_{j,l} + 6\tilde{G}^{u}_{j+1,l} - 7\tilde{\Delta}_{j,l}\right)}\right\},$$

$$\sigma_{j,l+1} > \max\left\{0, \frac{2\left(\tilde{G}^{u}_{j,l+1} - \tilde{\Delta}_{j,l+1}\right)}{\left(-\tilde{G}^{u}_{j+1,l+1} - 6\tilde{G}^{u}_{j,l+1} + 7\tilde{\Delta}_{j,l+1}\right)}\right\},$$

$$\varrho_{j,l+1} > \max\left\{0, \frac{2\left(\tilde{\Delta}_{j,l+1} - \tilde{G}^{u}_{j+1,l+1}\right)}{\left(\tilde{G}^{u}_{j,l+1} + 6\tilde{G}^{u}_{j+1,l+1} - 7\tilde{\Delta}_{j,l+1}\right)}\right\},$$

$$\bar{\sigma}_{j,l} > \max\left\{0, \frac{2\left(\tilde{G}^{v}_{j,l} - \check{\Delta}_{j,l}\right)}{\left(-\tilde{G}^{v}_{j,l+1} - 6\tilde{G}^{v}_{j,l} + 7\check{\Delta}_{j,l}\right)}\right\}, \bar{\varrho}_{j,l} > \max\left\{0, \frac{2\left(\check{\Delta}_{j,l} - \tilde{G}^{v}_{j,l+1}\right)}{\left(\tilde{G}^{v}_{j,l} + 6\tilde{G}^{v}_{j,l+1} - 7\check{\Delta}_{j,l}\right)}\right\},$$

$$\bar{\sigma}_{j+1,l} > \max\left\{0, \frac{2\left(\tilde{G}^{v}_{j+1,l} - \check{\Delta}_{j+1,l}\right)}{\left(-\tilde{G}^{v}_{j+1,l+1} - 6\tilde{G}^{v}_{j+1,l} + 7\check{\Delta}_{j+1,l}\right)}\right\},$$

$$\bar{\varrho}_{j+1,l} > \max\left\{0, \frac{2\left(\check{\Delta}_{j+1,l} - \tilde{G}^{v}_{j+1,l+1}\right)}{\left(\tilde{G}^{v}_{j+1,l} + 6\tilde{G}^{v}_{j+1,l+1} - 7\check{\Delta}_{j+1,l}\right)}\right\}.$$

Adjusting the above constraints as:

$$\sigma_{j,l} = a_{j,l} + \max\left\{0, \frac{2\left(\tilde{G}^{u}_{j,l} - \tilde{\Delta}_{j,l}\right)}{\left(-\tilde{G}^{u}_{j+1,l} - 6\tilde{G}^{u}_{j,l} + 7\tilde{\Delta}_{j,l}\right)}\right\}, \qquad a_{j,l} > 0$$

$$\varrho_{j,l} = b_{j,l} + \max\left\{0, \frac{2\left(\tilde{\Delta}_{j,l} - \tilde{G}^{u}_{j+1,l}\right)}{\left(\tilde{G}^{u}_{j,l} + 6\tilde{G}^{u}_{j+1,l} - 7\tilde{\Delta}_{j,l}\right)}\right\}, \qquad b_{j,l} > 0$$

$$\sigma_{j,l+1} = c_{j,l} + \max\left\{0, \frac{2\left(\tilde{G}^{u}_{j,l+1} - \tilde{\Delta}_{j,l+1}\right)}{\left(-\tilde{G}^{u}_{j+1,l+1} - 6\tilde{G}^{u}_{j,l+1} + 7\tilde{\Delta}_{j,l+1}\right)}\right\}, \qquad c_{j,l} > 0$$

$$\varrho_{j,l+1} = d_{j,l} + \max\left\{0, \frac{2\left(\tilde{\Delta}_{j,l+1} - \tilde{G}^{u}_{j+1,l+1}\right)}{\left(\tilde{G}^{u}_{j,l+1} + 6\tilde{G}^{u}_{j+1,l+1} - 7\tilde{\Delta}_{j,l+1}\right)}\right\}, \qquad d_{j,l} > 0$$

$$\bar{\sigma}_{j,l} = e_{j,l} + \max\left\{0, \frac{2\left(\tilde{G}^{v}_{j,l} - \check{\Delta}_{j,l}\right)}{\left(-\tilde{G}^{v}_{j,l+1} - 6\tilde{G}^{v}_{j,l} + 7\check{\Delta}_{j,l}\right)}\right\}, \qquad e_{j,l} > 0$$

$$\bar{\varrho}_{j,l} = g_{j,l} + \max\left\{0, \frac{2\left(\check{\Delta}_{j,l} - \tilde{G}^{v}_{j,l+1}\right)}{\left(\tilde{G}^{v}_{j,l} + 6\tilde{G}^{v}_{j,l+1} - 7\check{\Delta}_{j,l}\right)}\right\}, \qquad g_{j,l} > 0$$

$$\bar{\sigma}_{j+1,l} = m_{j,l} + \max\left\{0, \frac{2\left(\tilde{G}^{v}_{j+1,l} - \check{\Delta}_{j+1,l}\right)}{\left(-\tilde{G}^{v}_{j+1,l+1} - 6\tilde{G}^{v}_{j+1,l} + 7\check{\Delta}_{j+1,l}\right)}\right\}, \qquad m_{j,l} > 0$$

$$\bar{\varrho}_{j+1,l} = n_{j,l} + \max\left\{0, \frac{2\left(\check{\Delta}_{j+1,l} - \tilde{G}^{v}_{j+1,l+1}\right)}{\left(\tilde{G}^{v}_{j+1,l} + 6\tilde{G}^{v}_{j+1,l+1} - 7\check{\Delta}_{j+1,l}\right)}\right\}. \qquad n_{j,l} > 0$$

6. RESULTS AND DISCUSSIONS

This section describes algorithm for the proposed shape preserving techniques in section 4 and verify its effectiveness through graphical results in the subsequent numerical examples.

6.1. Algorithm. Convex Curve Model

Step 1: Compute $(n+1)$ convex data points $\{(u_j, v_j); j = 0,1,2, \dots, n\}$

Step 2: Approximate the derivatives $\check{\Delta}_j$ at the nots using Arithmetic mean method.

Step 3: Using Theorem 1, evaluate free parameters σ_j and ϱ_j.

Step 4: Insert the above values in **Eq.** (**4.1**).

Example 1. The data in Table 1 encloses convex data set. MATLAB programming software packet was used to implement constraints on shape parameter in order to visualize convex curve. Numerical results were recorded in Table 5. Figure 1 clearly reflects the shape characteristic of convexity.

Table 1. A Convex 2D Data Set

u_i	-3	-2	-1	0	1	2	3	4	5
v_i	17	10	5	1.8	1	1.8	5	10	17

Example 2. Another convex data set was considered to implement the proposed algorithm using MATLAB software packet and results are shown in Table 6, while Figure 2 clearly depicts convexity of data.

Table 2. A Convex 2D Data Set

u_i	1	2	3	4	4.9	6
v_i	4.11	9.39	20.3	54.2	163.89	438.1

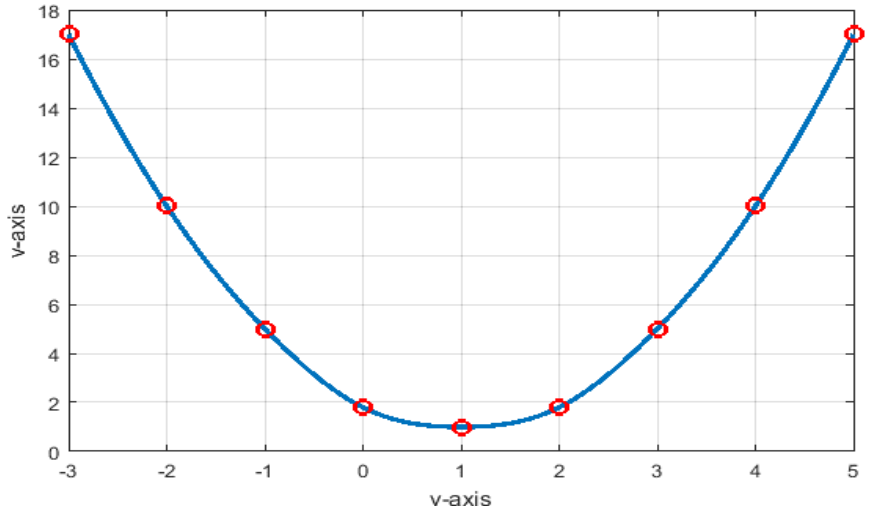

Figure 1. Convexity Preserving Curve of Convex 2D Data Set in Table 1 Using Convex Rational Cubic Spline Function

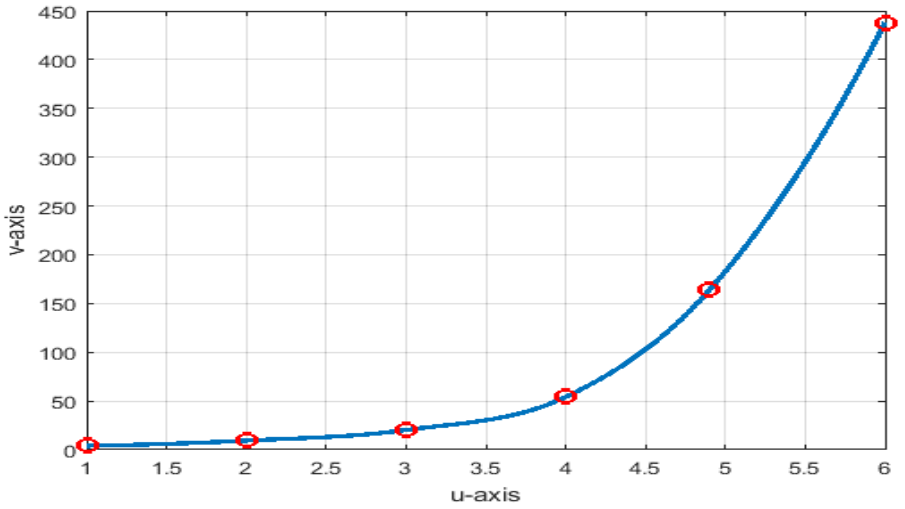

Figure 2. A Convex Curve of Data Set taken in Table 2 Using Convex Rational Cubic Spline Function

Algorithm 2. Convex Surface Model

Step 1: Compute $(n+1) \times (m+1)$ convex data point points $\{(u_j, v_j, \tilde{G}_{j,l}): j = 0,1,2,\dots,n;\ l = 0,1,2,\dots,m\}$.

Step 2: Approximate the derivatives $\tilde{G}_{j,l}^{u}$ and $\tilde{G}_{j,l}^{v}$at the nots using Arithmetic mean method.

Step 3: Using Theorem 2, evaluate free parameters $\varrho_{j,l}$, $\sigma_{j,l}$, $\varrho_{j,l+1}$, $\sigma_{j,l+1}$, $\bar{\varrho}_{j,l}$, $\bar{\sigma}_{j,l}$. $\bar{\varrho}_{j+1,l}$ and $\bar{\sigma}_{j+1,l}$.

Step 4: Insert the above values in (3).

Example 3. A convex 3D data set is prescribed in Table 3 which is created by the function particularized in the following **Eq.** (**6.1**). Convexity is conserved by utilizing convex bi-cubic rational function with the graphical representation illustrated in Figure 3. Numerical results are displayed in Table 7. The uz-view and the vz-view of the convex surface is given in the Figure 4 and Figure 5, respectively.

$$\tilde{G}(u,v) = u^2 + v^2 + 0.1. \qquad (6.1)$$

Table 3. A Convex 3D Data set

u/v	-5	-4	-3	-2	-1	0	1	2	3	4	5	6
-5	50.1	41.1	34.1	29.1	26.1	25.1	26.1	29.1	34.1	41.1	50.1	61.1
-4	41.1	32.1	25.1	20.1	17.1	16.1	17.1	20.1	25.1	32.1	41.1	52.1
-3	34.1	25.1	18.1	13.1	10.1	9.1	10.1	13.1	18.1	25.1	34.1	45.1
-2	29.1	20.1	13.1	8.1	5.1	4.1	5.1	8.1	13.1	20.1	29.1	40.1
-1	26.1	17.1	10.1	5.1	2.1	1.1	2.1	5.1	10.1	17.1	26.1	37.1
0	25.1	16.1	9.1	4.1	1.1	0.1	1.1	4.1	9.1	16.1	25.1	36.1
1	26.1	17.1	10.1	5.1	2.1	1.1	2.1	5.1	10.1	17.1	26.1	37.1
2	29.1	20.1	13.1	8.1	5.1	4.1	5.1	8.1	13.1	20.1	29.1	40.1
3	34.1	25.1	18.1	13.1	10.1	9.1	10.1	13.1	18.1	25.1	34.1	45.1
4	41.1	32.1	25.1	20.1	17.1	16.1	17.1	20.1	25.1	32.1	41.1	52.1
5	50.1	50.1	41.1	34.1	29.1	26.1	25.1	26.1	29.1	34.1	41.1	50.1
6	61.1	52.1	45.1	40.1	37.1	36.1	37.1	40.1	45.1	52.1	61.1	72.1

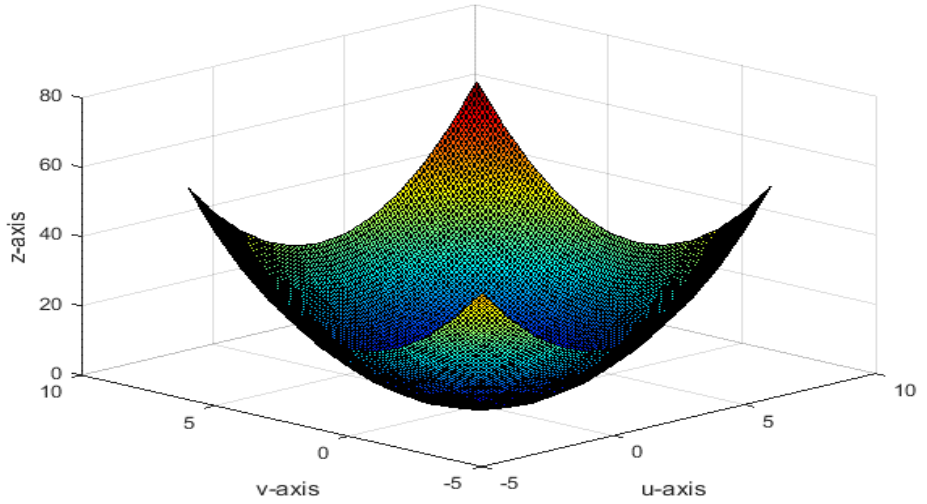

Figure 3. A Convex Surface produced from the Convex Data Set in Table 3

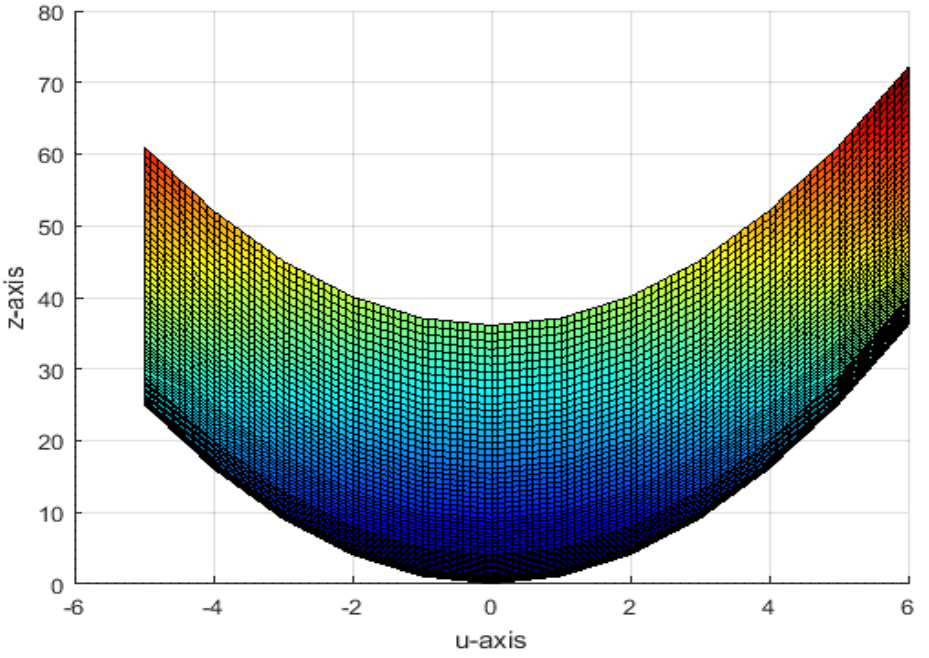

Figure 4. A uz-view of the Convex Surface

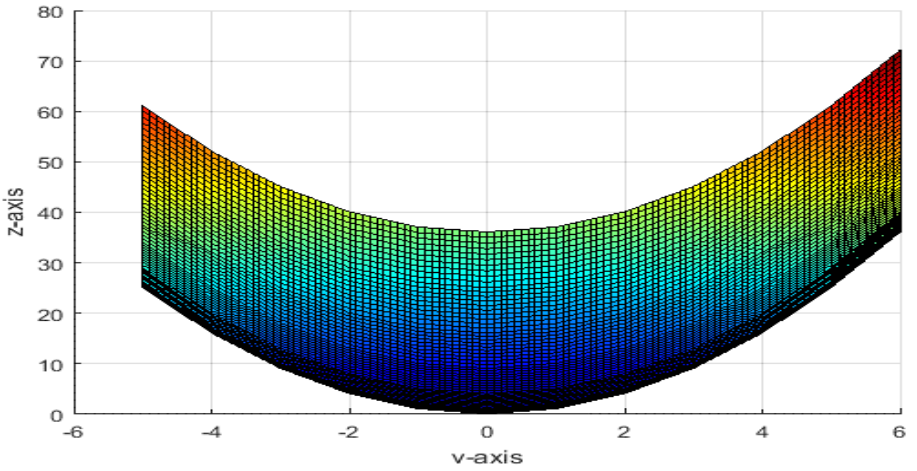

Figure 5. A vz-view of the Convex Surface

Example 4. Another convex 3D data set in Table 4 is made up by the function given by the subsequent equation (17). The convex rational bi-cubic functions help to preserve the convexity of the data which can be visualized in Figure 6. Figures 7, and Figure 8 give the uz-view and vz-view of the convex surface, respectively. Numerical results are shown in Table 8.

$$\tilde{G}(u,v) = (u^2 + v^2 - 1)^2 + 0.2. \qquad (6.2)$$

Table 4. A Convex 3D Data set

u/v	0	1	2	3	4	5	6	7
0	1.2	0.2	9.2	64.2	225.2	576.2	1225.2	2304.2
1	0.2	1.2	16.2	81.2	256.2	625.2	1296.2	2401.2
2	9.2	16.2	49.2	144.2	361.2	784.2	1521.2	2704.2
3	64.2	81.2	144.2	289.2	576.2	1089.2	1936.2	3249.2
4	225.2	256.2	361.2	576.2	961.2	1600.2	2601.2	4096.2
5	576.2	625.2	784.2	1089.2	1600.2	2401.2	3600.2	5329.2
6	1225.2	1296.2	1521.2	1936.2	2601.2	3600.2	5041.2	7056.2
7	2304.2	2401.2	2704.2	3249.2	4096.2	5329.2	7056.2	9409.2

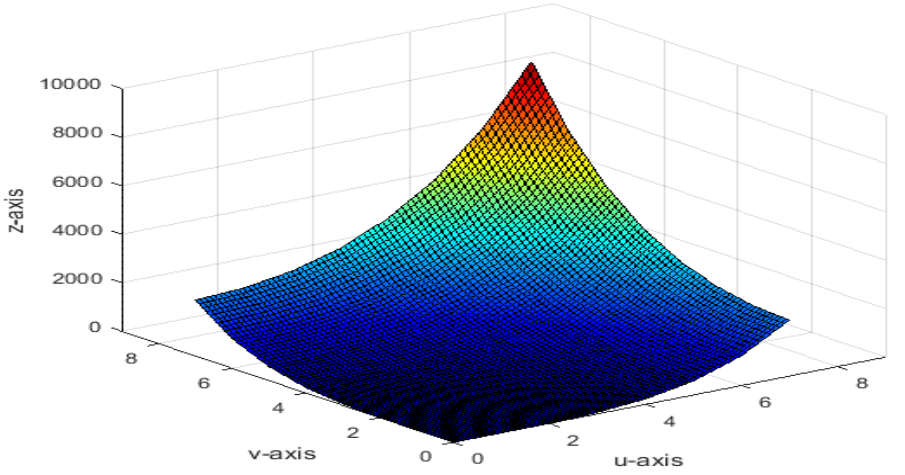

Figure 6. A Convex Surface Constructed from the Convex Data set in Table 4

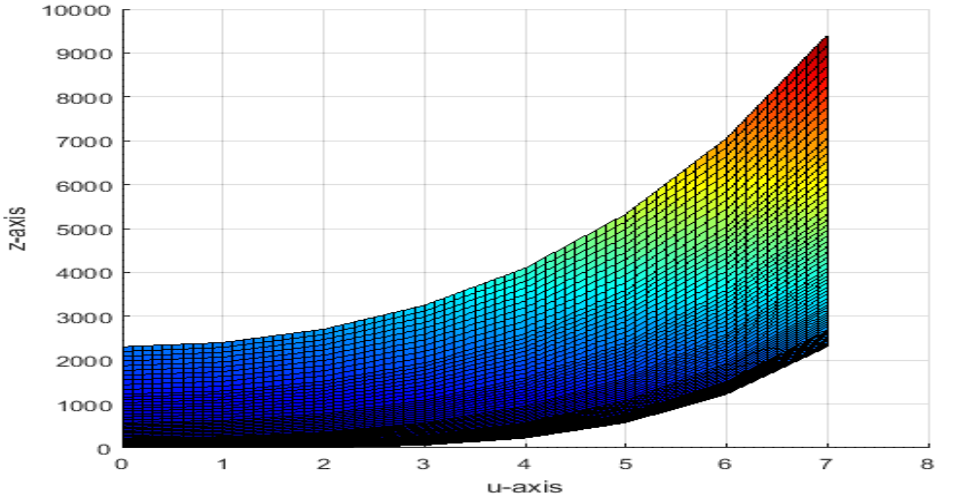

Figure 7. A uz-view of the Convex Surface

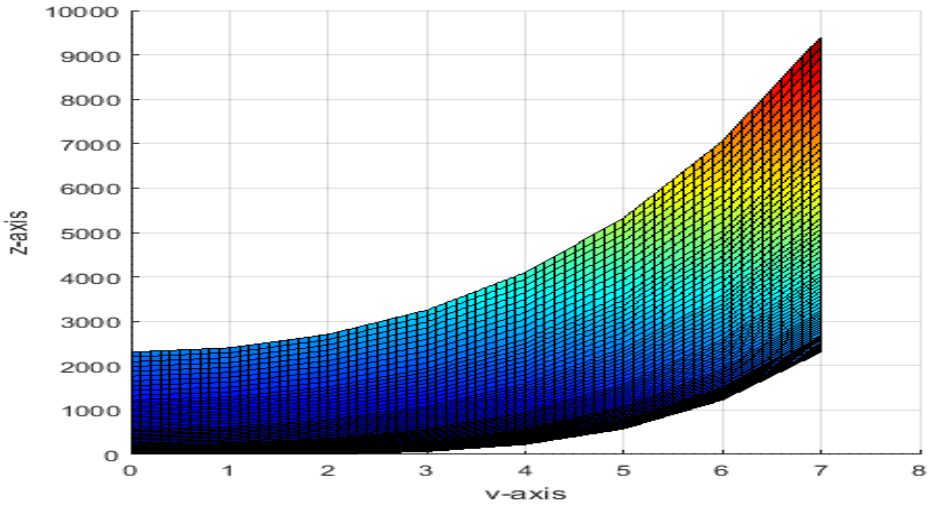

Figure 8. A vz-view of the Convex Surface

7. NUMERICAL RESULTS

This section presents the numerical results when proposed algorithm was implemented on 2D convex data set in Table 1 and Table 2. Similarly, for 3D convex data in Table 3 and Table 4, numerical results are given in Table 7 and Table 8. MATLAB software packets were used for programming and visualizing convex curves and surfaces.

Table 5. Numerical Results Parallel to Figure 1

i	1	2	3	4	5	6	7	8	9
d_i	-8.000	-6.000	-4.100	-2.000	0	2.000	4.100	6.000	8.000
ϱ_i	1	1	1	1	1	1	1	1	____
σ_i	1	1	1	1	1	1	1	1	____

Table 6. Numerical Results for Figure 2

i	1	2	3	4	5	6
d_i	2.4650	8.0950	22.4050	77.8889	185.5798	319.3540
ϱ_i	1	1	1	1	1	____
σ_i	1	1	1	1	1	____

Table 7. Numerical Results for Figure 3

u/v	-5	-4	-3	-2	-1	0	1	2	3	4	5	6
Numerical results for $\tilde{G}_{j,l}^{u}$												
-5	-10.0	-10.0	-10.0	-10.0	-10.0	-10.0	-10.0	-10.0	-10.0	-10.0	-10.0	-10.0
-4	-8.00	-8.00	-8.00	-8.00	-8.00	-8.00	-8.00	-8.00	-8.00	-8.00	-8.00	-8.00
-3	-6.00	-6.00	-6.00	-6.00	-6.00	-6.00	-6.00	-6.00	-6.00	-6.00	-6.00	-6.00
-2	-4.00	-4.00	-4.00	-4.00	-4.00	-4.00	-4.00	-4.00	-4.00	-4.00	-4.00	-4.00
-1	-2.00	-2.00	-2.00	-2.00	-2.00	-2.00	-2.00	-2.00	-2.00	-2.00	-2.00	-2.00
0	0	0	0	0	0	0	0	0	0	0	0	0
1	2.00	2.00	2.00	2.00	2.00	2.00	2.00	2.00	2.00	2.00	2.00	2.00
2	4.00	4.00	4.00	4.00	4.00	4.00	4.00	4.00	4.00	4.00	4.00	4.00
3	6.00	6.00	6.00	6.00	6.00	6.00	6.00	6.00	6.00	6.00	6.00	6.00
4	8.00	8.00	8.00	8.00	8.00	8.00	8.00	8.00	8.00	8.00	8.00	8.00
5	10.0	10.0	10.0	10.0	10.0	10.0	10.0	10.0	10.0	10.0	10.0	10.0
6	12.0	12.0	12.0	12.0	12.0	12.0	12.0	12.0	12.0	12.0	12.0	12.0
Numerical results for $\tilde{G}_{j,l}^{v}$												
-5	-10.0	-8.00	-6.00	-4.00	-2.00	0	2.00	4.00	6.00	8.00	10.0	12.0
-4	-10.0	-8.00	-6.00	-4.00	-2.00	0	2.00	4.00	6.00	8.00	10.0	12.0
-3	-10.0	-8.00	-6.00	-4.00	-2.00	0	2.00	4.00	6.00	8.00	10.0	12.0

u/v	-5	-4	-3	-2	-1	0	1	2	3	4	5	6
-2	-10.0	-8.00	-6.00	-4.00	-2.00	0	2.00	4.00	6.00	8.00	10.0	12.0
-1	-10.0	-8.00	-6.00	-4.00	-2.00	0	2.00	4.00	6.00	8.00	10.0	12.0
0	-10.0	-8.00	-6.00	-4.00	-2.00	0	2.00	4.00	6.00	8.00	10.0	12.0
1	-10.0	-8.00	-6.00	-4.00	-2.00	0	2.00	4.00	6.00	8.00	10.0	12.0
2	-10.0	-8.00	-6.00	-4.00	-2.00	0	2.00	4.00	6.00	8.00	10.0	12.0
3	-10.0	-8.00	-6.00	-4.00	-2.00	0	2.00	4.00	6.00	8.00	10.0	12.0
4	-10.0	-8.00	-6.00	-4.00	-2.00	0	2.00	4.00	6.00	8.00	10.0	12.0
5	-10.0	-8.00	-6.00	-4.00	-2.00	0	2.00	4.00	6.00	8.00	10.0	12.0
6	-10.0	-8.00	-6.00	-4.00	-2.00	0	2.00	4.00	6.00	8.00	10.0	12.0
Numerical results for $\varrho_{j,l}$												
-5	1.00	1.00	1.00	1.00	1.000	1.000	1.000	1.000	1.000	1.000	1.000	___
-4	1.000	1.000	1.000	1.000	1.000	1.000	1.000	1.000	1.000	1.000	1.000	___
-3	1.000	1.000	1.000	1.000	1.000	1.000	1.000	1.000	1.000	1.000	1.000	___
-2	1.000	1.000	1.000	1.000	1.000	1.000	1.000	1.000	1.000	1.000	1.000	___
-1	1.000	1.000	1.000	1.000	1.000	1.000	1.000	1.000	1.000	1.000	1.000	___
0	1.000	1.000	1.000	1.000	1.000	1.000	1.000	1.000	1.000	1.000	1.000	___
1	1.000	1.000	1.000	1.000	1.000	1.000	1.000	1.000	1.000	1.000	1.000	___
2	1.000	1.000	1.000	1.000	1.000	1.000	1.000	1.000	1.000	1.000	1.000	___

u/v	-5	-4	-3	-2	-1	0	1	2	3	4	5	6
3	1.000	1.000	1.000	1.000	1.000	1.000	1.000	1.000	1.000	1.000	1.000	___
4	1.000	1.000	1.000	1.000	1.000	1.000	1.000	1.000	1.000	1.000	1.000	___
5	1.000	1.000	1.000	1.000	1.000	1.000	1.000	1.000	1.000	1.000	1.000	___
6	___	___	___	___	___	___	___	___	___	___	___	___
Numerical results for $\sigma_{j,l}$												
-5	1.000	1.000	1.000	1.000	1.000	1.000	1.000	1.000	1.000	1.000	1.000	___
-4	1.000	1.000	1.000	1.000	1.000	1.000	1.000	1.000	1.000	1.000	1.000	___
-3	1.000	1.000	1.000	1.000	1.000	1.000	1.000	1.000	1.000	1.000	1.000	___
-2	1.000	1.000	1.000	1.000	1.000	1.000	1.000	1.000	1.000	1.000	1.000	___
-1	1.000	1.000	1.000	1.000	1.000	1.000	1.000	1.000	1.000	1.000	1.000	___
0	1.000	1.000	1.000	1.000	1.000	1.000	1.000	1.000	1.000	1.000	1.000	___
1	1.000	1.000	1.000	1.000	1.000	1.000	1.000	1.000	1.000	1.000	1.000	___
2	1.000	1.000	1.000	1.000	1.000	1.000	1.000	1.000	1.000	1.000	1.000	___
3	1.000	1.000	1.000	1.000	1.000	1.000	1.000	1.000	1.000	1.000	1.000	___
4	1.000	1.000	1.000	1.000	1.000	1.000	1.000	1.000	1.000	1.000	1.000	___
5	1.000	1.000	1.000	1.000	1.000	1.000	1.000	1.000	1.000	1.000	1.000	___
6	___	___	___	___	___	___	___	___	___	___	___	___
Numerical results for $\varrho_{j,l+1}$												

u/v	-5	-4	-3	-2	-1	0	1	2	3	4	5	6
-5	1.000	1.000	1.000	1.000	1.000	1.000	1.000	1.000	1.000	1.000	1.000	___
-4	1.000	1.000	1.000	1.000	1.000	1.000	1.000	1.000	1.000	1.000	1.000	___
-3	1.000	1.000	1.000	1.000	1.000	1.000	1.000	1.000	1.000	1.000	1.000	___
-2	1.000	1.000	1.000	1.000	1.000	1.000	1.000	1.000	1.000	1.000	1.000	___
-1	1.000	1.000	1.000	1.000	1.000	1.000	1.000	1.000	1.000	1.000	1.000	___
0	1.000	1.000	1.000	1.000	1.000	1.000	1.000	1.000	1.000	1.000	1.000	___
1	1.000	1.000	1.000	1.000	1.000	1.000	1.000	1.000	1.000	1.000	1.000	___
2	1.000	1.000	1.000	1.000	1.000	1.000	1.000	1.000	1.000	1.000	1.000	___
3	1.000	1.000	1.000	1.000	1.000	1.000	1.000	1.000	1.000	1.000	1.000	___
4	1.000	1.000	1.000	1.000	1.000	1.000	1.000	1.000	1.000	1.000	1.000	___
5	1.000	1.000	1.000	1.000	1.000	1.000	1.000	1.000	1.000	1.000	1.000	___
6	___	___	___	___	___	___	___	___	___	___	___	___
Numerical results for $\sigma_{j,l+1}$												
-5	1.000	1.000	1.000	1.000	1.000	1.000	1.000	1.000	1.000	1.000	1.000	___
-4	1.000	1.000	1.000	1.000	1.000	1.000	1.000	1.000	1.000	1.000	1.000	___
-3	1.000	1.000	1.000	1.000	1.000	1.000	1.000	1.000	1.000	1.000	1.000	___
-2	1.000	1.000	1.000	1.000	1.000	1.000	1.000	1.000	1.000	1.000	1.000	___
-1	1.000	1.000	1.000	1.000	1.000	1.000	1.000	1.000	1.000	1.000	1.000	___

u/v	-5	-4	-3	-2	-1	0	1	2	3	4	5	6
0	1.000	1.000	1.000	1.000	1.000	1.000	1.000	1.000	1.000	1.000	1.000	___
1	1.000	1.000	1.000	1.000	1.000	1.000	1.000	1.000	1.000	1.000	1.000	___
2	1.000	1.000	1.000	1.000	1.000	1.000	1.000	1.000	1.000	1.000	1.000	___
3	1.000	1.000	1.000	1.000	1.000	1.000	1.000	1.000	1.000	1.000	1.000	___
4	1.000	1.000	1.000	1.000	1.000	1.000	1.000	1.000	1.000	1.000	1.000	___
5	1.000	1.000	1.000	1.000	1.000	1.000	1.000	1.000	1.000	1.000	1.000	___
6	___	___	___	___	___	___	___	___	___	___	___	___
Numerical results for $\bar{\varrho}_{j,l}$												
-5	1.000	1.000	1.000	1.000	1.000	1.000	1.000	1.000	1.000	1.000	1.000	___
-4	1.000	1.000	1.000	1.000	1.000	1.000	1.000	1.000	1.000	1.000	1.000	___
-3	1.000	1.000	1.000	1.000	1.000	1.000	1.000	1.000	1.000	1.000	1.000	___
-2	1.000	1.000	1.000	1.000	1.000	1.000	1.000	1.000	1.000	1.000	1.000	___
-1	1.000	1.000	1.000	1.000	1.000	1.000	1.000	1.000	1.000	1.000	1.000	___
0	1.000	1.000	1.000	1.000	1.000	1.000	1.000	1.000	1.000	1.000	1.000	___
1	1.000	1.000	1.000	1.000	1.000	1.000	1.000	1.000	1.000	1.000	1.000	___
2	1.000	1.000	1.000	1.000	1.000	1.000	1.000	1.000	1.000	1.000	1.000	___
3	1.000	1.000	1.000	1.000	1.000	1.000	1.000	1.000	1.000	1.000	1.000	___
4	1.000	1.000	1.000	1.000	1.000	1.000	1.000	1.000	1.000	1.000	1.000	___

u/v	-5	-4	-3	-2	-1	0	1	2	3	4	5	6
5	1.000	1.000	1.000	1.000	1.000	1.000	1.000	1.000	1.000	1.000	1.000	___
6	___	___	___	___	___	___	___	___	___	___	___	___
Numerical results for $\bar{\sigma}_{j,l}$												
-5	1.000	1.000	1.000	1.000	1.000	1.000	1.000	1.000	1.000	1.000	1.000	___
-4	1.000	1.000	1.000	1.000	1.000	1.000	1.000	1.000	1.000	1.000	1.000	___
-3	1.000	1.000	1.000	1.000	1.000	1.000	1.000	1.000	1.000	1.000	1.000	___
-2	1.000	1.000	1.000	1.000	1.000	1.000	1.000	1.000	1.000	1.000	1.000	___
-1	1.000	1.000	1.000	1.000	1.000	1.000	1.000	1.000	1.000	1.000	1.000	___
0	1.000	1.000	1.000	1.000	1.000	1.000	1.000	1.000	1.000	1.000	1.000	___
1	1.000	1.000	1.000	1.000	1.000	1.000	1.000	1.000	1.000	1.000	1.000	___
2	1.000	1.000	1.000	1.000	1.000	1.000	1.000	1.000	1.000	1.000	1.000	___
3	1.000	1.000	1.000	1.000	1.000	1.000	1.000	1.000	1.000	1.000	1.000	___
4	1.000	1.000	1.000	1.000	1.000	1.000	1.000	1.000	1.000	1.000	1.000	___
5	1.000	1.000	1.000	1.000	1.000	1.000	1.000	1.000	1.000	1.000	1.000	___
6	___	___	___	___	___	___	___	___	___	___	___	___
Numerical results for $\bar{\varrho}_{j+1,l}$												
-5	1.000	1.000	1.000	1.000	1.000	1.000	1.000	1.000	1.000	1.000	1.000	___
-4	1.000	1.000	1.000	1.000	1.000	1.000	1.000	1.000	1.000	1.000	1.000	___

u/v	-5	-4	-3	-2	-1	0	1	2	3	4	5	6
-3	1.000	1.000	1.000	1.000	1.000	1.000	1.000	1.000	1.000	1.000	1.000	___
-2	1.000	1.000	1.000	1.000	1.000	1.000	1.000	1.000	1.000	1.000	1.000	___
-1	1.000	1.000	1.000	1.000	1.000	1.000	1.000	1.000	1.000	1.000	1.000	___
0	1.000	1.000	1.000	1.000	1.000	1.000	1.000	1.000	1.000	1.000	1.000	___
1	1.000	1.000	1.000	1.000	1.000	1.000	1.000	1.000	1.000	1.000	1.000	___
2	1.000	1.000	1.000	1.000	1.000	1.000	1.000	1.000	1.000	1.000	1.000	___
3	1.000	1.000	1.000	1.000	1.000	1.000	1.000	1.000	1.000	1.000	1.000	___
4	1.000	1.000	1.000	1.000	1.000	1.000	1.000	1.000	1.000	1.000	1.000	___
5	1.000	1.000	1.000	1.000	1.000	1.000	1.000	1.000	1.000	1.000	1.000	___
6	___	___	___	___	___	___	___	___	___	___	___	___
Numerical results for $\bar{\sigma}_{j+1,l}$												
-5	1.000	1.000	1.000	1.000	1.000	1.000	1.000	1.000	1.000	1.000	1.000	___
-4	1.000	1.000	1.000	1.000	1.000	1.000	1.000	1.000	1.000	1.000	1.000	___
-3	1.000	1.000	1.000	1.000	1.000	1.000	1.000	1.000	1.000	1.000	1.000	___
-2	1.000	1.000	1.000	1.000	1.000	1.000	1.000	1.000	1.000	1.000	1.000	___
-1	1.000	1.000	1.000	1.000	1.000	1.000	1.000	1.000	1.000	1.000	1.000	___
0	1.000	1.000	1.000	1.000	1.000	1.000	1.000	1.000	1.000	1.000	1.000	___
1	1.000	1.000	1.000	1.000	1.000	1.000	1.000	1.000	1.000	1.000	1.000	___

u/v	-5	-4	-3	-2	-1	0	1	2	3	4	5	6
2	1.000	1.000	1.000	1.000	1.000	1.000	1.000	1.000	1.000	1.000	1.000	___
3	1.000	1.000	1.000	1.000	1.000	1.000	1.000	1.000	1.000	1.000	1.000	___
4	1.000	1.000	1.000	1.000	1.000	1.000	1.000	1.000	1.000	1.000	1.000	___
5	1.000	1.000	1.000	1.000	1.000	1.000	1.000	1.000	1.000	1.000	1.000	___
6	___	___	___	___	___	___	___	___	___	___	___	___

Table 8. Numerical Results for Figure 4

u/v	0	1	2	3	4	5	6	7
Numerical Results for $\tilde{G}^{u}{}_{j,l}$								
0	-0.0060	-0.0060	-0.0060	-0.0060	-0.0060	-0.0060	-0.0060	-0.0060
1	0.0040	0.0080	0.0200	0.0400	0.0680	0.1040	0.1480	0.2000
2	0.0320	0.0400	0.0640	0.1040	0.1600	0.2320	0.3200	0.4240
3	0.1080	0.1200	0.1560	0.2160	0.3000	0.4080	0.5400	0.6960
4	0.2560	0.2720	0.3200	0.4000	0.5120	0.6560	0.8320	1.0400
5	0.5000	0.5200	0.5800	0.6800	0.8200	1.000	1.2200	1.4800
6	0.8640	0.8880	0.9600	1.0800	1.2480	1.4640	1.7280	2.0400
7	1.2940	1.3220	1.4060	1.5640	1.7420	1.9940	2.3020	2.6660
Numerical Results for $\tilde{G}^{v}{}_{j,l}$								
0	-0.0060	0.0040	0.0320	0.1080	0.2560	0.5000	0.8640	1.2940
1	-0.0060	0.0080	0.0400	0.1200	0.2720	0.5200	0.8880	1.3220
2	-0.0060	0.0200	0.0640	0.1560	0.3200	0.5800	0.9600	1.4060
3	-0.0060	0.0400	0.1040	0.2160	0.4000	0.6800	1.0800	1.5460

u/v	0	1	2	3	4	5	6	7
4	-0.0060	0.0680	0.1600	0.3000	0.5120	0.8200	1.2480	1.7420
5	-0.0060	0.1040	0.2320	0.4080	0.6560	1.000	1.4640	1.9940
6	-0.0060	0.1480	0.3200	0.5400	0.8320	1.2200	1.7280	2.3020
7	-0.0060	0.2000	0.4240	0.6960	1.0400	1.4800	2.0400	2.6660
Numerical results for $\varrho_{j,l}$								
0	1.000	1.000	1.000	1.000	1.000	1.000	1.000	___
1	1.000	1.000	1.000	1.000	1.000	1.000	1.000	___
2	1.000	1.000	1.000	1.000	1.000	1.000	1.000	___
3	1.000	1.000	1.000	1.000	1.000	1.000	1.000	___
4	1.000	1.000	1.000	1.000	1.000	1.000	1.000	___
5	1.000	1.000	1.000	1.000	1.000	1.000	1.000	___
6	1.000	1.000	1.000	1.000	1.000	1.000	1.000	___
7	___	___	___	___	___	___	___	___
Numerical results for $\sigma_{j,l}$								
0	1.000	1.000	1.000	1.000	1.000	1.000	1.000	___
1	1.000	1.000	1.000	1.000	1.000	1.000	1.000	___
2	1.000	1.000	1.000	1.000	1.000	1.000	1.000	___
3	1.000	1.000	1.000	1.000	1.000	1.000	1.000	___
4	1.000	1.000	1.000	1.000	1.000	1.000	1.000	___
5	1.000	1.000	1.000	1.000	1.000	1.000	1.000	___
6	1.000	1.000	1.000	1.000	1.000	1.000	1.000	___
7	___	___	___	___	___	___	___	___
Numerical results for $\varrho_{j,l+1}$								
0	1.000	1.000	1.000	1.000	1.000	1.000	1.000	___

u/v	0	1	2	3	4	5	6	7
1	1.000	1.000	1.000	1.000	1.000	1.000	1.000	___
2	1.000	1.000	1.000	1.000	1.000	1.000	1.000	___
3	1.000	1.000	1.000	1.000	1.000	1.000	1.000	___
4	1.000	1.000	1.000	1.000	1.000	1.000	1.000	___
5	1.000	1.000	1.000	1.000	1.000	1.000	1.000	___
6	1.000	1.000	1.000	1.000	1.000	1.000	1.000	___
7	___	___	___	___	___	___	___	___
Numerical results for $\sigma_{j,l+1}$								
0	1.000	1.000	1.000	1.000	1.000	1.000	1.000	___
1	1.000	1.000	1.000	1.000	1.000	1.000	1.000	___
2	1.000	1.000	1.000	1.000	1.000	1.000	1.000	___
3	1.000	1.000	1.000	1.000	1.000	1.000	1.000	___
4	1.000	1.000	1.000	1.000	1.000	1.000	1.000	___
5	1.000	1.000	1.000	1.000	1.000	1.000	1.000	___
6	1.000	1.000	1.000	1.000	1.000	1.000	1.000	___
7	___	___	___	___	___	___	___	___
Numerical results for $\bar{\varrho}_{j,l}$								
0	1.000	1.000	1.000	1.000	1.000	1.000	1.000	___
1	1.000	1.000	1.000	1.000	1.000	1.000	1.000	___
2	1.000	1.000	1.000	1.000	1.000	1.000	1.000	___
3	1.000	1.000	1.000	1.000	1.000	1.000	1.000	___
4	1.000	1.000	1.000	1.000	1.000	1.000	1.000	___
5	1.000	1.000	1.000	1.000	1.000	1.000	1.000	___
6	1.000	1.000	1.000	1.000	1.000	1.000	1.000	___

u/v	0	1	2	3	4	5	6	7
7	___	___	___	___	___	___	___	___
Numerical results for $\bar{\sigma}_{j,l}$								
0	1.000	1.000	1.000	1.000	1.000	1.000	1.000	___
1	1.000	1.000	1.000	1.000	1.000	1.000	1.000	___
2	1.000	1.000	1.000	1.000	1.000	1.000	1.000	___
3	1.000	1.000	1.000	1.000	1.000	1.000	1.000	___
4	1.000	1.000	1.000	1.000	1.000	1.000	1.000	___
5	1.000	1.000	1.000	1.000	1.000	1.000	1.000	___
6	1.000	1.000	1.000	1.000	1.000	1.000	1.000	___
7	___	___	___	___	___	___	___	___
Numerical results for $\bar{\varrho}_{j+1,l}$								
0	1.000	1.000	1.000	1.000	1.000	1.000	1.000	___
1	1.000	1.000	1.000	1.000	1.000	1.000	1.000	___
2	1.000	1.000	1.000	1.000	1.000	1.000	1.000	___
3	1.000	1.000	1.000	1.000	1.000	1.000	1.000	___
4	1.000	1.000	1.000	1.000	1.000	1.000	1.000	___
5	1.000	1.000	1.000	1.000	1.000	1.000	1.000	___
6	1.000	1.000	1.000	1.000	1.000	1.000	1.000	___
7	___	___	___	___	___	___	___	___
Numerical results for $\bar{\sigma}_{j+1,l}$								
0	1.000	1.000	1.000	1.000	1.000	1.000	1.000	___
1	1.000	1.000	1.000	1.000	1.000	1.000	1.000	___
2	1.000	1.000	1.000	1.000	1.000	1.000	1.000	___
3	1.000	1.000	1.000	1.000	1.000	1.000	1.000	___

u/v	0	1	2	3	4	5	6	7
4	1.000	1.000	1.000	1.000	1.000	1.000	1.000	___
5	1.000	1.000	1.000	1.000	1.000	1.000	1.000	___
6	1.000	1.000	1.000	1.000	1.000	1.000	1.000	___
7	___	___	___	___	___	___	___	___

8. CONCLUSION

In the current research, shape preserving rational schemes were devised for convex curve and surface data. A C^1 rational cubic piecewise function, composed of cubic numerator and quadratic denominator with two free parameters σ_j and ϱ_j, was used to retain the intrinsic shape characteristic of 2D convex data. Mathematical derivation was performed to derive the data dependent constraints on free parameter and results were summarized in Theorem 1. MATLAB software packet was used to implement the developed scheme and visualize 2D convex data. Furthermore, the function was then advanced to partially blended rational bi-cubic function with eight free parameters for the 3D convex data positioned over rectangular grid. These eight parameters $\sigma_{j,l}$, $\varrho_{j,l}$, $\sigma_{j,l+1}$, $\varrho_{j,l+1}$, $\bar{\sigma}_{j,l}$, $\bar{\varrho}_{j,l}$, $\bar{\sigma}_{j+1,l}$, and $\bar{\varrho}_{j+1,l}$ by means of mathematical derivation, were conditioned to preserve the inherent curvature of 3D data and findings were summarized in Theorem 2. The proposed algorithm controls the shape of visual model locally. Convex surfaces were realized with the help of MATLAB software packet. The suggested shape-preserving techniques in this study are applicable to both data and derivatives and do not alter basis functions. The proposed scheme, however, does not use free parameters which provides the users with minimal flexibility to change the shape of the data as they desire. Work on curvature preserving scheme for scatter data is in process by the authors.

REFERENCES

1. Ebrahimi AR, Loghmani GB, Sarfraz M. Capturing outlines of generic shapes with cubic B´ezier curves using the Nelder–Mead simplex method**.** *Irn J Numer Anal Optim*. 2019;9(2):103–121. https://doi.org/10.22067/IJNAO.V9I2.70045
2. Ebrahimi AR, Loghmani GB, Sarfraz M. Capturing outlines of planar generic images by simultaneous curve fitting and sub-division. *J AI Data Mining*. 2020;8(1):105–118. https://doi.org/10.22044/JADM.2019.6727.1788
3. Ebrahimi AR, Loghmani GB. B-spline curve fitting by diagonal approximation BFGS methods. *Iran J Sci Technol Trans A*. 2019;43(3):947–958. https://doi.org/10.1007/s40995-017-0347-1
4. Jahanshahloo A, Ebrahimi AR. Reconstruction of 3D shapes with B-spline surface using diagonal approximation BFGS methods. *Multimed Tools Appl*. 2022;81:38091–38111. https://doi.org/10.1007/s11042-022-13024-6

5. Jahanshahloo A, Ebrahimi AR. Reconstruction of the initial curve from a two-dimensional shape for the B-spline curve fitting. *Eur Phys J Plus*. 2022;137:e411. https://doi.org/10.1140/epjp/s13360-022-02604-y
6. Kvasov BI. Monotone and convex interpolation by weighted quadratic splines. *Adv Comput Math*. 2014;40(1): 91–116. https://doi.org/10.1007/s10444-013-9300-9
7. Verlan I. Convexity preserving interpolation by splines of arbitrary degree. *Comput Sci J Mold*. 2010;18(1):54–58.
8. Clements JC. A convexity preserving parametric C^2 rational cubic interpolant. *Numer Math*. 1992;63(1):165–171. https://doi.org/10.1007/BF01385853
9. Merrian JL, Sablonniere P. Rational splines for hermite interpolation with shape constraints. *Comput Aided Geom Des*. 2013;30:296–309. https://doi.org/10.1016/j.cagd.2013.01.004
10. Carnicer JM, Garcia-Esnaol M, Peña JM. Convexity of rational curves and total positivity. *J Comput App Math*. 1996;71(2):365–382. https://doi.org/10.1016/0377-0427(95)00240-5
11. Brodlie KW, Butt S. Preserving convexity using piecewise cubic interpolation. *Comput Graphs*. 1991;15:15–23. https://doi.org/10.1016/0097-8493(91)90026-E
12. Hussain M, Hussain MZ, Waseem A, Javaid M. GC^1 Shape-preserving trigonometric surfaces. *J Math Imaging Vis*. 2015;53(1):21–41. https://doi.org/10.1007/s10851-014-0544-x
13. Sarfraz M, Hussain MZ, Nisar A. Positive data modelling using spline functions. *Appl Math Comput*. 2010;216:2036–2049. https://doi.org/10.1016/j.amc.2010.03.034
14. Sarfraz M, Hussain MZ, Hussain F. Shape preserving convex data interpolation. *Appl Comput Math*. 2017;16(3):205–227.
15. Sarfraz M, Hussain MZ, Hussain M. Shape preserving curve interpolation. *Int J of Comput Math*. 2012;89(1):35–53. https://doi.org/10.1080/00207160.2011.627434
16. Tian M, Li SL. Convexity-Preserving piecewise rational cubic interpolation. *J Shand Univ*. 2007;42(10):80–83.
17. Floater MS. A weak condition for the convexity of tensor-product Bézier and B-spline surfaces. *Adv Comput Math*. 1994;2(1):67–80. https://doi.org/10.1007/BF02519036

18. Hussain MZ, Hussain M, Waseem A. Shape-preserving trigonometric functions. *Comput App Math*. 2014;33:411–431. https://doi.org/10.1007/s40314-013-0071-1

19. Hussain MZ, Hussain M. Visualization of 3D data preserving convexity. *J App Math Comput*. 2006;2:170–186. https://doi.org/10.1007/BF02831986

20. Hussain MZ, Hussain M. Convex surface interpolation. In: Chen F, Jüttler B. eds., *Advances in Geometric Modeling and Processing. GMP 2008. Lecture Notes in Computer Science*. Springer, Berlin, Heidelberg. https://doi.org/10.1007/978-3-540-79246-8_36

21. Costantini P. On monotone and convex spline interpolation. *Math Comput*. 1986;46(173):203–214. https://doi.org/10.2307/2008224

22. Costantini P, Fontanella F. Shape preserving bivariate interpolation. *SIAM J Numer Anal*. 1990;27(2):488–506. https://doi.org/10.1137/0727030

23. Asaturyan S. *Shape Preserving Surface Interpolation Scheme* [Doctoral dissertation]. University of Dundee; 1992.

24. Asaturyan S, Costantini P, Manni C. Local shape preserving interpolation by space curves. *IMA J Numer Anal*. 2001;21(1):301–325. https://doi.org/10.1093/imanum/21.1.301

25. Dodd SL, McAllister DF, Roulier J. Shape-Preserving spline interpolation for specifying bivariate functions on grids. *IEEE Comput Graph App*. 1983;3(6):70–79.

26. Han X. Shape-preserving piecewise rational Interpolant with quartic numerator and quadratic denominator. *App Math Comput*. 2015;251:258–274. https://doi.org/10.1016/j.amc.2014.11.067

Scientific Inquiry and Review (SIR)
Volume 7 Issue 2, 2023
ISSN (P): 2521-2427, ISSN (E): 2521-2435
Homepage: https://journals.umt.edu.pk/index.php/SIR

Article QR

Title:	**Potential of Antioxidant Enzymes as biochemical biomarkers for glyphosate-based herbicide in *Oreochromis niloticus***
Author (s):	Ahmad Manan Mustafa Chatha[1], Saima Naz[2], Syeda Saira Iqbal[3], Azka Kiran[2], Maria Lateef[2], Anab Zahra[2]
Affiliation (s):	[1]Islamia University of Bahawalpur, Pakistan; [2]Government Sadiq College University, Bahawalpur, Pakistan; [3]Government College University, Lahore.
DOI:	https://doi.org/10.32350/sir.72.02
History:	Received: February 15, 2023, Revised: April 05, 2023, Accepted: April 05, 2023, Published: June 15, 2023
Citation:	Chatha AMM, Naz S, Kiran A, Iqbal SS, Lateef M, Zahra A. Potential of antioxidant enzymes as biochemical biomarkers for glyphosate-based herbicide in Oreochromis niloticus. *Sci Inq Rev.* 2023;7(2),38-53. https://doi.org/10.32350/sir.72.02
Copyright:	© The Authors
Licensing:	This article is open access and is distributed under the terms of Creative Commons Attribution 4.0 International License
Conflict of Interest:	Author(s) declared no conflict of interest

A publication of
The School of Science
University of Management and Technology, Lahore, Pakistan

Potential of Antioxidant Enzymes as Biochemical Biomarkers for Glyphosate-Based Herbicide in *Oreochromis niloticus*

Ahmad Manan Mustafa Chatha[1], Saima Naz[2], Syeda Saira Iqbal[3*], Azka Kiran[2], Maria Lateef[2], and Anab Zahra

[1]Department of Entomology, Faculty of Agriculture and Environment, Islamia University of Bahawalpur, Pakistan
[2]Department of Zoology, Government Sadiq College University, Bahawalpur, Pakistan
[3]University of Management and Technology, Lahore, Pakistan

ABSTRACT

The current study examined the toxicity of Roundup, which is a herbicide containing glyphosate that is commonly used in agriculture, on *Oreochromis niloticus*, a type of freshwater fish. The researchers investigated the effectiveness of using antioxidant enzymes as biochemical biomarkers to assess the potentially toxic impact of Roundup on the fish. The sub-lethal concentration of Roundup in tilapia is 1.05 mg/l for 96 hours of exposure. The fish were exposed to sub-lethal concentration (36.8 to 46.9 mg/L) of Roundup for a period of 24, 48, 72, and 96 hours, and their antioxidant enzyme activities were measured, respectively. According to the findings, Roundup exposure led to a noticeable rise in the levels of superoxide dismutase, catalase, and peroxidase activities in both the liver and gill tissues of the fish, which suggested the occurrence of oxidative stress. These changes in antioxidant enzyme activities were concentration-dependent, suggesting that Roundup exposure can induce oxidative damage in fish. The study concluded that Roundup affects the enzymatic activity of both organs in a concentration- and time-dependent manner. Catalase and peroxidase activities were generally inhibited, while superoxide dismutase activity was affected differently depending on the organ, concentration, and time of exposure.

Keywords: biochemical, biomarkers, enzyme, fish, gills, liver

1. INTRODUCTION

Due to the fact that approximately 70% of Pakistan's population relies on the agricultural sector, there has been a significant increase in the use of

* Corresponding Author: saira.iqbal@umt.edu.pk

pesticides over the last 30 years to meet the growing demands of the population [1]. The accessibility and affordability of these pesticides have led to their indiscriminate use, resulting in significant ecological changes in major freshwater resources such as water, sediment, and fish [2]. Glyphosate, an organophosphorus herbicide, is currently the most commonly used herbicide on a global scale [3]. It is marketed under numerous brands and commercialized in over 100 countries worldwide [4]. The primary toxic component of formulated glyphosate-based products for aquatic organisms are surfactants like POEA found in Roundup. Several previous studies have suggested that pesticides can cause alterations in the water present in the ponds surrounding the cultivation regions, as well as rainwater and groundwater [5] through mechanisms such as volatilization, spray drift, surface runoff, chemical-biological degradation, leaching, and sorption [6].

Antioxidant enzymes, including CAT, POD, and SOD, are important in fish because they protect the fish from oxidative stress caused by factors such as pollution and diseases. These enzymes help to neutralize harmful free radicals and reactive oxygen species, which can damage cells and tissues. Additionally, these enzymes play a crucial role in the overall health and survival of fish, as oxidative stress can lead to a range of negative effects, including reduced growth rates, decreased immune function, and increased mortality. Therefore, understanding the role of antioxidant enzymes in fish can help to inform efforts to protect and maintain healthy fish populations [7].

There is limited information available in the previous literature regarding the harmful effects of glyphosate on organisms exposed to it in their natural environment. However, certain synthetic agrochemical compounds like glyphosate may become more toxic to non-target species due to differences in their bioactive properties. These compounds often cause sub-lethal damage to tissues, disrupt endocrine function, induce immunotoxicity and neurotoxicity, and alter the metabolism of the affected animals [8]. According to Naz et al. [9], industrial and agricultural water sources release a range of toxins into both rivers and canals, which then accumulate in sand. This accumulation of toxins in aquatic environments has emerged as a global issue, leading to health issues for both humans and aquatic animals [10]. Nile tilapia (*Oreochromis niloticus*) is a popular commercial fish species and is often used as a bio indicator to assess the

quality of aquatic ecosystems, particularly for pollutants such as herbicides [11]. It is also considered a suitable biological model for toxicological studies due to its sensitivity to diazinon, an organophosphate pesticide herbicides [12]. Aquatic organisms exposed to pesticides often experience oxidative stress, which is caused by the production of ROS in response to toxicants [13]. The effects of lufenuron exposure on *Oreochromis niloticus* were examined through histopathological analysis of various organs, including the gills, kidneys, livers, brain, and hearts. The findings revealed severe alterations and indicated that lufenuron caused DNA damage and oxidative stress in the fish. The study aimed to investigate the mechanisms behind lufenuron's toxicity, as well as to raise concerns about the use and disposal of lufenuron in terms of its potential to cause environmental pollution. The study also proposed measures to mitigate contamination in aquatic populations [14]. The comet assay, also known as Single Cell Gel Electrophoresis (SCGE), as a genotoxicity technique that detects DNA damage caused by alkylating chemicals, intercalating agents, and oxidizing agents. The comet assay is a useful method for monitoring genotoxicity in aquatic environments, where fish are often used as test organisms to detect DNA damage resulting from the ingestion of mutagens and pro-mutagens in freshwater and saltwater. This technique has also been employed to determine the genotoxic potential of water resources such as rivers and lakes. The purpose of the current study was to investigate the adverse effects of lufenuron exposure on various health biomarkers of *Oreochromis niloticus* [14].

The objective of the current study was to examine the Roundup exposure affects oxidative stress in fish by assessing variations in the activities of antioxidant enzymes. The aim wato obtain an understanding of the possible adverse impacts of Roundup exposure on the well-being of freshwater fish and the general health of aquatic ecosystems. The aim of the research is to increase our knowledge about the dangers related to the usage of herbicides that contain glyphosate in freshwater ecosystems. Additionally, it seeks to lay the groundwork for more extensive investigations into the lasting consequences of Roundup exposure on aquatic creatures such as fish.

2. MATERIAL AND METHODOLOGY

At the laboratory of Government Sadiq College Women University in Bahawalpur, Pakistan, an experimental study was conducted, adhering to

the ethical principles for laboratory animal usage set by the Ethical Committee of Government Sadiq College Women University Bahawalpur.

2.1. Sample Collection and Management

Thirty freshwater fish of the species *Oreochromis niloticus*, with a weight range of 75-80g, were procured from the nearby Fish Seed Hatchery in Bahawalpur. The fish were fed with the commercial feed palettes. These fish were transferred to the Zoology department testing laboratory of Government Sadiq College Women University Bahawalpur in plastic bags equipped with enough oxygen. The fish were subsequently relocated to glass tanks filled with 100 liters of water. The experiment employed five 100L tanks for each concentration, with each tank measuring 36 inches in length and 12 inches in width, housing six fish in each tank. Prior to commencing the experiment, the fish were given a period of 15 days to acclimate. To ensure that the fish had enough oxygen, continuous air pumps were utilized. The temperature of the aquarium water was kept constant, and measurements of the water's physical properties were taken before and after the study, as outlined in Table 1. The study was carried out in compliance with the ethical standards set forth by the Ethical Committee of Government Sadiq College Women University Bahawalpur.

Table 1. Physical Parameters of Water

Parameters	Values
Dissolved oxygen (mg/L)	6.70±0.1
Electrical conductivity at 25°(µmhos/cm)	393.10±2.2
PH	6.89±0.05
Total dissolved solid (mg/L)	153.89±3.9
Total hardness (CaCO3, mg/L)	174.59±2.1
Water temperature (°C)	23.80±0.3

2.2. Experimental Design

During the acclimation period, 30 fish [14] were distributed randomly into the control group (without exposure) and four experimental groups, which were subjected to different concentrations of Roundup original (46.9, 44.4, 40.0, and 36.8 mg L−1). The selection of these concentrations was informed by previous research, which examined the impact of acute

exposure to Roundup® at comparable concentrations in other fish species [15].

2.3. Evaluation of Antioxidant Enzymes

After exposure, fish from each group were euthanized at different time points (24, 48, 72, and 96 hours), and their gills and liver were extracted. Briefly, for removal of erythrocytes, all the organs were washed using phosphate buffer solution having 6.5 PH. After that all the organs were triturated using 0.2 mL normal saline and then homogenate was prepared (1:4 w/v) by adding cold buffer. The homogenate from each tissue was centrifuged (10000 rpm) at 40C for 15 minutes. After centrifugation, the supernatants were removed and placed at -800C for enzyme profiling. By using UV-visible spectrophotometer, the amount of (reactive oxygen species) ROS in the gills and liver of each fish was measured by different antioxidant enzymes, which were such as peroxidase [16], catalase [17], and superoxide dismutase (SOD) were measured according to previous protocols [16]. Additionally, the gill tissue homogenates from individual fish, which were used to quantify the level of antioxidant enzymes, such as catalase, superoxide dismutase (SOD), and peroxidase described by [16, 17].

At the Zoology Lab of the Department of Zoology, Government Sadiq College Women University, Bahawalpur, 36 fish samples were carefully dissected for the laddering assay. The dissection process was performed with great care to avoid contamination and the fish muscles were preserved in plastic bottles containing 0.9% saline solution. The bottles were properly labeled and stored at a temperature of -20^{o}C, with plans to process the samples within two weeks. It is advisable to store muscle tissues at a temperature of -20^{o}C or lower for future use, as this can enhance their usability [18].

2.4. DNA Extraction and Laddering assay

The Phenol Chloroform Isoamyl method was used to extract DNA from muscle tissue samples weighing 100-200 milligrams [18]. The samples were homogenized and mixed with 1 ml of lysis buffer containing 1 M Tris, 5 M NaCl, 0.5 M EDTA, 10% SDS, and 20 µl of Proteinase K. The mixture was then incubated overnight in a water bath at 50 degrees Celsius. On the following day, 1 ml of PCI (phenol chloroform isoamyl alcohol) was added in the prepared solution and the contents were centrifuged at 15,000 rpm for

10 minutes. The supernatant was transferred to fresh tubes and 20 µl of glycogen blue and 1 ml of chilled isopropyl alcohol were added in the mixture. The mixture was frozen overnight at 30 degrees Celsius and centrifuged at 15,000 rpm for 10 minutes. The resulting DNA pellet was washed three times with 70% ethanol and later dried for 15 minutes at the room temperature. Finally, 100 µl of injection water was added to the dried DNA pellet and the extracted DNA was stored at -8 degrees Celsius. To identify any genomic DNA damage, the extracted DNA was separated at 1% agarose gels and visualized with ethidium bromide (6 µg/ml) under 300 nm UV light.

2.5. Statistical analysis

SPSS software (version 15) was utilized for statistical analysis and ANOVA was employed to evaluate the significance of differences between the Roundup-treated and untreated fish groups. The results were expressed as mean ± SE, and a significance level of $P<0.05$ was adopted.

3. RESULTS

3.1. Antioxidant enzyme activities

The study investigated the impact of various pesticide doses on the antioxidant enzymes in different organs of fish, such as the liver and gills. The results revealed that the levels of catalase [17] and superoxide dismutase (SOD) were significantly lower in the heart, gills, liver, and brain tissues of fish exposed to different concentrations of insecticides as compared to untreated fish. Conversely, fish, which were exposed to the same concentrations of insecticides had higher levels of peroxidase [16] in their gills, liver, and brain tissues than those, which were untreated. According to the results of the study, there was a significant decrease in the levels of antioxidant enzymes (POD, CAT, and SOD) in the gills of fish exposed to Roundup GBH at concentrations of 0.80, 1.30, 1.90, 2.50 µg/L mg L^{-1} for 24, 48, 72, and 96 hours as compared to the control group. The fish in group-E exhibited a substantial reduction in SOD and CAT levels in their liver tissue after 24 hours of exposure. Meanwhile, groups D-E demonstrated lower SOD and CAT levels in their liver tissue after 48 and 72 hours of exposure as compared to the control group. Furthermore, the concentration of peroxidase in the liver, kidneys, and gills tissues of treated fish in groups D-E was significantly lower ($p < 0.05$) than in the non-treated fish. All results were presented as mean ± SE, and statistical significance

was assessed using one-way ANOVA analysis with a significance threshold of $p<0.05$. (Table 2, 3).

Table 2. Different Antioxidant Enzymes in Liver of Fish *Oreochromis niloticus*

Parameter/hour	Groups				
	A (control)	B (0.80ppm)	C (1.30 ppm)	D (1.90ppm)	E (2.50)
Catalase (units/min)					
24	4.92 ± 0.02	6.67 ± 0.02	4.72 ± 0.02	6.54 ± 0.01	5.67 ± 0.06*
48	4.83 ± 0.03	5.64 ± 0.03	4.46 ± 0.04	5.61 ± 0.08*	5.38 ± 0.07*
72	4.56 ± 0.06*	5.78 ± 0.01	6.47 ± 0.03	4.91 ± 0.04	4.62 ± 0.06*
96	5.61 ± 0.05*	5.64 ± 0.04	5.78 ± 0.06*	4.56 ± 0.07*	4.90 ± 0.03
Superoxide dismutase (units/mg)					
24	12.98 ± 0.11	12.91 ± 0.01	12.86 ± 0.01	11.67 ± 0.05	9.11 ± 0.03*
48	13.04 ± 0.03	12.75 ± 0.06	12.50 ± 0.02	9.20 ± 0.49*	9.00± 0.05*
72	13.07 ± 0.05	12.80 ± 0.04	12.29 ± 0.05	8.22 ± 0.29*	8.37 ± 0.01*
96	11.91 ± 0.07*	13.45 ± 0.02	11.77 ± 0.05	9.41 ± 0.07*	9.45 ± 0.01
Peroxidase (units/min)					
24	5.21 ± 0.01	6.11 ± 0.02	5.07 ± 0.02	4.79 ± 0.02*	4.23 ± 0.01*
48	5.20 ± 0.05	6.12 ± 0.02	2.96 ± 0.02	2.61 ± 0.03*	4.11 ± 0.01*
72	5.23 ± 0.02	6.09 ± 0.08	2.85 ± 0.04	2.24 ± 0.04*	4.02 ± 0.01*
96	3.94 ± 0.02	6.07 ± 0.05	5.19 ± 0.02	5.71 ± 0.01	3.10 ± 0.03

Table 3. Enzymes in Gills of Fish *Oreochromis niloticus*

Parameter/hour	Groups				
Catalase (units/min)	A (control)	B (0.80)	C (1.30 ppm)	D (1.90 ppm)	E (2.50)
24	3.23 ± 0.00	3.25 ± 0.01	3.18 ± 0.03	3.68 ± 0.01	3.34 ± 0.04*
48	3.42 ± 0.00	3.11 ± 0.02	3.17 ± 0.02	2.83 ± 0.06*	3.27 ± 0.03*
72	3.06 ± 0.00	2.87 ± 0.01	3.47 ± 0.06	3.23 ± 0.04*	3.01 ± 0.01
96	3.11 ± 0.00	3.36 ± 0.02	3.12 ± 0.02	3.45 ± 0.01	2.26 ± 0.01
Superoxide dismutase (units/mg protein)					
24	5.85 ± 0.04	5.73 ± 0.04	5.63 ± 0.01	4.89 ± 0.10	5.64 ± 0.04*
48	5.79 ± 0.03	5.56 ± 0.01	5.88 ± 0.03	4.16 ± 0.03*	5.29 ± 0.01*
72	5.93 ± 0.04	5.94 ± 0.02	6.26 ± 0.01	4.99 ± 0.04*	5.48 ± 0.11*

Parameter/hour	Groups				
Catalase (units/min)	A (control)	B (0.80)	C (1.30 ppm)	D (1.90 ppm)	E (2.50)
96	5.97 ± 0.03	6.45 ± 0.02	5.35 ± 0.02	5.02 ± 0.05*	4.96± 0.09*
Peroxidase (units/min)					
24	1.42 ± 0.01	1.29 ± 0.01	1.22 ± 0.01	1.31 ± 0.04*	0134 ± 0.02
48	1.34 ± 0.01	1.31 ± 0.03	1.28 ± 0.02	1.29 ± 0.05*	1.32 ± 0.01
72	1.37 ± 0.01	1.28 ± 0.02	1.26 ± 0.01	1.25 ± 0.03*	1.29 ± 0.02
96	1.45± 0.03	1.31± 0.01	1.31± 0.02	1.34± 0.01	1.41± 0.01

3.2. DNA Quantification

Nano Drop technology measures the absorbance of the light by a DNA sample to determine its concentration and purity. A quick and easy method, which requires only a small amount of the sample. The technique is commonly used in research and diagnostic laboratories for DNA quantification [19]. The Nanodrop technique was employed to measure both the quantity and quality of genomic DNA using a Spectrophotometer (Agilent 8453, California, USA). The absorbance values of the DNA sample, measured at 260/280 nm, were recorded for 5 seconds (Figure 1) to determine the quantity and purity of the sample**.**

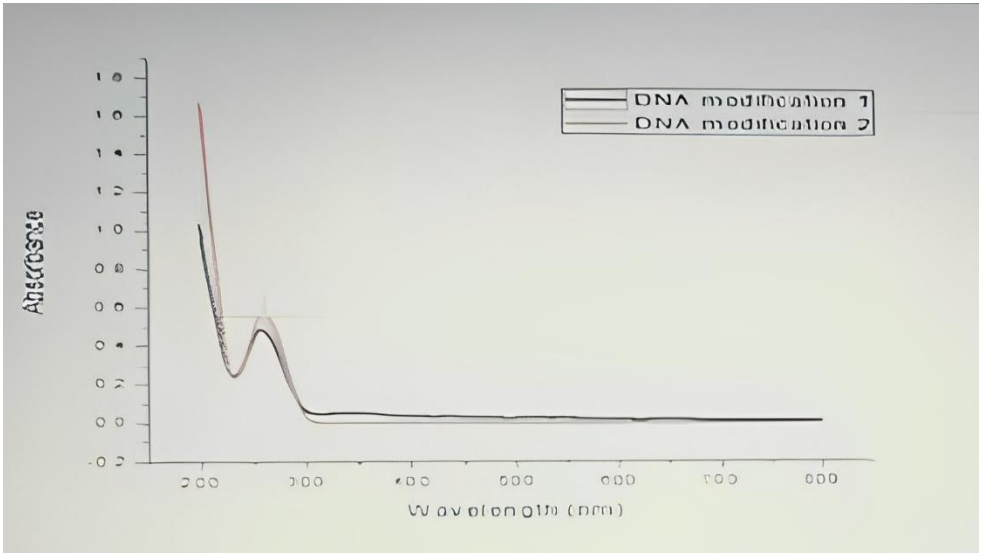

Figure 1. Absorbance Peaks Showing Good Quality of DNA

The quality and quantity of genomic DNA were assessed using the Nanodrop technique and a spectrophotometer (Agilent 8453, California, USA). The absorbance values at 260-280 nm wavelength were used to evaluate the DNA quality and DNA concentration values (ng/µl) and the ratio of 260/280, which were noted for purification purposes. The following equation was utilized to calculate the DNA concentration: volume (g/ml) = OD 260 × 100 (dilution factor) × 50g/ml/1000. The results were acceptable only if the ratio of OD 260/OD 280 was 1.8-2.0, indicating good DNA quality. Table 4 summarizes the obtained data.

Table 4. DNA Quantification using Spectrophotometer (Agilent 8453, California, USA) DNA damage

24 days	Insecticide concentration	260/280 ratio	DNA concentration
Gills	0.80µg/L	1.49	44.9µg/ml
Liver		1.28	44.65µg/ml
Gills	1.30µg/ml	1.28	41µg/ml
Liver		1.95	24.1µg/ml
Gills	1.90µg/ml	1.67	24.25µg/ml
Liver		1.65	23.45µg/ml
Gills	2.50g/ml	1.67	24.25µg/ml
Liver		1.65	23.45µg/ml
48 days	Insecticide concentration	260/280 ratio	DNA concentration
Gills	0.80µg/L	1.58	22.7µg/ml
Liver		1.47	21µg/ml
Gills	1.30µg/ml	1.41	20.5µg/ml
Liver		1.71	18.75µg/ml
Gills	1.90µg/ml	1.24	17.65µg/ml
Liver		1.13	16.35µg/ml
Gills	2.50g/ml	1.41	20.5µg/ml
Liver		1.58	22.7µg/ml
72 days	Insecticide concentration	260/280 ratio	DNA concentration
Gills	0.80µg/L	1.54	16.25µg/ml

72 days	Insecticide concentration	260/280 ratio	DNA concentration
Liver		1.47	14.65µg/ml
Gills	1.30µg/ml	1.60	14.35µg/ml
Liver		1.40	13.3µg/ml
Gills	1.90µg/ml	1.37	13µg/ml
Liver		1.26	12.3µg/ml
Gill	2.50g/ml	1.44	16.26µg/ml
Liver		1.46	14.66µg/ml
96 days	Insecticide concentration	260/280 ratio	DNA concentration
		1.54	16.24µg/ml
Gill	0.80µg/L	1.46	14.63µg/ml
Liver		1.68	14.34µg/ml
Gill	1.30µg/ml	1.47	13.3µg/ml
Liver		1.36	13.00µg/ml
Gill	1.90µg/ml	1.25	12.10µg/ml
Liver		1.45	16.21µg/ml
Gill	2.50g/ml	1.47	14.61µg/ml
Liver		1.46	14.66µg/ml

4. DISCUSSION

Glyphosate, a primary component in numerous herbicides, is extensively employed in agriculture industry to eliminate unwanted weeds and in non-agricultural areas for vegetation clearance. Its usage can lead to contamination of nearby water bodies through irrigated food crops, which can cause various abnormalities in the organisms inhabiting the polluted water. Due to its frequent use and specificity, glyphosate has been found to induce several toxicological problems in exposed species, including humans. Organisms' antioxidant systems play a crucial role in responding to oxidative stress by generating antioxidant metabolites and enzymes. Catalase is a significant enzyme among these enzymes, as it helps in preventing the harmful impacts of ROS on cells [20]. In the current investigation, the liver tissue levels of lipid peroxidation, which is the primary immune organ, exhibited a significant decrease ($P < 0.05$) in groups

exposed to ≥20 mg/L of GBH. Moreover, the catalase activities in liver tissues also increased. Previous research has reported significant alterations in oxidative stress in fish upon exposure to GBH [21]. The current study found that fish exposed to glyphosate had increased levels of ROS and TBARS, while their levels of GSH and total proteins decreased, respectively. The liver tissues of treated fish showed these effects throughout the experiment. Additionally, the kidneys of fish in groups D-E showed significantly higher levels of oxidative stress and ROS contents after the 4th day of exposure as compared to unexposed fish [22]. The levels of lipid peroxidation in liver tissues of fish exposed to GBH exhibited diverse outcomes, either increasing, decreasing, or remaining stable, depending mainly on the fish weight (or age) and exposure time, similar to the levels of catalase. Such oxidative conditions have been observed in various fish species upon exposure to different pollutants, including GBH, as per earlier studies. In this study, the DNA fragments displayed irregular and stepped smears due to the inaccurate process of DNA cleavage that occurs during apoptosis. This result is consistent with earlier findings [23] conjecture that more than one mechanism could be responsible for the fragmentation patterns leading to cell death and the cumulative effect of these events can trigger apoptosis and necrotic cell death. The ends were employed to assess the intricate genotoxic effects of the insecticide at the DNA level of many fish species under study. Various tissues are commonly used to determine DNA damage, namely , gills and liver [24]. In this study, the liver -detoxification organ- and the gills were selected as organs that are directly exposed to environmental contaminants. Gills and liver, being metabolically active organs that have higher metal accumulation than other organs, share this characteristic. Metal ion complexes formation can cause DNA damage. During apoptosis, DNA cleavage occurs at sites between nucleosomes, leading to DNA damage, which is a typical feature [25]. Moreover, chromatin is broken down by proteases and endonucleases into a smearing pattern, which is an indication of necrosis when proteases break down the histones and expose the entire length of the nucleases.

4.1. Conclusion

By analyzing the activities of antioxidant enzymes as biochemical biomarkers in freshwater fish *Oreochromis niloticus* (glyphosate-based herbicide) exposed to Roundup, it was concluded that the exposure to Roundup resulted in oxidative stress as well as DNA damage in the fish.

Therefore, the current conclusion was supported by the changes noticed in the activities of antioxidant enzymes. The study found a significant increase in oxidative stress by the activities of superoxide dismutase (SOD), catalasend peroxidase. The active ingredient in Roundup and glyphosate, can generate reactive oxygen species, which can damage the DNA molecules. This damage can lead to mutations and genetic instability, potentially increasing the risk of cancer and other diseases. Moreover, this sort of damage can lead to reduced growth, reproduction, and survival of fish populations. Additionally, glyphosate can also affect the aquatic food chain, potentially affecting the health of other species, which rely on fish as a prime food source. These findings emphasized the need for proper regulation and management of herbicide usage in aquatic ecosystems to minimize the impact on fish and other aquatic organisms. Thus, it is crucial to monitor the use of glyphosate-based herbicides in freshwater environments and take measures to reduce their potential negative impacts on aquatic organisms. Exposure to Roundup herbicide led to changes in the DNA concentration and 260/280 ratio in fish organs such as the liver and gills. The gills showed higher vulnerability to Roundup herbicide exposure than the liver. This suggested that Roundup herbicide exposure could cause DNA damage in fish organs. Hence, further research is required to evaluate the long-term effects of Roundup herbicide exposure on fish populations and the broader ecosystem. For this purpose, measures should be taken to reduce Roundup herbicide usage and minimize its potential negative impacts on aquatic life. Further research can also comprehensively understand the long-term effects of Roundup exposure on fish and other aquatic organisms.

REFERENCES

1. Tariq MI, Afzal S, Hussain I. Pesticides in shallow groundwater of Bahawalnagar, Muzafargarh, D.G. Khan and Rajan Pur districts of Punjab, Pakistan. *Environ Int*. 2004;30(4):471–79. https://doi.org/10.1016/j.envint.2003.09.008

2. Rana SM, Asi MR, Niazi F, Sultana S, Ghazala, Al-Ghanim KA. Determination of organochlorine and nitrogen containing pesticide residues in Labeo rohita. *Toxicol Environ Chem*. 2011;93(10):1851–1855. https://doi.org/10.1080/02772248.2011.585746

3. Soares D, Silva L, Duarte S, Pena A, Pereira A. Glyphosate use, toxicity and occurrence in food. *Foods*. 2021;10(11):e2785. https://doi.org/10.3390/foods10112785

4. Benbrook CM. Trends in glyphosate herbicide use in the United States and globally. *Environ Sci Eur*. 2016;28(1):e3. https://doi.org/10.1186/s12302-016-0070-0

5. Belo MSdSP, Pignati W, Dores EFGdC, Moreira JC, Peres F. Pesticide use in soybean production in Mato Grosso state, Brazil: A preliminary occupational and environmental risk characterization. *Rev Brasil de Saúde Ocup*. 2012;37:78–88.

6. Uddin MH, Shahjahan M, Ruhul Amin AKM, Haque MM, Islam MA, Azim ME. Impacts of organophosphate pesticide, sumithion on water quality and benthic invertebrates in aquaculture ponds. *Aquacul Rep*. 2016;3:88–92. https://doi.org/10.1016/j.aqrep.2016.01.002

7. Karadag H, Fırat Ö, Fırat Ö. Use of oxidative stress biomarkers in *Cyprinus carpio* L. for the evaluation of water pollution in Ataturk Dam Lake (Adiyaman, Turkey). *Bulletin Environ Cont Toxicol*. 2014;92(3):289–293. https://doi.org/10.1007/s00128-013-1187-0

8. Nardi J, Moras PB, Koeppe C, Dallegrave E, Leal MB, Rossato-Grando LG. Prepubertal subchronic exposure to soy milk and glyphosate leads to endocrine disruption. *Food Chem Toxicol*. 2017;100:247–252. https://doi.org/10.1016/j.fct.2016.12.030

9. Naz S, Mansouri B, Chatha AMM, et al. Water quality and health risk assessment of trace elements in surface water at Punjnad Headworks, Punjab, Pakistan. *Environ Sci Pollut Res Int*. 2022;29(40):61457–61469. https://doi.org/10.1007/s11356-022-20210-4

10. Naz S, Hussain R, Ullah Q, Chatha AMM, Shaheen A, Khan RU. Toxic effect of some heavy metals on hematology and histopathology of major carp (*Catla catla*). *Environ Sci Pollut Res*. 2021;28(6):6533–6539. https://doi.org/10.1007/s11356-020-10980-0

11. Parrino V, De Marco G, Minutoli R, et al. Effects of pesticides on Chelon labrosus (Risso, 1827) evaluated by enzymatic activities along the north eastern Sicilian coastlines (Italy). *Euro Zoolog J*. 2021;88(1):540–48. https://doi.org/10.1080/24750263.2021.1905090

12. Díaz-Resendiz K, Ortiz-Lazareno P, Covantes-Rosales C, et al. Effect of diazinon, an organophosphate pesticide, on signal transduction and death induction in mononuclear cells of Nile tilapia fish (*Oreochromis niloticus*). *Fish Shellfish Immunol*. 2019;89:12–17. https://doi.org/10.1016/j.fsi.2019.03.036

13. Oropesa A, García Cambero J, Soler F. Effect of long-term exposure to simazine on brain and muscle acetylcholinesterase activity of common carp *(Cyprinus carpio)*. *Environ Toxicol: An Int J*. 2008;23(3):285–293. https://doi.org/10.1002/tox.20342

14. Al-Saeed FA, Naz S, Saeed MH, et al. Oxidative stress, antioxidant enzymes, genotoxicity and histopathological profile in oreochromis niloticus exposed to lufenuron. *Pak Veter J*. 2023;43(1):160–166. http://dx.doi.org/10.29261/pakvetj/2023.012

15. Glusczak L, dos Santos Miron D, Crestani M, et al. Effect of glyphosate herbicide on acetylcholinesterase activity and metabolic and hematological parameters in piava (*Leporinus obtusidens*). *Ecotoxicol Environ Saf*. 2006;65(2):237–241. https://doi.org/10.1016/j.ecoenv.2005.07.017

16. Selionova MI, Podkorytov NA. Polymorphism of the gene *GDF9* in sheep of Prikatun type of Altai Mountains breedand its correlation with indices of meat rate productivity. *Theory Prac Meat Proc*. 2021;6(1):4–9. https://doi.org/10.21323/2414–438X-2021–6–1–4–9

17. Ferreira L, Soares MAM, Rodrigues MT, et al. *UCP2* and *PPARG* gene polymorphisms and their association with milk yield and composition traits in goats. *Small Rum Res.* 2020;192:e106210. https://doi.org/10.1016/j.smallrumres.2020.106210

18. Javadi A, Shamaei M, Mohammadi Ziazi L, et al. Qualification study of two genomic DNA extraction methods in different clinical samples. *Tanaffos*. 2014;13(4):41–47

19. Au - Desjardins P, Au - Conklin D. NanoDrop microvolume quantitation of nucleic acids. *JoVE*. 2010(45):e2565. https://doi.org/doi:10.3791/2565

20. Das SK, Fanburg BL. Hyperoxia elevates cu,zn-superoxide dismutase of endothelial cells as detected by a sensitive ELISA. *Enzyme*. 1992;46:188–195. https://doi.org/10.1159/000468787

21. Li Y, Ding W, Li X. Acute exposure of glyphosate-based herbicide induced damages on common carp organs via heat shock proteins-related immune response and oxidative stress. *Toxin Rev*. 2021;40(4):1071–1083. https://doi.org/10.1080/15569543.2019.1621903

22. Ghaffar A, Hussain R, Ahmad N, et al. Evaluation of hemato-biochemical, antioxidant enzymes as biochemical biomarkers and genotoxic potential of glyphosate in freshwater fish (*Labeo rohita*). *Chem.* 2021;37(7):646–667. https://doi.org/10.1080/02757540.2021.1937141

23. Bortner CD, Oldenburg NB, Cidlowski JA. The role of DNA fragmentation in apoptosis. *Tren Cell Biol*. 1995;5(1):21–26. https://doi.org/10.1016/s0962-8924(00)88932-1

24. Lee RF, Steinert S. Use of the single cell gel electrophoresis/comet assay for detecting DNA damage in aquatic (marine and freshwater) animals. *Mut Res*. 2003;544(1):43–64. https://doi.org/10.1016/s1383-5742(03)00017-6

25. Williams JR, Little JB, Shipley WU. Association of mammalian cell death with a specific endonucleolytic degradation of DNA. *Nature*. 1974;252(5485):754–755. https://doi.org/10.1038/252754a0

Scientific Inquiry and Review (SIR)
Volume 7 Issue 2, 2023
ISSN (P): 2521-2427, ISSN (E): 2521-2435
Homepage: https://journals.umt.edu.pk/index.php/SIR

Article QR

Title:	**Assessing the Impact of Prolonged Screen Time on Ophthalmic Health among Students: A Post-COVID-19 Study in Pakistan**
Author (s):	Basit Ali[1], Kaniz Fatima[2], Mahnoor[3], Amen Fatima[3], Kinza Mazhar[3]
Affiliation (s):	[1]Department of Electrical Engineering, Bahria University, Karachi, Pakistan [2]Department of Humanities & Social Sciences, Bahria University, Karachi, Pakistan [3]DOW University of Health Sciences, Karachi, Pakistan
DOI:	https://doi.org/10.32350/sir.72.03
History:	Received: December 16, 2022, Revised: March 12, 2023, Accepted: March 13, 2023, Published: June 15, 2023
Citation:	Ali B, Fatima K, Mahnoor, Fatima A, Mazhar K. Assessing the impact of prolonged screen time on ophthalmic health among students: A Post-COVID-19 study in Pakistan. *Sci Inq Rev.* 2023;7(2):54–70. https://doi.org/10.32350/sir.72.03
Copyright:	© The Authors
Licensing:	This article is open access and is distributed under the terms of Creative Commons Attribution 4.0 International License
Conflict of Interest:	Author(s) declared no conflict of interest

A publication of
The School of Science
University of Management and Technology, Lahore, Pakistan

Assessing the Impact of Prolonged Screen Time on Ophthalmic Health among Students: A Post-COVID-19 Study in Pakistan

Basit Ali[1*], Kaniz Fatima[2], Mahnoor[3], Amen Fatima[3], Kinza Mazhar[3]

[1]Department of Electrical Engineering, Bahria University, Karachi, Pakistan
[2]Department of Humanities & Social Sciences, Bahria University, Karachi, Pakistan
[3]DOW College of Pharmacy, DOW University of Health Sciences, Karachi, Pakistan

ABSTRACT

Human beings heavily rely on the sense of sight, as sight mainly controls approximately 80% of our perception. During the COVID-19 pandemic, students had to take their online classes by using different electronic devices. By not following the proper instructions to use these devices, primary students faced eyesight issues during the COVID-19 pandemic. Low Vision is a commonly diagnosed issue in ophthalmology in Pakistan. Therefore, the current study is a survey-based research. For this purpose, a population of 100 primary students was gathered who took online classes during the pandemic and developed eyesight issues after their online classes. Based on statistical analysis, the logistic regression model was used to analyze the eyesight issues among the primary students considering several variables including gender, age, distance with devices, duration of using the devices, and analyzing previous eyesight issues. The findings indicated that male students have a more chance of developing eyesight issues than female students. Hence, it was deduced that female students who used their devices from a distance of more than 16 inches for less than 3 hours had the least possibility of developing any eyesight issues.

Keywords: COVID-19, eyesight issues, ophthalmology, logistic regression

1. INTRODUCTION

Throughout history, notable pandemics such as AIDS, dengue, cholera, plague, influenza, smallpox, and severe acute respiratory syndrome have had far-reaching consequences, affecting not only the healthcare system but also the economy, society, and security. Several key factors contribute to the facilitation of a pandemic, including its global reach, novelty, severity,

* Corresponding Author: Basitali.bukc@bahria.edu.pk

reduced immunity, high infection rates, and other related aspects [1].

Prior to early December 2019, numerous symptoms resembling pneumonia were documented in Wuhan, located in Hubei province, China [2]. These symptoms occurred because of the re-emergence of the coronavirus in the form of SARS-COV 2 [3]. In Pakistan, authorities reported the first two COVID-19 cases in March 2020 in Islamabad [4]. The lockdown was imposed countrywide and people were forced to isolate themselves in their houses. The traditional mode of education was shifted to an online education medium, which opened new gateways and new opportunities for students to learn this new medium of education [5]. Online education brought many challenges, which include a lack of proper infrastructure for educational setup, technical issues like internet lagging leading to voice and video disruption, and a lack of face-to-face interaction among teachers. Primary-level of students were dependent on their parents for their academic work and the online education system was new to their parents. Thereby, students or teachers developed several health conditions that were also connected to the online education system including eyestrain, cervical pain, lumbago, vertigo, headaches, psychological issues, lack of physical activity, and eyesight issues.

The eye is the most delicate and sensitive organ of the human body. It is susceptible to any damage that could be chemical, physical, environmental, and others, which may affect its ability to envisage leading numerous eye-related issues. The structure of the eye mainly comprises the conjunctiva, sclera, iris, pupil, lens, and retina. The conjunctiva is a mucous membrane made up of non-keratinizing squamous epithelium containing goblet cells, langerhans cells, and dendritic melanocytes [6]. It protects and lubricates the eye by producing mucous and tears [7]. As light strikes the retina, several chemical reactions take place within different cell layers such as rods and cones. These chemical reactions in the form of electrical signals disseminate through nerve cells into the second cranial nerve [8]. Several abnormalities associated with the eye include ageing, increased exposure to unshielded screens, trauma, infections, and family history. The main issues that could occur due to prolonged exposure to screens are eye itching, irritation, burning, redness, drying, and fatigue. Long-sightedness (hypermetropia) and shortsightedness (myopia), which are the most common abnormalities in growing ages. Hypermetropia occurs when the eyeball is too short so the focus point is behind the retina at the back of the

eye. If this condition occurs in students, a squint may be noticed, for instance, one eye turning inward. On the other hand, myopia occurs when a person is unable to see only nearby objects.This condition occurs when the length of the eye is excessive, causing the light to converge in front of the retina located at the back of the eye. Myopia is a serious condition because if a child becomes myopic before nine years old, there are chances that he or she may develop a high level of myopia in the future, which makes them prone to glaucoma, retinal detachments, and myopic retinal degeneration. There are also chances of complete loss of eyesight for the high-level myopic person [9]. Dry eye is an eye condition that leads to ocular tenderness. It is characterized by a disruption in the tear film, resulting in the drying of tears. This condition is commonly associated with decreased intervals between blinking [10, 11]. Continuous use of screens can cause eye fatigue and soreness, which contributes to the eye injury and diseases like refractive error, myopia, cataract, and glaucoma [12]. Recently, eye abnormalities are associated with increased exposure time to screens among all age groups. In the last couple of years, as the COVID-19 lockdown prompted a global shift towards online education, numerous reports in the literature have highlighted the prevalence of eyesight problems. During the COVID-19 pandemic lockdown in the past two years, the traditional education system shifted to online educational medium. Reportedly, many eyesight cases were noted during this particular time of the COVID-19 pandemic.

However, in Pakistan, such issues remained unnoticed due to the dearth concerns, such as financial issues and regular checkup. People in this crucial time avoided visiting hospitals because of fear of getting COVID from the hospitals of infected patients. According to WHO, 2.2 billion people around the world suffered from eye conditions [13]. *Bahkir* reported that the increase in the usage of digital devices during COVID-19 led to an adverse effect on ocular health in all age groups. Therefore, 90.42% of the respondents reportedly experienced eye abnormalities due to the excessive usage of digital devices. In their study, they identified a high incidence of dry eye and headache in females. A percentage of 43.5% of people experienced headaches, 29% had eye pain, 23.8% had heavy eyelids, and 74.2% had sleep disturbances [14]. *Balsam Alabdulkader* through a self-reported questionnaire estimated that the prolonged use of digital devices increased during the COVID-19 pandemic and reported that 78% of students faced digital eyestrains [15]. *Bengi Demirayak* elaborated increase

in digital device use during COVID-19 exacerbated the digital eyestrain problem in students. Hence, 52.2% of students experienced headaches as the most common symptom [16]. *Abdullah Altalhi* conducted an electronic self-administered survey on KSAUHS students in Saudi Arabia of Computer Vision Syndrome (CVS). It was reported that CVS symptoms were reportedly higher in female students who used to wear spectacles and observed glare on the screen. Reportedly, the most common symptoms noticed among students were headache (68%), feeling of affected eyesight (65%), eye itchiness (63%), burning sensation (62%), excessive blinking (40%), and difficulty moving eyelids (9%) [17].

In China, more than 180 million of primary and secondary school students were circumscribed to their homes. It was observed that students were less physically active with longer screen time and irregular diet resulted in cardiorespiratory weaknesses [18]. Homeschooling is a unique and alternative format of education. According to the student demographic questionnaire, 17.6% of students were identified as having behavioural and emotional effects. However, low-grade students were more at risk with 19.3% as compared to high-grade students having 13.7% effects [19]. According to the Indian Journal of Ophthalmology, a survey conducted among 217 individuals showed the frequency of digital eyestrain to be 50.23%. Common manifestations observed were itching in the eyes and headache (53.9%). This survey-based research highlighted the prevalence of digital eyestrain causing ocular health issues due to increased usage of digital devices [20]. Increased usage of digital devices among students for online sessions showed the progression of myopia in individuals. The percentage of myopic individuals reached up to 10.40% in Chongqing, China [21]. Researchers used the chi-square test for analyzing the immense use of computers by university students and it was identified that burning eyes and tired eyes were the common symptoms reported among students [22]. Computer vision syndrome was reported in 75% of visual display terminal workers as compared to other workers [23].

Ugam Usgaonkar through his e-survey-based research estimated that most of the respondents were involved in more than two digital activities on more than two digital devices. The symptoms observed were watery eyes, headache, dry eyes, shoulder pain, pain behind the eye, and back pain. The increase in ocular symptoms was due to an increase in time spent on digital devices [24]. *Richa Gupta* elaborated on the adverse effect of e-learning on

the eye health of school students during COVID-19 through survey-based research. A percentage of 92.8% of students reportedly had eyestrain symptoms. The most common symptoms were eye redness, which was 69.1% and heaviness of the eyelid, which was 79.7% [25]. *Pratyusha Ganne* analyzed the digital eyestrain problem due to the increase in digital device usage during COVID-19. The prevalence of eyestrain was found to be higher in students, which were attending online classes. The prime factors, which were involved, were pre-existing eye disease, greater screen time, screen distance, and using the screen in the dark [26].

In this paper, a survey-based research regarding the ophthalmic health of primary school students was conducted as a result of attending online classes through different digital devices during COVID-19. The current study was designed to analyze the impact of online education on their eyesight is qualitative, based on survey of 100 primary students, 59 female, and 41 male students conducted for the age group 4 to 12 years. It was also observed that some students were already facing eye abnormalities, which may include eyestrain, red eyes, night blindness, uveitis, presbyopia, floaters, dry eyes, cataracts, retinal disorders, corneal diseases, and others. For this purpose, Logistic regression analysis would help to estimate the probability of the eyesight issues of the primary students after online education. This dichotomous variable would be used as a dependent variable, which depends on gender, age, the distance of the device with the eyes, duration of the user device, and already facing any eye health issues.

2. METHODOLOGY

2.1. Statistical Model and Analysis

The relationship between a dichotomous dependent variable and one or more independent categorical variables was illustrated by binary logistic regression analysis. This model provides odds, odds ratio, and probability statistics, which can be highly useful in properly expressing the research goal [27]. Generally, this model is used while discussing a dependent variable, which is binary, dichotomous, or alternative, rather than continuous variables [28, 29]. There are other statistical models, which can be applied in previous literature related to statistical convergence [30, 31].

The IBM SPSS version 25.0 software was used to find out the relationship between eyesight issues with the explanatory variables of gender, age, the distance of the device with the eyes, duration of using the

device, and people who were already facing any eye abnormalities. In the study population 100 primary students who have taken online classes during the pandemic, 59 were female and 41 were male students with different age groups ranging from 4-12 years. The device distance could be less or greater than 16 inches. The duration of using devices for online education was noticeably more or less than 3 hours. Another significant aspect to consider is whether the student had experienced any eye-related issues prior to the onset of the COVID-19 pandemic. After executing the logistic regression in IBM SPSS, some information was obtained, which helped to estimate the impact of the devices used for online education on primary students' eyes.

2.2. Model Diagnosis

Model diagnosis shows the complete analysis of the model execution. Table 1 provides a complete indication of how well the model executes. This is also termed as a "Goodness of fit test". It is utilized to decide the rate of an exact number of expectations in total predictions. The significant value in the Omnibus test is less than 0.05, which reflects that the model is significant. The chi-square statistic is 19.224 with 5 degrees of freedom. Therefore, the overall model is statistically significant, χ^2 (5) = 19.224, $p < 0.05$. The Hosmer and Lemeshow tests were also used to support the current model but their interpretation is completely different from the omnibus test. In this test, the significance value should be higher than 0.05 so that the model does fit the data. Table 1 shows that the chi-square value for the Hosmer and Lemeshow Test is 11.980 with a significance level of 0.101. This value is larger than 0.05; therefore, indicating accuracy for the model.

Table 1. Omnibus & Hosmer Tests of Model Coefficients

Test	Chi-square	Degrees of freedom	Significant value
Omnibus	19.224	5	0.002
Hosmer and Lemeshow	11.980	7	0.101

To calculate the variations in the dependent variable, the method of the Cox & Snell R^2 and Nagelkerke R^2 were supportive. According to these methods, Table 2 shows that around 17.5%-23.5% of the variability in the eyesight issues after the COVID-19 pandemic were considered by all the independent variables.

Table 2. Model Summary

-2 Log likelihood	Cox & Snell R Square	Nagelkerke R Square
116.835	0.175	0.235

2.3. Model Characteristics

The classification table depicted in Table 3, which is obtained after the execution of logistic regression in IBM SPSS, explains how well the model is going to predict the correct category (facing eyesight issues/no eyesight issues after the COVID-19 pandemic) for each case. The sensitivity of the model is the percentage of the students having eyesight issues after COVID-19 pandemic, which were identified by the model in Table 3, which is primarily 52.4% of the students who are facing eyesight issues after COVID-19 pandemic.

Table 3. Classification Table

Observed		Predicted		
		Is the child facing any eyesight issues after COVID-19 pandemic?		Percentage Correct
		no	yes	
Is the child facing any eyesight issues after COVID-19 pandemic?	no	44	14	75.9
	yes	20	22	52.4
Overall Percentage				66.0

The model's specificity refers to the percentage of students who do not have eyesight issues after COVID-19 pandemic. In this model, the specificity is 75.9%. The model accurately predicted that students who did not have eyesight problems after the COVID-19 pandemic were indeed free of such issues.

3. RESULTS AND DISCUSSION

The model shows a complete picture of all the parameters measured in this study. Table 4 provides a detaileddata about the contributions of every

independent variable.

Table 4. Coefficients of Logistic Regression Model for Different Eyesight Issues Parameters

Independent variables	Coefficients (*B*)	S.E.	Wald	*df*	Sig.	Exp(*B*)	95% C.I. for EXP(*B*)	
							Lower	Upper
Gender of child	0.774	0.465	2.774	1	0.096	2.168	.872	5.389
Age of child	0.204	0.107	3.616	1	0.057	1.226	.994	1.513
What was the distance of eyes of the child from computer/phone screen?	-0.748	0.581	1.653	1	0.199	0.474	0.152	1.480
What is the maximum hours of screen exposure of the child?	0.876	0.517	2.867	1	0.090	2.402	0.871	6.622
Did the child have any eyesight issue before COVID-19 pandemic?	0.903	0.484	3.478	1	0.062	2.466	0.955	6.369
Constant	-3.206	0.998	10.316	1	0.001	0.041		

The direction and quality of the relationship between the dependent and independent variables are shown in the column B. In the model, the B value of the distance of eyes of the students from computer/phone screen is negative, which means that the distance is more than 16 inches and has less probability of having eyesight issues than if the distance is less than 16 inches. The other B values are positive, which reflects that if the age of students increased, the chances of having eyesight issues increases. Furthermore, the B value of gender is also positive, which means that female students has less probability of having eyesight issues than male

students. More than 3 hours of screening time is more harmful for the students and create more eyesight issues than the other students whose screening time is less than 3 hours. Similarly, students who were already facing vision problems have more possibility to have more severe vision problems after online education.

These values of B can be utilized in an equation to find the probability of the primary students having eyesight issues. These values are in log-odds units, which can be converted to probabilities. The following is the expression for the binary logistic regression model considering the aforementioned variables:

$$\log\left(\frac{p}{1-p}\right) = b_0 + b_1 x_{gender} + b_2 x_{age} + b_3 x_{distance} + b_4 x_{duration} + b_5 x_{already\ eyesight\ issues} \quad (3.1)$$

Where p, is the probability of having eyesight issues after COVID-19 pandemic $\log\left(\frac{p}{1-p}\right)$ in **Eq. (3.1)** is considered as a log of odds or link logit function while $\frac{p}{1-p}$ is taken as the odds ratio. The logistic regression equation in variables form is:

$$\log\left(\frac{p}{1-p}\right) = -3.206 + 0.774\, x_{gender} + 0.204\, x_{age} - 0.748 x_{distance} + 0.876\, x_{duration} + 0.903\, x_{already\ eye\ issues} \quad (3.2)$$

Applying antilog on both sides, the odds ratio will be equal to,

$$\left(\frac{p}{1-p}\right) = e^{-3.206+0.774\, x_{gender}+0.204\, x_{age}-0.748 x_{distance}+0.876\, x_{duration}+0.903\, x_{already\ eye\ issues}} \quad (3.3)$$

The probability of each eyesight issue parameter with different covariates can be easily depicted. **Eq. (3.4)** represents the probability equation generated from the model.

$$p = \frac{e^{-3.206+0.774\, x_{gender}+0.204\, x_{age}-0.748 x_{distance}+0.876\, x_{duration}+0.903\, x_{already\ eyesight\ issues}}}{1 + e^{-3.206+0.774\, x_{gender}+0.204\, x_{age}-0.748 x_{distance}+0.876\, x_{duration}+0.903\, x_{already\ eyesight\ issues}}} \ldots \quad (3.4)$$

In Table 4, column Exp (B) is the value of the odd ratio for each

independent variable. It shows the increase in probability of occurrence as the independent variable increases by one unit. In the model, the odds of a student having eyesight issues is 0.474 times higher for the student whose distance of eyes from the device is less than 16 inches than a child whose distance of eyes from the device is more than 16 inches, if all other factors are supposed to be constant. Similarly, the odds of a student having eyesight issues is 2.402 times higher for the student whose screen time is more than 3 hours than those students having screen time is less than 3 hours. Same as in the situation of suffering any other eyesight issues before COVID-19 pandemic, those students who are suffering any eyesight issues before COVID-19 pandemic, the eyesight issues is 2.466 times higher than those who not suffering any eyesight issues before online education, taking all other factors constant. The odd ratio of the gender is greater than 1, which represents that mostly male students have reported eyesight issues than female students. The odds of eyesight issues in female students decrease by a factor of 2.168 to male students when all other factors are kept constant. In the model, one continuous variable, age, is also included. The odd ratio of age is increased by a factor of 1.226 for a one-year increase in age. In Table 4, the 95% confidence intervals provide lower and upper bounds associated with the corresponding odds ratios. These are the limits where you can be 95% confident that they cover the true value of the odds ratio. Using the probability equation obtained in (4), Table 5 shows that all probabilities of having eyesight issues were measured with the impact of all independent variables.

As age is the continuous variable, maximum, minimum, and average age has been taken to estimate the probabilities. The lowest probability of having eyesight issues is 0.04156, which depicts a female primary student who is not suffering any eyesight issues before online education, at the age of 4 years, with the distance of more than 16 inches with screen and her exposure duration is less than 3 hours. While the maximum probability of having eyesight issues is 0.85753, which represents a male student who is already facing eyesight issues at the age of approximately 12 years, with a distance of fewer than 16 inches and his exposure duration is more than 3 hours. Figure 1 shows the probability of having eyesight issues in male students with the consideration of all the independent variables. While, Figure 2 shows the probability of having eyesight issues in female students with the consideration of all the independent variables.

Table 5. Probability Table of Having Eyesight Issues with the Covariates

Distance		Less than 16 inches				More than 16 inches			
Duration		Less than 3 hours		More than 3 hours		Less than 3 hours		More than 3 hours	
Eyesight condition before pandemic		Healthy	Unhealthy	Healthy	Unhealthy	Healthy	Unhealthy	Healthy	Unhealthy
Female	4 year	0.083	0.184	0.180	0.351	0.041	0.096	0.094	0.204
	≤8 year	0.171	0.338	0.332	0.551	0.089	0.194	0.190	0.367
	≤12 year	0.319	0.536	0.529	0.735	0.181	0.353	0.347	0.567
Male	4 year	0.165	0.328	0.323	0.540	0.085	0.188	0.184	0.357
	≤8 year	0.310	0.525	0.518	0.726	0.175	0.344	0.338	0.557
	≤12 year	0.503	0.714	0.709	0.857	0.324	0.542	0.535	0.740

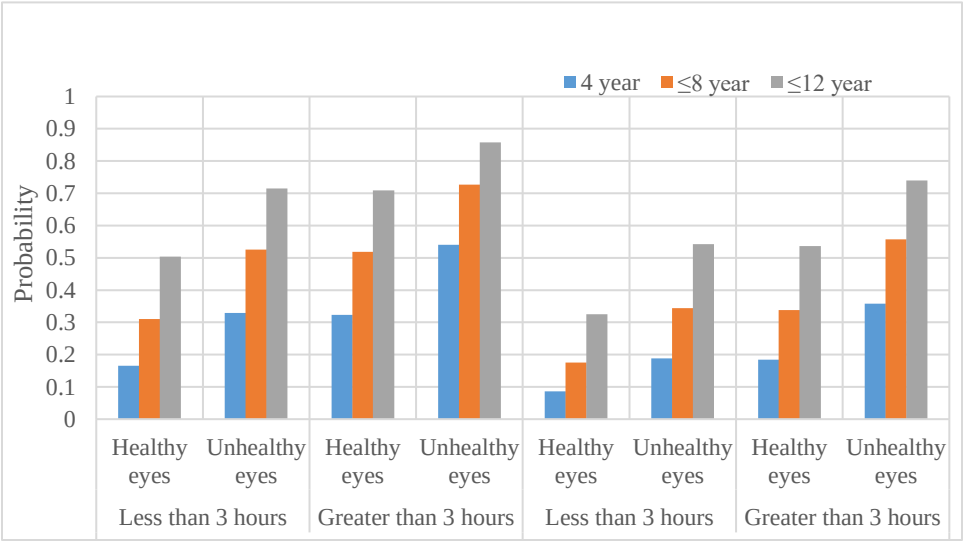

Figure 1. Probability of Eyesight Issues in Male Students

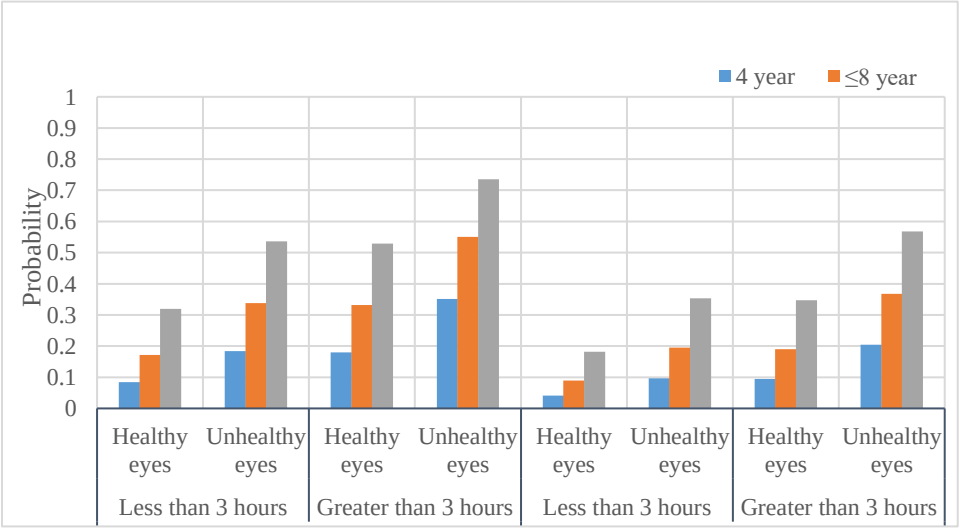

Figure 2. Probability of Eyesight Issues in Female Students

3.1. Conclusion

The current study deployed a logistic regression analysis, which estimated the probability of optical impairment in primary school children. Noticeably, these children were taking online classes during the COVID-19 pandemic. This research paper indicated that a logistic regression model

considered the explanatory variables of gender, age, eye distance from the device, duration of use, and previous vision problems to model eyesight abnormalities in primary school children. With the help of this model, it has been observed that male students have more chances than female students of developing eyesight issues. Furthermore, it was observed that the probability of experiencing eye problems increases when factors such as age, distance, and duration of online classes are extended. Additionally, if the child has preexisting eye disorders, the likelihood of developing eye issues increase. Thereby, it was identified that female students of 4 years of age have the lowest chance of having eyesight problems if they use devices with 16 inches of distance. This is because they are exposed for less than 3 hours and do not have any prior eye problems. Male students ranging between 9-12 years, using a screen with a distance of less than 16 inches over an extended period of up to 3 hours and who have already faced vision issues have the highest risk of having vision issues. Therefore, it is recommended that male students should wear eyeglasses or should maintain a proper screen distance to reduce the impact on their eyesight. Additionally, periodic eye exams enable them to detect earlier symptoms of any developing problems.

REFERENCES

1. Qiu W, Rutherford S, Mao A, Chu C. The pandemic and its impacts. *Health Cul Soc*. 2022;9:1–11. https://doi.org/10.5195/hcs.2017.221
2. Seah I, Agrawal R. Can the coronavirus disease 2019 (COVID-19) affect the eyes? A review of coronaviruses and ocular implications in humans and animals. *Ocular Immunol Inflam*. 2020;28(3):391–395. http://doi.org/10.1080/09273948.2020.1738501
3. Lone SA, Ahmad A. (2020). COVID-19 pandemic–an African perspective. *Emerg Microbes Infec*. 2020;9(1):1300–1308. https://doi.org/10.1080/22221751.2020.1775132
4. Li YP, Ma Y, Wang N, Jin ZB. Eyes on coronavirus. *Stem Cell Res*. 2021;51(102200):e102200. https://doi.org/10.1016/j.scr.2021.102200
5. Karim H, Hafeez M. The impact of online education system at student's and teacher's during covid-19 pandemic in Pakistan. *Sci Educ J*. 2022;6(1):61–69. https://doi.org/10.21070/sej.v6i1.1541

6. Yanoff M. Ocular pathology of diabetes mellitus. *Am J Ophthalmol*. 1969;67(1):21–38. https://doi.org/10.1016/0002-9394(69)90004-x

7. Bhattacharya K, Bhattacharya N, Bhattacharya AS. Tubarial salivary gland – A new kid on the block. *Ind J Anat Surg Head Neck Brain*. 2022;8(2):80–81. https://doi.org/10.18231/j.ijashnb.2022.018

8. Marra AR, Edmond MB, Popescu SV, Perencevich EN. examining the need for eye protection for coronavirus disease 2019 (COVID-19) prevention in the community. *Infect Control Hosp Epidemiol*. 2021;42(5):646–647. https://doi.org/10.1017/ice.2020.314

9. Gegúndez-Fernández JA, Zarranz-Ventura J, Garay-Aramburu G, et al. Recommendations for eye care during the alarm state by the coronavirus disease pandemic COVID-19. *Arch Soc Esp Oftalmol*. 2020;95(6):300–310. https://doi.org/10.1016/j.oftal.2020.04.002

10. Mufti M, Imran Sayeed S, Jaan I, Nazir S. Does digital screen exposure cause dry eye? *Ind J Clin Anat Physiol*. 2019;6(1):68–72. https://doi.org/10.18231/2394-2126.2019.0017

11. Sodani P, Manhas A, Gupta D, Syed T, Dolma YC, Sangra S. A study of prevalence and association of dry eye disease with visual display terminal use in students-a cross sectional observational study. *J Evolution Med Dent Sci*. 2019;8:3707–3711. https://doi.org/10.14260/jemds/2019/802

12. Lee CC, Chiang HS, Hsiao MH. Effects of screen size and visual presentation on visual fatigue based on regional brain wave activity. *J Supercomput*. 2021;77(5):4831–4851. https://doi.org/10.1007/s11227-020-03458-w1

13. Gupta R, Chauhan L, Varshney A. Impact of e-schooling on digital eye strain in Coronavirus disease era: A survey of 654 students. *J Curr Ophthalmology*. 2021;33(2):158–164. https://doi.org/10.4103/joco.joco_89_202

14. Lawrenson JG, Buckley RJ. COVID-19 and the eye. *Ophthalmic Physio Opt*. 2020;40(4):383–388. https://doi.org/10.1111/opo.12708

15. Bahkir FA, Grandee SS. Impact of the COVID-19 lockdown on digital device-related ocular health. *Indian J Ophthalmology*. 2020;68(11):2378–2383. https://doi.org/10.4103/ijo.IJO_2306_20

16. Alabdulkader B. Effect of digital device use during COVID-19 on digital eye strain. *Clin Exp Optom*. 2021;104(6):698–704. https://doi.org/10.1080/08164622.2021.1878843

17. Demirayak B, Tugan BY, Toprak M, Çinik R. Digital eye strain and its associated factors in students during the COVID-19 pandemic. *Indian J Ophthalmol*. 2022;70(3):988–992. https://doi.org/10.4103/ijo.IJO_1920_21

18. Altalhi A, Khayyat W, Khojah O, Alsalmi M, Almarzouki H. Computer vision syndrome among Health Sciences students in Saudi Arabia: Prevalence and risk factors. *Cureus*. 2020;12(2):e7060. https://doi.org/10.7759/cureus.7060

19. Wang G, Zhang Y, Zhao J, Zhang J, Jiang F. Mitigate the effects of home confinement on students during the COVID-19 outbreak. *Lancet*. 2020;395:945–947.

20. Zhao Y, Guo Y, Xiao Y, et al. The effects of online homeschooling on students, parents, and teachers of grades 1-9 during the COVID-19 pandemic. *Medical Sci Moni*. 2020;26:925591–925591. https://doi.org/10.12659/MSM.925591

21. Mohan A, Sen P, Shah C, Jain E, Jain S. Prevalence and risk factor assessment of digital eye strain among students using online e-learning during the COVID-19 pandemic: Digital eye strain among kids (DESK study-1). *Indian J Ophthalmol*. 2021;69(1):140–144. https://doi.org/10.4103/ijo.IJO_2535_20

22. Wang W, Zhu L, Zheng S, et al. Survey on the progression of myopia in students and adolescents in Chongqing during COVID-19 pandemic. *Front Public Health*. 2021;9:e646770. https://doi.org/10.3389/fpubh.2021.646770

23. Shantakumari N, Eldeeb R, Sreedharan J, Gopal K. Computer use and vision. related problems among university students in Ajman, United Arab Emirate. *Ann Med Health Sci Res*. 2014;4(2):258–263.

24. Blehm C, Vishnu S, Khattak A, Mitra S, Yee RW. Computer vision syndrome: A review. *Surv Ophthalmol*. 2005;50(3):253–262. https://doi.org/10.1016/j.survophthal.2005.02.008

25. Usgaonkar U, Shet Parkar SR, Shetty A. Impact of the use of digital

devices on eyes during the lockdown period of COVID-19 pandemic. *Indian J Ophthalmol*. 2021;69(7):1901–1906. https://doi.org/10.4103/ijo.IJO_3500_20

26. Gupta R, Chauhan L, Varshney A. impact of E-schooling on digital eye strain in Coronavirus disease era: A survey of 654 students. *J Current Ophthalmology*. 2021;33(2):158–164. https://doi.org/10.4103/joco.joco_89_20

27. Ganne P, Najeeb S, Chaitanya G, Sharma A, Krishnappa NC. Digital eye strain epidemic amid COVID-19 pandemic-a cross-sectional survey. *Ophthalmic Epidemiol*. 2021;28(4):285–292. https://doi.org/10.1080/09286586.2020.1862243

28. Klieštik T, Kočišová K, Mišanková M. Logit and probit model used for prediction of financial health of company. *Procedia Econ Finance*. 2015;23:850–855. https://doi.org/10.1016/s2212-5671(15)00485-2

29. Hayes AF, Matthes J. Computational procedures for probing interactions in OLS and logistic regression: SPSS and SAS implementations. *Behav Res Methods*. 2009;41(3):924–936. https://doi.org/10.3758/BRM.41.3.9242

30. Maduraiveeran J, Kanna SS, Silamparasan B, Johnsy J. Recent developments regarding Lacunary-Statistical convergence in Neutrosophic n-Normed linear spaces. *Sci Inq Rev*. 2022;6(3):61–78. https://doi.org/10.32350/sir.63.04

31. Ali U, Ishtiaq U, Ahmad K. Statistically convergent sequences in Neutrosophic metric spaces. *Sci Inq Rev*. 2022;6(1) :37–54. https://doi.org/10.32350/sir.61.03

Scientific Inquiry and Review (SIR)
Volume 7 Issue 2, 2023
ISSN (P): 2521-2427, ISSN (E): 2521-2435
Homepage: https://journals.umt.edu.pk/index.php/SIR

Article QR

Title: **Isolation and Identification of *Lawsonia* Content from Leaves of Henna (*Lawsonia inermis)***

Author (s): Muhammad Aslam[1], Sana Siddique[1], Muhammad Zaheer[2], Muhammad Zia-Ur-Rehman[2], Zahra Noreen[3], Yousuf Abbas[1], Aamir Sohail[1], Muhammad Aneeq Javed[1], Madiha Rashid[3], Aamir Ali[4]

Affiliation (s):
[1]Department of Chemistry, University of Education, Lahore, Pakistan
[2]Applied Chemistry Research Center (ACRC), Pakistan Council of Scientific and Industrial Research (PCSIR), Lahore, Pakistan
[3]Department of Botany, University of Education, Lahore, Pakistan
[4]Geological Survey of Pakistan, Lahore, Pakistan

DOI: https://doi.org/10.32350/sir.72.04

History: Received: January 14, 2023, Revised: March 05, 2023, Accepted: March 06, 2023, Published: June 15, 2023

Citation: Aslam M, Siddique S, Zaheer M, et al. Isolation and identification of Lawsonia content from leaves of Henna (Lawsonia inermis). *Sci Inq Rev.* 2023;7(2):71–80. https://doi.org/10.32350/sir.72.04

Copyright: © The Authors

Licensing: This article is open access and is distributed under the terms of Creative Commons Attribution 4.0 International License

Conflict of Interest: Author(s) declared no conflict of interest

A publication of
The School of Science
University of Management and Technology, Lahore, Pakistan

Isolation and Identification of Lawsonia Content from the Leaves of Henna (*Lawsonia inermis*)

Muhammad Aslam[1*], Sana Siddique[1], Muhammad Zaheer[2], Muhammad Zia-Ur-Rehman[2], Zahra Noreen[3], Yousuf Abbas[1], Aamir Sohail[1], Muhammad Aneeq Javed[1], Madiha Rashid[3], and Aamir Ali[4]

[1]Department of Chemistry, Division of Science and Technology, University of Education, Lahore, Pakistan
[2]Applied Chemistry Research Center (ACRC), Pakistan Council of Scientific and Industrial Research (PCSIR), Lahore, Pakistan
[3]Department of Botany, Division of Science and Technology, University of Education, Lahore, Pakistan
[4]Geological Survey of Pakistan, Lahore, Pakistan

ABSTRACT

Lawsone is an orange red dye mainly isolated from *Lawsonia inermis* plant leaves. *L. inermis* is commonly known as henna plant, Egyptian privet, or mignonette tree. In Pakistan, henna is known as *mehndi*. Paste from thick henna leaves has been used to dye hairs, fingernails, palms of hands, and eyebrows for more than 5000 years. The characteristic colour of henna is because of the natural dye lawsone present in it. In this study, lawsone was extracted from four samples of henna leaves collected from various parts of Pakistan. Moreover, the impact of the environment on the leaves was examined. Lawsone was extracted using diethyl ether, so that the maximum amount of lawsone could be isolated from the leaves. The maximum and minimum amount of lawsone isolated during this work was 1.01% and 0.745% of dry weight, respectively. Afterwards, IR and HPLC were used to identify the isolated reddish-brown substance known as lawsone which is useful in textile, cosmetics, and pharmaceutical sectors.

Keywords: dye, Henna, *Lawsonia inermis*, lawsone, plant

1. INTRODUCTION

Lawsonia inermis is commonly known as henna plant, Egyptian privet, or mignonette tree [1, 2]. In Pakistan, henna is known as mehndi. The principal colouring component of this plant is known as lawsone. This plant is grown on a large scale in Sindh and Baluchistan, two provinces of Pakistan [3]. However, due to its medicinal and cosmetic applications, it is

* Corresponding Author: maslamchemist@hotmail.com

cultivated throughout the world [4]. It is a significant medicinal plant that has drawn the attention of scientists from all over the world due to its amazing pharmacological properties [5]. It is a mid-sized, highly branched shrub. Several medicinal uses have been reported for its flower, seed, roots, and stem [6]. It is used to dye hair, skin, and nails [7]. Skin and hair colour are extracted from lawsone by using the technique based on Michael addition reaction theory. A non-permanent colouration that can last up to two to three weeks is produced when Lawsone makes a covalent link with the keratin protein present in skin and hair. The interaction between lawsone and keratin determines colour intensity [8]. Darker colouration results from a greater lawsone-keratin interaction. However, with the passage of time, lawsone is dissolved in water. As a result, lawsone concentration decreases and henna stain fades away [9].

Chemically, lawsone is a 2-hydroxy-1,4-naphthoquinone, also known as hennotannic acid [10]. Lawsone is an orange-red dye mainly found in *Lawsonia inermis* leaves. It is also present in other plant components, although the amount is quite small [11]. Lawsone gets its name from the plant it is derived from, that is, *Lawsonia inermis*. The genus *Lawsonia* includes only two species, that is, *L. inermis* and *L. odorata*. Lawsone is present in very small amounts in *Lawsonia odorata*. A minor quantity of lawsone was also observed in water hyacinth bloom [12].

Human beings have been using henna extracts containing lawsone for at least 5000 years to dye their hair and skin [13]. Lawsone shows an excellent antifungal, antibacterial, antitumor, antiviral, and pesticidal activity [14, 15]. The amount of lawsone in henna plant leaves varies by region. Geological conditions and a number of environmental factors affect its concentration [16]. Moreover, soil temperatures between 25°C and 30°C are ideal for the germination of this plant. Although, it may also survive in the temperature range of 35°C to 45°C [17]. In comparison to winter, a higher concentration of lawsone is observed in henna leaves during summer [18]. The current study highlights the effect of environmental conditions on lawsone content cultivated in different areas of Pakistan.

2. MATERIALS AND METHOD

Experimental work regarding the isolation and identification of lawsone content from the leaves of henna was carried out in the laboratory of Pakistan Council of Scientific and Industrial Research (PCSIR), Lahore.

HPLC instrument used in this experiment was designed by Shimadzu Corporation, Japan. While, the column used was LC-18 and SPD 6AV UV-detector, adjusted at 260nm. Henna leaves used in this work were collected from different areas of Sindh and Punjab. The identification of samples was confirmed by the Department of Botany, University of Education, Lahore. All the samples were shade dried.

Dried henna leaves sample (100g) was added in a 5L Erlenmeyer flask containing 5000ml distilled water and refluxed at 80^0C till the vapours stopped coming out of the flask. The suspension was stirred continuously with the help of magnetic stirrer to avoid any sort of coagulation. After approximately 3 hours, the colour of suspension turned brown and the reflux assembly was removed. Suspension was left overnight. Then, the suspension was made alkaline by adding sodium bicarbonate (20g). Alkaline suspension was then filtered and the filtrate was made acidic by adding 0.12M hydrochloric acid till the pH of the solution became 3. Lawsone was extracted by using diethyl ether. Excessive solvent was evaporated on a hot plate at 30^0C to avoid the burning of lawsone. Isolated reddish-brown material was then scratched and stored in a pre-weigh vial. The same procedure was reported for other samples and the isolated lawsone was stored in pre-weighed vials, separately (Figure 1 and 2) [16].

Figure 1. Powdered Henna Leaves Sample Collected from Different Areas

3. RESULTS AND DISCUSSION

The amount of lawsone isolated from four different henna leaves samples was not more than 1% of the dry weight of samples (Table 1). The percentage of the isolated reddish-brown material depicted the effect of environmental conditions on the lawsone content. The material was identified by using IR and HPLC and the results were compared with the standard chemical lawsone.

Table 1. Percentage of Lawsone Isolated from Different Henna Samples

Henna Leaves Samples	Percentage of Lawsone Extracted
Sample leaves 1 (S1)	1.010
Sample leaves 2 (S2)	0.845
Sample leaves 3 (S3)	0.785
Sample leaves 4 (S4)	0.744

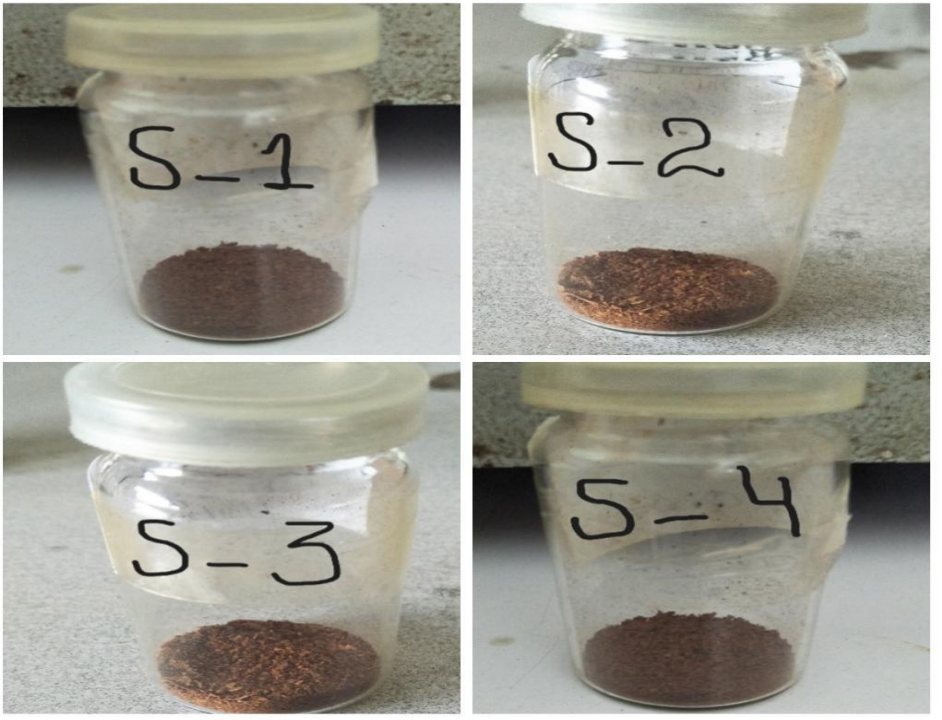

Figure 2. Reddish Brown Material Isolated from Different Henna Leaves Samples

3.1. IR Spectra

The IR spectra of the isolated material shows different peaks. Each peak corresponds to a specific functional group. The stretching of the O-H functional group, overlaid by the naphthalene ring's C-H vibrations, reached its maximum at 3159 cm^{-1}. Carbonyl stretching caused peak formation at 1675 cm-1 and 1636 cm^{-1}. These peaks were expected to divide due to internal hydrogen bonds. Peaks at 1216 cm^{-1} were related to the stretching C-O, while peaks at 1584 and 1510 cm^{-1} were related to the naphthalene ring's C=C vibrational bands. The IR spectra peaks confirmed the chemical nature of the reddish-brown substance, namely lawsone (Figure 3).

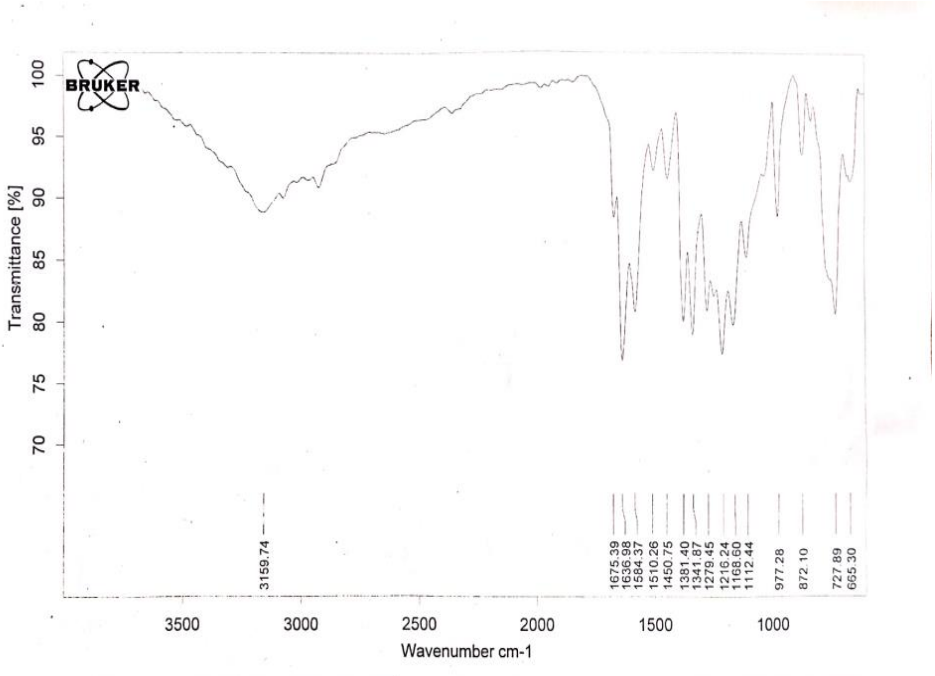

Figure 3. IR Spectra of Isolated Reddish-Brown Material

3.2. HPLC Analysis

The nature of the isolated material was further confirmed by HPLC. For this purpose, standard lawsone was purchased from Merck. A total of 50mg of standard and isolated material was used to prepare standard and sample solutions, respectively. Mobile phase used during the experiment was 70% methanol and 30% water. A significant resemblance between the separated

material's HPLC spectra and the standard lawsone HPLC spectra was observed. This resemblance proved that the isolated chemical was lawsone (Figure 4).

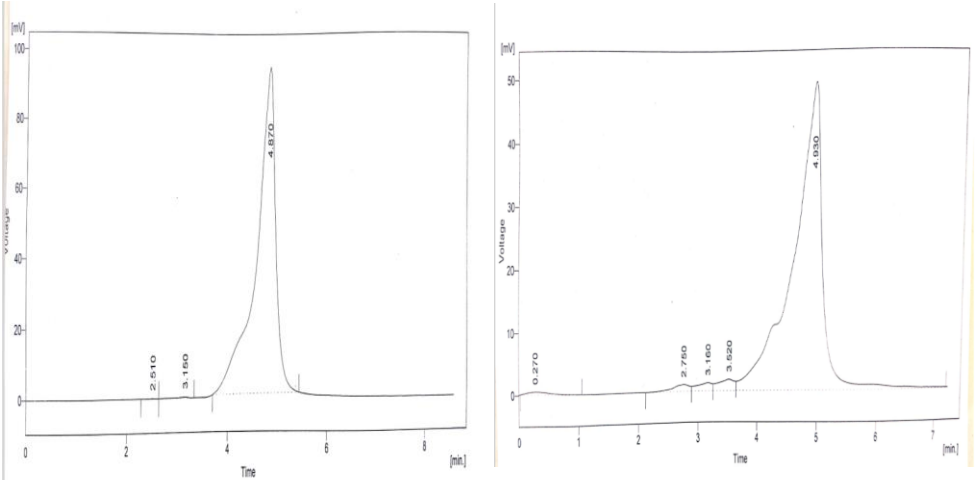

Figure 4. HPLC Spectra of Standard and Isolated Reddish-Brown Material

3.3. Effect of Geological Conditions on Lawsone Content

Henna leaves collected from areas with a high temperature and dry air have more lawsone. High temperature is favorable for lawsone content in henna leaves. Moreover, henna plants cultivated during summer have more lawsone content in their leaves than those cultivated in winter.

3.4. Factors Effecting Lawsone Content

3.4.1. Effect of Temperature. Temperature has a strong influence on the amount of lawsone extracted from *Lawsonia inermis* leaves [19]. This is because if the extraction temperature exceeds 80^0C, then most of lawsone is either dissolved in water or burned out. Similarly, if the temperature exceeds the boiling temperature of the solvent during the isolation of lawsone from diethyl ether, then all the lawsone is burnt.

3.4.2. Effect of pH. Change in pH does affect lawsone concentration but its effects are less harsh as compared to temperature. A slight change in pH can be neglected but a major change does affect the lawsone yield. The greater the pH of solution the lesser is the amount of the isolated lawsone. pH also affects the colour of the extract [20].

4. CONCLUSION

The primary colouring component of the *Lawsonia inermis* plant is lawsone. The identification of environmental conditions and their impact on lawsone content were studied in this research. Lawsone was extracted from four different kinds of henna leaves samples. The maximum and minimum amount of lawsone isolated during this work was 1.01% and 0.745% of dry weight, respectively. The percentage yield made it evident that sample leaves from Sindh contained more lawsone than sample leaves from Punjab. Thus, it was concluded that the weather conditions of Sindh are in favor of lawsone content in *Lawsonia inermis* leaves. Moreover, it was also determined that henna plants harvested in the summer season have more lawsone than those harvested in winters. Thus, isolated lawsone can be used in the pharmaceutical industry and as a dying agent in cosmetic and textile industries.

REFERENCES

1. Adam AEA. *Toxicity of the Aqueous and Ethanol Extracts of Ginger (Zingiber Officinale L.) Rhizome and Henna (Lawsonia inermis L.) Leaves on Mosquitoes (Anopheles and Culex) larvae* [doctoral dissertation]. University of Gezira; 2015.

2. Talab TA, Alfuraiji N, Al-Snafi AE. The analgesic and anti-inflammatory effect of lawsone isolated from *lawsonia inermis*. *Pharm Sci*. 2022;1(35):77–84. https://doi.org/10.15587/2519-4852.2022.253555

3. Younas A, Kiran S, Abrar S, Javed S, Gulzar T. Ultrasonic-assisted extraction and characterization of natural colorants from plants and evaluation of their therapeutic properties and cytotoxicity. *Pol J Environ Stud*. 2022;31(6):5945–5954. https://doi.org/10.15244/pjoes/151862

4. Sankar J, Kini M, Mhaskar S, Sangle P. Estimation of lawsone release from *Lawsonia inermis* Leaf Powder. *Trend Agric Sci*. 2022;1(1):28–34. https://doi.org/10.17311/tas.2022.28.34

5. Dixit K, Mohapatra D, Senapat PC, Panda R, Sahu AN. Formulation development and evaluation of *Lawsonia inermis* extract loaded hydrogel for wound dressing application. *Indian J Pharm Sci*. 2022;84(4):848–862. http://doi.org/10.36468/pharmaceutical-sciences.980

6. Bakkali AT, Jaziri M, Foriers A, Heyden YV, Vanhaelen M, Homes J. Lawsone accumulation in normal and transformed cultures of henna, Lawsonia inermis. *Plant Cell Tissue Organ Cult.* 1997;51:83–87. https://doi.org/10.1023/A:1005926228301

7. Rostowski H, Nowak MJ, Lapinski L, Adamowicz L. Molecular structure and infrared spectra of 2-hydroxy-1,4- naphthoquinone; Experimental matrix isolation and theoretical Hartree–Fock and post Hartree–Fock study. *Spectrochim Acta A Mol Biomol Spectrosc*. 1998; 54(8):1091–1103. https://doi.org/10.1016/S1386-1425(98)00032-8

8. Umadevi R, Gursharanpreet KB, Mariam-Aisha F. Characterisation of henna as a determinant for organic fabric integrity. *J Manag Sci*. 2016;14(2):45–55.

9. Jordao AK, Vargas MD, Pinto AC, da Silva FDC, Ferreira VF. Lawsone in organic synthesis. *RSC Adv*. 2015;5:67909–67943. https://doi.org/10.1039/C5RA12785H

10. Hijji YM, Barare B, Zhang Y. Lawsone (2-hydroxy-1,4-naphthoquinone) as a sensitive cyanide and acetate sensor. *Sens Actuators B Chem*. 2012;169(5):106–112. https://doi.org/10.1016/j.snb.2012.03.067

11. Ostovari A, Hoseinieh SM, Peikari M, Shadizadeh SR, Hashemi SJ. Corrosion inhibition of mild steel in 1 M HCl solution by henna extract: A comparative study of the inhibition by henna and its constituents (Lawsone, Gallic acid, α-D-Glucose and Tannic acid). *Corros Sci*. 2009;51(9):1935–1949. https://doi.org/10.1016/j.corsci.2009.05.024

12. Dweck C. Natural ingredients for colouring and styling. *Int J Cosmet Sci*. 2002;24(5):287–302. https://doi.org/10.1046/j.1467-2494.2002.00148.x

13. Petkewich, R. Henna dye derived from green leaves is used to decorate the body with intricate designs. *J Am Chem Soc*. 2006;84:15–20. https://doi.org/10.1021/cen-v084n006.p028

14. Kapadia GJ, Rao GS, Sridhar R, et al. Chemoprevention of Skin Cancer: Effect of *Lawsonia inermis* L. (Henna) Leaf Powder and its Pigment Artifact, Lawsone in the Epstein- Barr Virus Early Antigen Activation Assay and in Two-Stage Mouse Skin Carcinogenesis Models.

Anticancer Agents Med Chem. 2013;13(10):1500–1507. http://doi.org/10.2174/18715206113139990096

15. Rahmoun NM, Boucherit-Otmani Z, Boucherit K, Benabdallah M, Villemin D, Choukchou-Braham N. Antibacterial and antifungal activity of lawsone and novel naphthoquinone derivatives. *Med Mal Infect*. 2012;42(6):270–275. https://doi.org/10.1016/j.medmal.2012.05.002
16. Alem FZ, Gita SA, Cougnaud L, et al. Lawsone quantification in *Lawsonia inermis L.* by HPLC-MS: How does the temperature and pluviometry affect lawsone concentration. *Ind Crops Prod*. 2020;158(15):e112960. https://doi.org/10.1016/j.indcrop.2020.112960
17. Bechtold T, Mussak R. *Handbook of Natural Colorants*. Wiley Publishers; 2009.
18. Karawya MS, Wahhab SMA, Zaki AY. A study of the lawsone content in henna. *Lloydia*. 1969;32:76–78.
19. Barani M, Mirzaei M, Torkzadeh-Mahani M, Nematollahi MH. Lawsone-loaded Niosome and its antitumor activity in MCF-7 breast cancer cell line: a Nano-herbal treatment for cancer. *J Pharm Sci*. 2018;26:11–17. https://doi.org/10.1007/s40199-018-0207-3
20. Saeed G, Sayeed SA, Ashraf S, et al. A new method for the isolation and purification of Lawsone from Lawsonia Inermis and its ROS inhibitory activity. *Pak J Bot*. 2013;45(4):1431–1436.

Scientific Inquiry and Review (SIR)
Volume 7 Issue 2, 2023
ISSN (P): 2521-2427, ISSN (E): 2521-2435
Homepage: https://journals.umt.edu.pk/index.php/SIR

Article QR

Title:	**Review of Pharmacological Activity of Ephedra Gerardiana**
Author (s):	Halima Nazar[1], Azalfa Amar[1], Mohmmad Younus[2], Ghazala Shaheen[3], Muhammad Asif[3], Farah Zafar[3], Sultan Ayaz[4]
Affiliation (s):	[1]Jinnah University for Women Karachi, Pakistan [2]Younus Dawakhana, Karachi, Pakistan [3]University College of Conventional Medicine, The Islamia University of Bahawalpur [4]Department of Eastern Medicine, GC University, Faisalabad
DOI:	https://doi.org/10.32350/sir.72.05
History:	Received: December 08, 2022, Revised: January 10, 2023, Accepted: January 10, 2023, Published: June 15, 2023
Citation:	Nazar H, Amar A, Younus M, et al. Review of pharmacological activity of Ephedra Gerardiana. *Sci Inq Rev.* 2023;7(2):81–100. https://doi.org/10.32350/sir.72.05
Copyright:	© The Authors
Licensing:	This article is open access and is distributed under the terms of Creative Commons Attribution 4.0 International License
Conflict of Interest:	Author(s) declared no conflict of interest

A publication of
The School of Science
University of Management and Technology, Lahore, Pakistan

Review of Pharmacological Activity of Ephedra Gerardiana

Halima Nazar[1], Azalfa Amar[1], Mohmmad Younus[2], Ghazala Shaheen[3*], Hafiz Muhammad Asif[3], Farah Zafar[3], and Sultan Ayaz[4]

[1]Department of Eastern Medicine, Jinnah University for Women Karachi, Pakistan
[2]Younus Dawakhana, Karachi, Pakistan
[3]University College of Conventional Medicine, The Islamia University of Bahawalpur, Pakistan
[4]Department of Eastern Medicine, GC University, Faisalabad, Pakistan

ABSTRACT

Ephedra gerardiana (E. gerardiana,), commonly known as "Ma-huang," is a medicinal plant native to the Himalayan region. Historically, it has a long traditional use in various indigenous systems for medicinal purpose. The current review aims to summarize the present knowledge on the botanical description, phytochemistry, traditional uses, and pharmacological properties of *E. gerardiana*. This study was thoroughly based on previous literature and was conducted by using electronic databases such as PubMed, Scopus, and Google Scholar. Relevant studies and recently published articles up till 2020 were included in this review. *E. gerardiana* is a small shrub-like plant characterized by jointed stems, scale-like leaves, and cylindrical cones. It belongs to the family Ephedraceae and is commonly found in arid and semi-arid regions. Phytochemical analysis has revealed the presence of various bioactive compounds in Ephedra gerardiana, including ephedrine, pseudoephedrine, norephedrine, and methyl ephedrine. These alkaloids are primarily responsible for their pharmacological activities. In traditional medicine, Ephedra gerardiana has been used for its bronchodilatory, diaphoretic, diuretic, and thermogenic properties. Additionally, it has been employed for the treatment of respiratory disorders, namely, asthma and nasal congestion, as a stimulant. Its bioactive alkaloids, particularly ephedrine, have been extensively studied for their potential therapeutic applications. However, caution should be exercised due to the potential side effects associated with ephedrine-containing products. Further research can explore its mechanisms of action, optimize dosage regimens, and investigate potential drug interactions to ensure its safe and effective use in clinical settings.

* Corresponding Author: Ghazala.shaheen@iub.edu.pk

Keywords: botanical description, *Ephedra gerardiana*, Ma-huang, phytochemistry, pharmacological properties, traditional uses

1. INTRODUCTION

Ephedra gerardiana is a herbal drug, which contains many useful features. This herbal drug has many medicinal uses. It belongs to the family of Ephedraceae and its plant is approximately 1-4 feet long. It has red berries because of this; the plant becomes more beautiful and attractive.

The red colour of berries is due to the presence of their chemical constituent Flavonones.

According to the Unani system of medicine temperament of ephedra is hot and dry in a second order. In the Unani system of medicine drugs, which belong to second-order temperament, are used to treat phlegmatic disorder more easily and rapidly.

The pharmacological activities include anti-inflammatory, alterative, diuretic, expectorant, anti-inflammatory, and bronchitis.

The most effective action of this herbal drug is on our respiratory system. In Chinese medicine, it is also known as Mahaung.

Its most important biomarkers are Ephedrine and Pseudo-ephedrine.

The plant parts, which are used in medicine, are branches, flowers, and fruits.

2. METHODOLOGY

Different online databases were examined to highlight the therapeutical potential of *Ephedra gerardiana*, including Springer-Link, Google, PubMed, MEDLINE Data, Wiley Online Library, Science Direct, and Google Scholar. Data were searched using different keywords, such as pharmacological/biological activities, chemical constituents, morphology, habitat, characteristics, and `distribution of *Ephedra gerardiana*.

2.1. Pharmacognostic Features

Latin Name: *Epheragerardiana* Wall, *Ephedra vulgaris*
Family: Epheraceae.
Arabic Name: ZanbulKhail.
Urdu Name: Somkalpana, Masania, Narom, Somkalpa
English Name: Ephedra, Joint Pine, Brigham Tea.

Hindi Name: Som, Tutgantha.

2.2. Characteristics

It is a small shrub, which grows up to 1-4 feet. The stem of the plant has a nodule with dark green branches.

The leaves are small and round. The flowers are 6-10 mm long and unisexual naturally. The fruit of the plant is sweet, round in shape, red in colour, and has 1-2 seeds.

2.3. Habitat

Endemic to the mountains of Afghanistan, Bhutan, Northem India, Nepal, Sikkim, and Tibet.

2.4. Chemical Constituent

In all types of herbal drugs, there are different chemicals, which give them different pharmacological activity and medicinal uses, along with different side effects.

The ephedra chemicals are:

lignans, flavonoids, pseudoephedrine, ephedrine.

The root contains spermine alkaloids, Phenylethylamine alkaloids, Polysaccharides, Catechols, Tyrosine Derivatives, and EphedranineA& B.

The most important chemicals are ephedrine and pseudo-ephedrine [1–3].

The chemical constituents , which are separated from the herbal plants are more than 145 including alkaloids, flavonoids, tannins, and polysaccharides. The compounds separated from each species are enlisted in Tables 1-4. Their chemical structures are given in Fig. 1–5.

Table 1. Alkaloids Different Species of the Genus Ephedra (the structures of main compounds are illustrated in Fig. 1)

Classification	Chemical name	Plant source	Ref
Macrocyclic spermine alkaloids	Ephedradine A (1)	E. sinica (root)	[4]
	Ephedradine B (2)	E. sinica (root)	[5]
	Ephedradine C (3)	E. sinica (root)	[5]

Classification	Chemical name	Plant source	Ref
	Ephedradine D (4)	E. sinica (root)	
Imidazole alkaloid	Feruloylhistamine (5)	E. sinica (root)	[6]
Amphetamine-type alkaloids	D(–)-Ephedrine (**6**)	*E.Sinica*,*E.nebrodensis*, *E. major*	[7]
	L(+)-Pseudoephedrine (**7**)	*E. sinica*, *E. nebrodensis*	[8]
	D(–)Norephedrine (**8**)	*E. sinica*, *E. nebrodensis*	[8]
	L(+)-Noreseudoephedrine (**9**)	*E. sinica*	[9]
	D(–)Methyl ephedrine (**10**)	*E. sinica*, *E. nebrodensis*	[8]
	L(+)-Methylpseudoephedrine(**11**)	*E. sinica*, *E. nebrodensis*	[10]
	Ephedroxane (**12**)	*E. sinica*	[11]
	3, 4-Dimethyl-5-pheyloxazolidine (**13**)	*E. sinica*	[11]
	2, 3, 4-Trimethyl-5-phenyloxazolidine (**14**)	*E. sinica*	[11]
	O-benzoyl-L(+)-pseudoephedrine (**15**)	*E. sinica*	[11]
	O-benzoyl-D(–)-ephedrine (**16**)	*E. aphylla*	
	Hordenine (**17**)		
Quinoline alkaloids	Transtorine (**18**)	*E. transitoria*	[12]
	6-Methoxykynurenic acid (**19**)	*E. pachyclada*ssp. *Sinaica*	[13]
	Kynurenic acid (**20**)	*E. pachyclada*ssp. *Sinaica*	[13]
	6-Hydroxykynurenic acids (**21**)	*E. foemine*assp. *Foliate*	[13]
	Ephedralone (**22**)	*E. Alata*, *E. aphylla*	[14]
Pyrrolidine alkaloid	*cis*-3, 4-Methanoproline (**23**)	*E. foemine*assp. *foliate* (seed)	[13]
Other alkaloids	Maokonine (**24**)	*E. sinica*(root)	[15]
	(±)-1-Phenyl-2-imido-1-propanol (**25**)	*E. sinica*	[16]
	Tetramethylpyrazine (**26)**	*E. sinica*	[16]
	N-methybenzlamine (**27)**	*E. sinica*	[16]
	(2*S*,3*S*,4*S*)-2(carboxycyclopropyl)glycine (**28)**	*E. altissima*	[13]

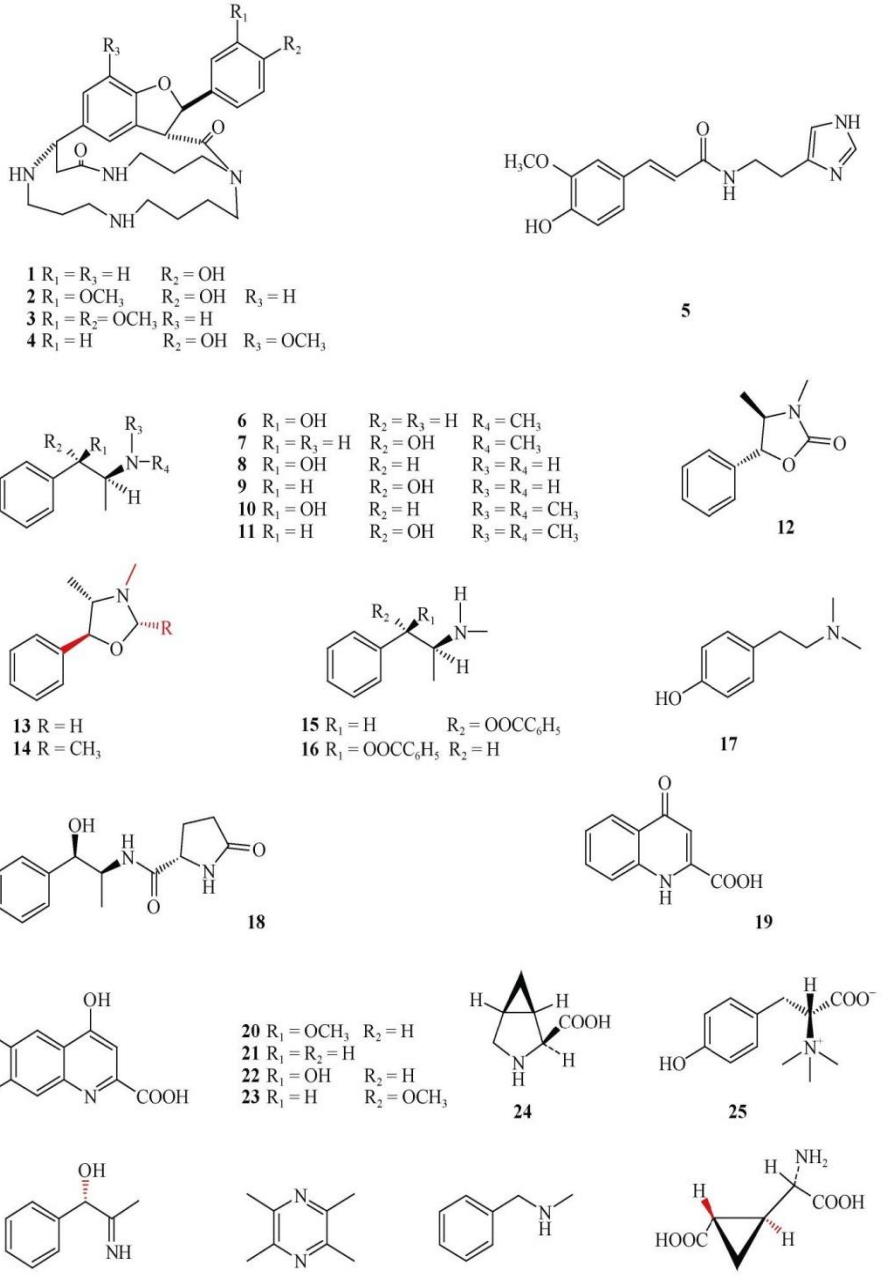
1 R1 = R3 = H R2 = OH
2 R1 = OCH3 R2 = OH R3 = H
3 R1 = R2 = OCH3 R3 = H
4 R1 = H R2 = OH R3 = OCH3
5
6 R1 = OH R2 = R3 = H R4 = CH3
7 R1 = R3 = H R2 = OH R4 = CH3
8 R1 = OH R2 = H R3 = R4 = H
9 R1 = H R2 = OH R3 = R4 = H
10 R1 = OH R2 = H R3 = R4 = CH3
11 R1 = H R2 = OH R3 = R4 = CH3
12
13 R = H
14 R = CH3
15 R1 = H R2 = OOCC6H5
16 R1 = OOCC6H5 R2 = H
17
18
19
20 R1 = OCH3 R2 = H
21 R1 = R2 = H
22 R1 = OH R2 = H
23 R1 = H R2 = OCH3
24
25

Figure 1. Structures of Different Alkaloids of *Ephedra*

Table 2. Flavonoids of Different Species of the Genus *Ephedra* (the structures of main compounds are illustrated in Fig. 2)

Classification	Chemical name	Plant source	Ref.
Flavonols	Herbacetin (29)	*E. sinica*	[17]
	Kaempferol (30)	*E. sinica*(root)	[18]
	Quercetin (31)	*E. sinica*(root)	[18]
	Herbacetin 7-methyl ether (32)	*E. sinica*	[17]
	Rutin (33)	*E. campylopoda*	[9] [19]
	Herbacetin 8-methyl ether3-*O*-glucoside-7-*O*-rutinoside (34)	*E. alata*	[19]
	Herbacetin 7-*O*-(6″-quinylglucoside) (35)	*E. alata*	[19]
	Herbacetin 3-*O*-rhamnoside 8-*O*-glucoside (36)	*E. aphylla*	[20]
	Pollenitin B (37)	*E. sinica*	[20]
	Herbacetin-8-methyl ether 3-*O*-glucoside (38)	*E. sinica*	[20]
	Herbacetin 7-*O*-glucoside (39)	*E. sinica*	[20]
	Kaempferol 3-*O*-rhamnoside 7-*O*-glucoside (40)	*E. sinica*	[20]
	Herbacetin 7-*O*-neohesperidoside (41)	*E. sinica*	[20]
	Kaempferol-3-*O*-glucoside-7-*O*-rhamnoside (42)	*E. sinica*	[19]
	Kaempferol 3-*O*-rhamnoside (43)	*E. alata*	[19]
	Quercetin 3-*O*-rhamnoside (44)	*E. alata*	[9]
	Quercetin-3-*O*-glucoside (45)	*E. campylopoda*	
Dihydroflavonol	Dihydroquercetin (46)	*E. sinica*(root)	[18]
	3-Hydroxynaringenin (47)	*E. sinica*(root)	[18]
Flavonone	3′, 4′, 5, 7-Tetrahydroxy flavanone (48)	*E. sinica*(root)	[18]
	Naringenin (49)	*E. sinica*(root)	[21]
	Hesperidin (50)	*E. sinica*(root)	[22]

Classification	Chemical name	Plant source	Ref.
		E. sinica	
Flavanols	(–)-epicatechin (51)	*E. sinica E. nebrodensis*	[23]
	(–)-epiafzelechin (52)		[18]
	Catechin (53)	*E. sinica*(root)	[20]
	Afzelechin (54)		[18]
	Leucocyanidin (55)	*E. sinica*	[20]
	Symplocoside (56)	*E. sinica*(root)	[20]
		E. sinica	
		E. sinica	
Flavones	Tricin (57)	*E. sinica*	
	Luteolin (58)	*E. sinica*	[24]
	Apigeni (59)	*E. sinica*(root)	[25]
	3-Methoxyherbacetin (60)		[18]
	Apigenin-5-rhamnoside (61)	*E. sinica*	[24]
	6-*C*-glycosyl-chrysoeriol (62)	*E. sinica*	[24]
	Swertisin (63)	*E. sinica*	[26]
	Isovitexin-2″-*O*-rhamnoside (64)	*E. sinica*	[27]
	Apigenin-7-*O*-glucoside (65)	*E. sinica*	[20]
	Vitexin (66)	*E. campylopoda*	[9]
	Lucenin III (67)	*E. sinica*	[20]
	2″, 2‴-Di-*O*-*β*-glucopyranosyl-vicenin II (68)	*E. alata*	[19]
		E. aphylla	[28]
Anthocyan	Leucodelphinidin (69)	*E. sinica*	[29]
	Leucopelargonin(70)	*E. sinica*	[29]

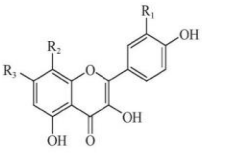

30 R_1 = H R_2 = R_3 =OH
31 R_1 = R_2 = H R_3 = OH
32 R_1 = OH R_2 = H R_3 = OH
33 R_1 = H R_2 = OH R_3 = OCH_3

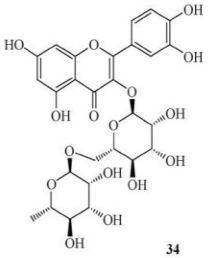

34

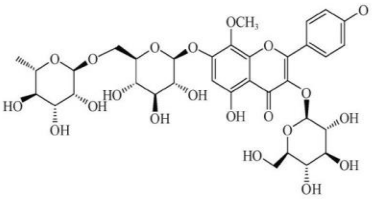

35

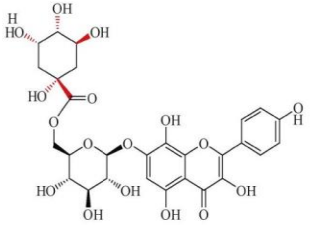

36

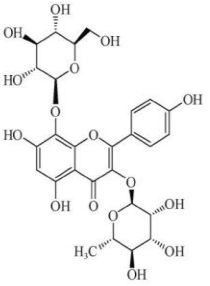

37

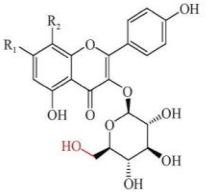

38 R_1 = OCH_3 R_2 = OH
39 R_1 = OH R_2 = OCH_3

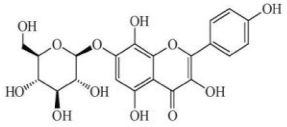

40

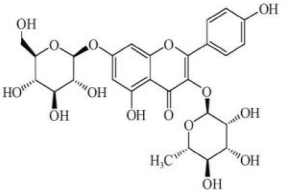

41

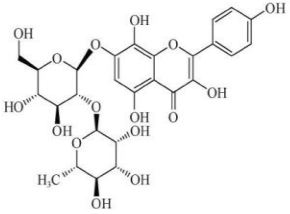

42

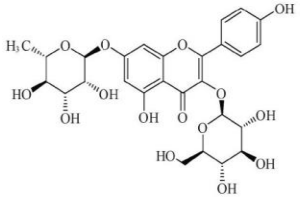

43

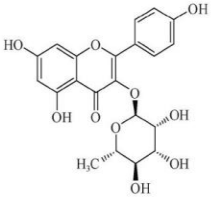

44

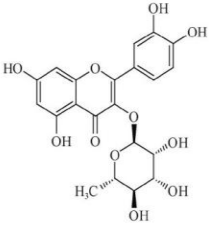

45

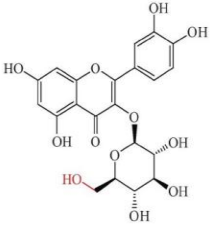

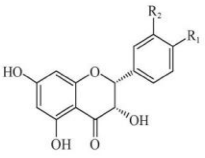

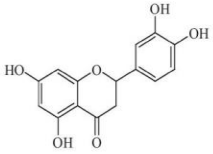

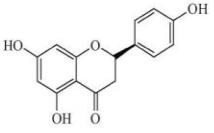

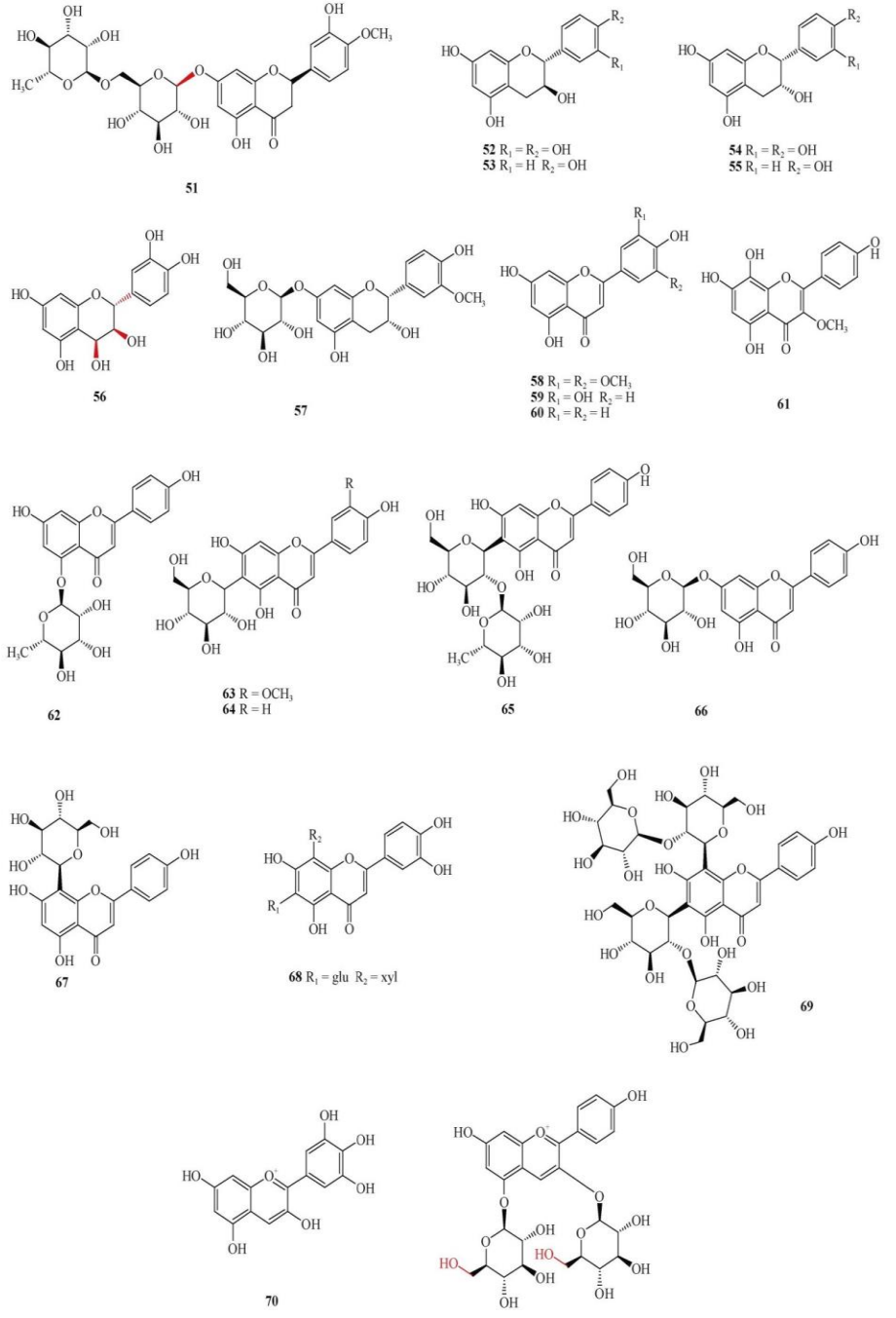

Figure 2. Structure of Different Flavonoids of *Ephedra*

Table 3. Tannins of Different Species of the Genus *Ephedra*

Classification	ChemicalName	PlantSource	Ref
Dimer proanthocyanidins	Ephedrannin A(71)		
	Ephedrannin B (**72**)		
	Muhuannin A (**73**)	*E. sinica*(root)	[30]
	Muhuannin D (**74**)	*E. sinica*(root)	[30]
	Muhuannin B (**75**)	*E. sinica*(root)	[31]
	Muhuannin E (**76**)	*E. sinica*(root)	[30]
	Muhuannin C (**77**)	*E. sinica*(root)	[30]
	Muhuannin F (**78**)	*E. sinica*(root)	[30]
	Muhuannin G (**79**)	*E. sinica*(root)	[30]
	Muhuannin H (**80**)	*E. sinica*(root)	[32]
	Muhuannin I (**81**)	*E. sinica*(root)	[32]
	Muhuannin J (**82**)	*E. sinica*(root)	[32]
	Muhuannin K (**83**)	*E. sinica*(root)	[32]
	Ephedrannin D1 (**84**)	*E. sinica*(root)	[32]
	Ephedrannin D2 (**85**)	*E. sinica*(root)	[32]
	Ephedrannin D3 (**86**)	*E. sinica*	[33]
	Ephedrannin D4 (**87**)	*E. sinica*	[33]
	Ephedrannin D5 (**88**)	*E. sinica*	[33]
	Ephedrannin D6 (**89**)	*E. sinica*	[33]
	Ephedrannin D7 (**90**)	*E. sinica*	[33]
	Ephedrannin D8 (**91**)	*E. sinica*	[33]
	Ephedrannin D9 (**92**)	*E. sinica*	[33]
	Ephedrannin D10 (**93**)	*E. sinica*	[33]
	Ephedrannin D11 (**94**)	*E. sinica*	[33]
	Ephedrannin D12 (**95**)	*E. sinica*	[33]
	Ephedrannin D13 (**96**)	*E. sinica*	[33]
	Ephedrannin D14 (**97**)	*E. herb*	[33]
Trimer proanthocyanidins	Ephedrannin Tr1 (**98**)	*E. sinica*	[33]
	Ephedrannin Tr2 (**99**)	*E. sinica*	[33]
	Ephedrannin Tr3 (**100**)	*E. sinica*	[33]
		E. sinica	[33]

Classification	ChemicalName	PlantSource	Ref
	Ephedrannin Tr4	*E. sinica*	[33]
	(**101**)	*E. sinica*	[33]
	Ephedrannin Tr5	*E. sinica*	[33]
	(**102**)	*E. sinica*	[33]
	Ephedrannin Tr6	*E. sinica*	[33]
	(**103**)	*E. sinica*	[33]
	Ephedrannin Tr7	*E. sinica*	[33]
	(**104**)	*E. sinica*	[33]
	Ephedrannin Tr8	*E. sinica*	[33]
	(**105**)	*E. sinica*	[33]
	Ephedrannin Tr9	*E. sinica*	[33]
	(**106**)		
	Ephedrannin Tr10		
	(**107**)		
	Ephedrannin Tr11		
	(**108**)		
	Ephedrannin Tr12		
	(**109**)		
	Ephedrannin Tr13		
	(**110**)		
	Ephedrannin Tr14		
	(**111**)		
	Ephedrannin Tr15		
	(**112**)		
Tetramer proanthocya- nidins	Ephedrannin Te1 (**113**)	*E. sinica*	[20]
	Ephedrannin Te2 (**114**)	*E. sinica*	[20]
	Ephedrannin Te3 (**115**)	*E. sinica*	[20]
	Ephedrannin Te4 (**116**)	*E. sinica*	[20]
	Ephedrannin Te5 (**117**)	*E. sinica*	[20]

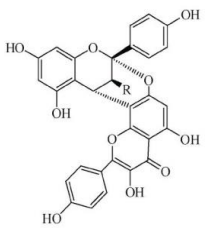

72 R = OH
73 R = H

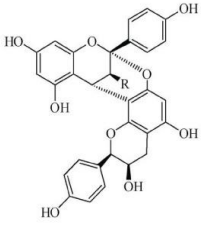

74 R = OH
75 R = H

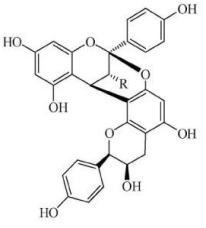

76 R = OH
77 R = H

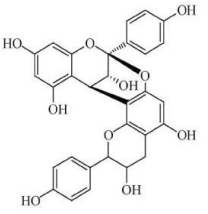

78

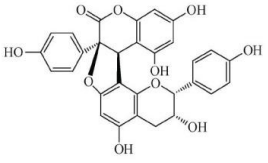

79

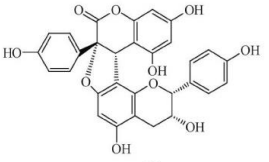

80

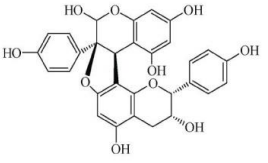

81

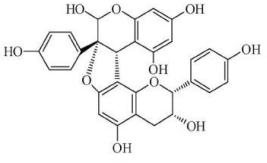

82

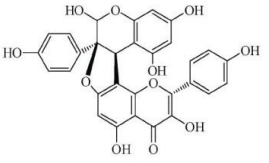

83

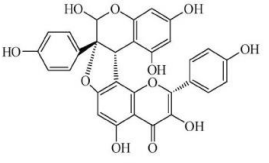

84

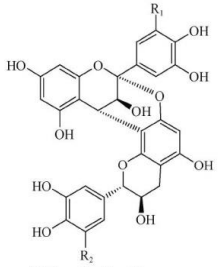

85 R_1 = OH R_2 = H
86 R_1 = OH R_2 = OH
87 R_1 = H R_2 = H

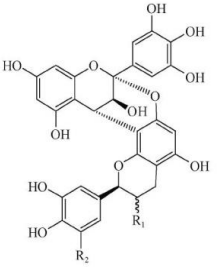

88 R_1 = —OH R_2 = H
89 R_1 = —OH R_2 = OH
90 R_1 = ····OH R_2 = OH
91 R_1 = ····OH R_2 = H

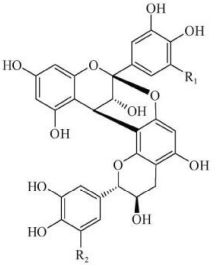

92 R_1 = OH R_2 = H
93 R_1 = OH R_2 = OH
94 R_1 = H R_2 = H

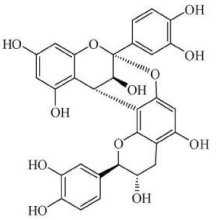

95

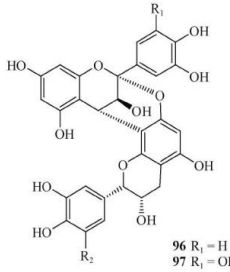

96 R_1 = H R_2 = H
97 R_1 = OH R_2 = H

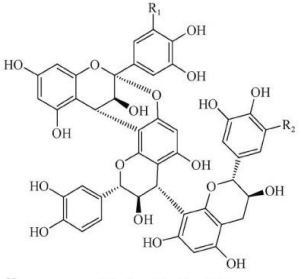

99 R_1 = H R_2 = OH
100 R_1 = OH R_2 = H

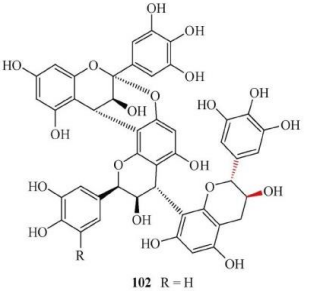

102 R = H

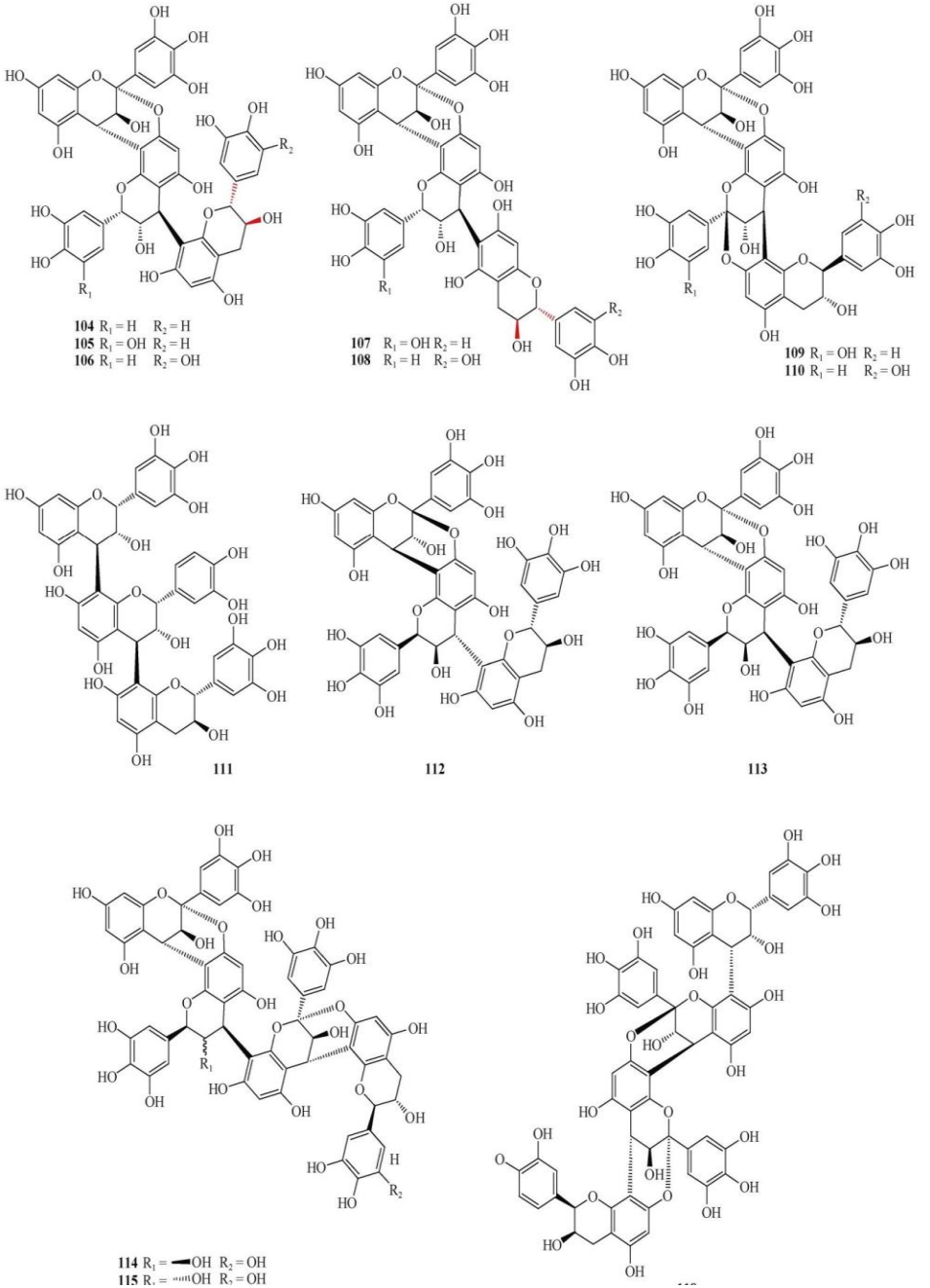

Figure 3. Different Tannins from *Ephedra*

3. PHARMACOLOGICAL ACTION

3.1. Cardiac Tonic

Ephedra is used as a cardiac tonic. It affects the CVS due to its biomarker Ephedrine, which is sympathomimetic amine activity. It increase the heart rate and also helps to manage low blood pressure to treat bradycardia, concerning hypotension. It also increases cardiac contractility mostly in hypotension conditions in which blood pressure usually droops [1].

A case of orthotic hypotension was observed in this condition having blood pressure, which suddenly dropped in the standing position, hence, use of infusion of ephedra very was considered effective in this condition in which the person's blood pressure became normal but it can not be used for a long time because it may also increase blood pressure [2, 34].

Ephedra has catechols constituents, which are alpha-receptor activity (vaso-constriction), due to which it can have vasoconstriction effects.

3.2. Respiratory System

Ephedra has two basic constituents' ephedrine and pseudoephedrine. Both of them gives a very good effect on the respiratory system. The constituents help to widen the lung's airway and also help to cure the nasal decongestant.

Additionally, they also help to treat asthma because these constituents have b-adrenergic receptors, which relax airway smooth muscles, hence, ephedra is noticed to be effective in asthma cases [2].

Ephedra has been effective in the respiratory system, especially in asthma that is why it is also known as DAMA BOTI.

3.3. Anti-Inflammatory

Ephedra also helped to reduce swelling. It has ephedranine A & B chemicals, which contain anti-inflammatory effects and reduce swelling, especially when applied in joint pain conditions like Rheumatoid Arthritis and Osteoarthritis. Paste of bark of ephedra should be applied on the affected area, which may give relief in pain and also in swelling [3].

Due to its effect on the joint, it is called Joint Pine.

3.4. Anti-Tumor Activity

Ephedra also has anti-tumor activity. It has two chemicals, namely, lignans, flavones both of which have anti-oxidant and anti-tumor properties, which suppress the growth of the tumor and also act as anti-bacterial medicine [2].

3.5. Renal System

Ephedra has another special property, which is Diuretic [1, 2].

It chemical ephedrine has multiple actions and one of them is Diuretic action. It produces a positive effect on renal system diseases such as renal calculi, urethritis, and UTI. , and those conditions in which dieresis is necessary through the kidney [1, 34]

3.6. Side Effects

Normally, any drug either it is herbal or synthetic, its excessive use can be harmful.

Prolong use of joint pine could elevate blood pressure because it has vasoconstriction property, which also helps to reduce lower blood pressure [2, 3].

It contraindicated in high blood pressure.

Some noticeable side effects include, vomiting, nausea, and minor abdominal pain [1, 35].

Some researches is also used in Obesity but in my point of view it not be useful for slimming medicine because it might be caused hypertension [1, 35].

4. CONCLUSION

Traditional medicine has employed *E. gerardiana* for its bronchodilatory, diaphoretic, diuretic, and thermogenic properties. The bronchodilatory effects of ephedrine have been extensively studied, leading to its inclusion in various over-the-counter medications for respiratory conditions. However, it is important to note that ephedrine-containing products have been associated with potential side effects and safety concerns. Adverse effects such as increased heart rate, elevated blood pressure, and central nervous system stimulation have been reported. Therefore, caution should be exercised when using E. gerardiana or

products containing ephedrine and it is advisable to consult with healthcare professionals before its usage. Further research is needed to elucidate the precise mechanisms of action of Ephedra gerardiana's bioactive compounds, optimize dosage regimens, and explore potential drug interactions. These studies would contribute to ensuring the safe and effective use of E. gerardiana in clinical settings and enhancing our understanding of its therapeutic potential. Concluding, E. gerardiana is a valuable medicinal plant but it should be used carefully, considering the potential risks associated with ephedrine-containing products.

REFERENCES

1. Zhang B-M, Zhi-Bin W, Ping X, Qiu-Hong W, He B, Kuang H-X. Phytochemistry and pharmacology of genus Ephedra. *Chin J Nat Med.* 2018;16(11):811–828. https://doi.org/10.1016/S1875-5364(18)30123-7
2. González-Juárez DE, Escobedo-Moratilla A, Flores J, et al. A review of the Ephedra genus: distribution, ecology, ethnobotany, phytochemistry and pharmacological properties. *Molecules.* 2020;25(14):e3283. https://doi.org/10.3390/molecules25143283
3. Chaudhary MK, Misra A, Srivastava S. Evaluation of ephedrine content and identification of elite chemotype (s) of Ephedra gerardiana (Wall.) from Kashmir Himalayas. *Proc National Acad Sci Ind Sec Biol Sci.* 2020;90(4):833–841. https://doi.org/10.1007/s40011-019-01153-2
4. Kurosawa W, Kan T, Fukuyama T. Stereocontrolled total synthesis of (−)-ephedradine A (orantine). *J Am Chem Soc.* 2003;125(27):8112–8113. https://doi.org/10.1021/ja036011k
5. Zhu J, Hesse M. The spermine alkaloids of chaenorhinum minus. *Planta Med.* 1988;54(05):430–433. https://doi.org/10.1055/s-2006-962490
6. Hikino H, Kiso Y, Ogata M, et al. Pharmacological actions of analogues of feruloylhistamine, an imidazole alkaloid of ephedra roots1. *Planta Med.* 1984;50(06):478–480. https://doi.org/10.1055/s-2007-969777
7. Krizevski R, Bar E, Shalit O, Sitrit Y, Ben-Shabat S, Lewinsohn E. Composition and stereochemistry of ephedrine alkaloids accumulation in Ephedra sinica Stapf. *Phytochemistry.* 2010;71(8–9):895–903. https://doi.org/10.1016/j.phytochem.2010.03.019

8. Ballero M, Foddis C, Sanna C, et al. Pharmacological activities on Ephedra nebrodensis Tineo. *Nat Product Res.* 2010;24(12):1115–1124. https://doi.org/10.1080/14786410802680902

9. Groves RA, Hagel JM, Zhang Y, et al. Transcriptome profiling of khat (Catha edulis) and Ephedra sinica reveals gene candidates potentially involved in amphetamine-type alkaloid biosynthesis. *PLoS One.* 2015;10(3):e0119701. https://doi.org/10.1371/journal.pone.0119701

10. Hikino H, Konno C, Takata H, Tamada M. Antiinflammatory principle of Ephedra herbs. *Chem Pharmac Bull.* 1980;28(10):2900–2904. https://doi.org/10.1248/cpb.28.2900

11. Krizevski R, Bar E, Shalit O, et al. Benzaldehyde is a precursor of phenylpropylamino alkaloids as revealed by targeted metabolic profiling and comparative biochemical analyses in Ephedra spp. *Phytochemistry.* 2012;81:71–79. https://doi.org/10.1016/j.phytochem.2012.05.018

12. Zhang D, Deng A-J, Ma L, et al. Phenylpropanoids from the stems of Ephedra sinica. *J Asian Nat Pro Res.* 2016;18(3):260–267. https://doi.org/10.1080/10286020.2015.1070831

13. Starratt AN, Caveney S. Quinoline-2-carboxylic acids from Ephedra species. *Phytochemistry.* 1996;42(5):1477–1478. https://doi.org/10.1016/0031-9422(96)00126-4

14. Nawwar M, Barakat H, Buddrust J, Linscheidt M. Alkaloidal, lignan and phenolic constituents of Ephedra alata. *Phytochemistry.* 1985;24(4):878–879. https://doi.org/10.1016/S0031-9422(00)84920-1

15. Tamada M, Endo K, Hikino H. Maokonine, hypertensive principle of Ephedra Roots1. *Planta Medica.* 1978;34(07):291–293. https://doi.org/10.1055/s-0028-1097453

16. Zhao W, Deng A-J, Du G-H, Zhang J-L, Li Z-H, Qin H-L. Chemical constituents of the stems of Ephedra sinica. *J Asian Nat Prod Res.* 2009;11(2):168–171. https://doi.org/10.1080/10286020802573552

17. Khan IA, Abourashed EA. *Leung's Encyclopedia of Common Natural Ingredients: Used In Food, Drugs And Cosmetics.* John Wiley & Sons; 2011.

18. Shuang-Man M, Zhang Q, Xiao-Bao B, Jin-Long C, Meng-Liang W. A review of the phytochemistry and pharmacological activities of Ephedra herb. *Chinese journal of natural Medicines.* 2020;18(5):321–344. https://doi.org/10.1016/S1875-5364(20)30040-6

19. Nawwar MA, El-Sissi HI, Barakat HH. Flavonoid constituents of Ephedra alata. *Phytochemistry.* 1984;23(12):2937–2939. https://doi.org/10.1016/0031-9422(84)83045-9

20. Amakura Y, Yoshimura M, Yamakami S, et al. Characterization of phenolic constituents from Ephedra herb extract. *Molecules.* 2013;18(5):5326-5334. https://doi.org/10.3390/molecules18055326

21. Pechini MP. Washington, DC: US patent and trademark office. *US patent.* 1967(3.330):697.

22. Bouchard NC, Howland MA, Greller HA, Hoffman RS, Nelson LS. Ischemic stroke associated with use of an ephedra-free dietary supplement containing synephrine. *InMayo Clinic Proc*. 2005;80(4):541–545. https://doi.org/10.4065/80.4.541

23. Cottiglia F, Bonsignore L, Casu L, et al. Phenolic constituents from Ephedra nebrodensis. *Nat Product Res.* 2005;19(2):117–123. https://doi.org/10.1080/14786410410001704714

24. Purev O, Pospíšil F, Motl O. Flavonoids from Ephedra sinica stapf. *Collection Czechoslovak Chem Commun.* 1988;53(12):3193–3196. https://doi.org/10.1135/cccc19883193

25. Porter PL, Wallace JW. C-glycosylflavones from species of Ephedra. *Biochem Syst Ecol.* 1988;16(3):261–262. https://doi.org/10.1016/0305-1978(88)90003-8

26. Wallace JW. C-Glycosylflavones in the gnetopsida: A preliminary report. *Am J Botany.* 1979;66(3):343–346. https://doi.org/10.1002/j.1537-2197.1979.tb06233.x

27. Ohba S, Yoshida K, Kondo T. Swertisin dihydrate. *Crystal Struc Commun.* 2004;60(12):o893–o896. https://doi.org/10.1107/S0108270104028355

28. Hussein SA, Barakat HH, Nawar MA, Willuhn G. Flavonoids from Ephedra aphylla. *Phytochemistry.* 1997;45(7):1529–1532. https://doi.org/10.1016/S0031-9422(97)00092-7

29. Friedrich H, Wiedemeyer H. Quantitative bestimmung der gerbstoffbildner und der gerbstoffe in ephedra helvetica. *Planta Medica.* 1976;30(07):223–231. https://doi.org/10.1055/s-0028-1097722

30. Tao H, Wang L, Cui Z, Zhao D, Liu Y. Dimeric proanthocyanidins from the roots of ephedra sinica. *Planta Med.* 2008;74(15):1823–1825. https://doi.org/10.1055/s-0028-1088321

31. Hikino H, Shimoyama N, Kasahara Y, Takahashi M, Konno C. Structures of mahuannin A and B, hypotensive principles of Ephedra roots. *Heterocycles*. 1982;19(8):1381–1384.

32. Tao H, Wang L, Cui Z. Study on chemical constituents of root of Ephedra sinica [J]. *Chin Tradit Herb Drugs.* 2010;41(4):533–536.

33. Zang X, Shang M, Xu F, et al. A-type proanthocyanidins from the stems of Ephedra sinica (Ephedraceae) and their antimicrobial activities. *Molecules.* 2013;18(5):5172–5189. https://doi.org/10.3390/molecules18055172

34. Ibragic S, Sofić E. Chemical composition of various Ephedra species. *Bosnian J Basic Med Sci.* 2015;15(3):21–27. https://doi.org/10.17305/bjbms.2015.539

35. Uttra AM, Shahzad M, Shabbir A, Jahan S. Ephedra gerardiana aqueous ethanolic extract and fractions attenuate Freund Complete Adjuvant induced arthritis in Sprague Dawley rats by downregulating PGE2, COX2, IL-1β, IL-6, TNF-α, NF-kB and upregulating IL-4 and IL-10. *J Ethnopharma.* 2018;224:482–496. https://doi.org/10.1016/j.jep.2018.06.018